INSTITUTE FOR AEROSPACE STUDIES

UNIVERSITY OF TORONTO

THE SCATTERING OF HIGH ENERGY ARGON ATOMS FROM A WELL CHARACTERIZED (100) TUNGSTEN SURFACE

by

D. R. O'Keefe

JULY 1968

UTIAS REPORT NO. 132

THE SCATTERING OF HIGH ENERGY ARGON ATOMS FROM A WELL CHARACTERIZED (100) TUNGSTEN SURFACE

by

D. R. O'Keefe

Manuscript received April 1968

JULY 1968 UTIAS REPORT NO. 132

ACKNOWLEDGEMENTS

The author wishes to thank Professor J. B. French for the supervisory assistance and advice rendered throughout this research endeavour, as well as Professor A. J. Howsmon for stimulating discussions on the theoretical aspects of the present work.

The advise and consultation received from fellow students especially J. W. Locke, E. J. Moskal, R. H. Prince and G. E. McMichael are gratefully acknowledged. Members of the UTIAS shop staff are thanked for their capable work in the fabrication of the equipment.

I would like to thank especially Dr. P. Sewell of the Applied Chemistry Division of the National Research Council of Canada for his assistance in the surface characterization studies, and Drs. Redhead and Armstrong of the Electron Physics Group of the N.R.C. for the valuable discussions which they provided on the adsorption and ultrahigh vacuum aspects of the work.

My thanks are also extended to my wife Gail for initial typing of the manuscript and Mrs. J. V. Dublack for final typing of the master sheets.

The work was conducted under the joint financial support of the National Aeronautics and Space Administration under Grant No. NsG-367, Defense Research Board Grant 9551-02 and National Research Council Grant A-2731. The author would like to thank the National Research Council of Canada for personal financial assistance in the form of scholarships.

SUMMARY

The scattered number flux distributions for nearly monoenergetic high energy (0.25 to ≈2.0 eV) argon atomic beams impinging on the (100) face of a single crystal of tungsten were obtained as part of a basic study of gas-surface interactions related to satellite aerodynamics. A fundamental study was chosen in order to allow direct comparison with existing and forthcoming theoretical analyses. To permit such comparisons, major emphasis was placed on surface preparation and characterization. The scattering studies were performed in an ultra-high vacuum environment, with prior surface characterization conducted through the use of optical microscopy and high energy electron diffraction. The amount and kind of adsorbed gas at the surface was inferred during beam bombardment by means of the retarding field diode method which indicates changes in surface work function. A seeded nozzle beam (argon-helium mixtures) was employed to obtain enhanced velocities approaching the satellite velocity range with very little velocity spread (< 10%). The use of an argon-helium beam circumvented the effects of beam contamination at the surface since these gases are physisorbed only slightly on a room temperature surface. Scattered number flux distributions were obtained for an angle of incidence of 45 degrees and for varying surface conditions and beam energies. The peak intensities for all distributions were found to lie below the specular angle and were narrower than the distributions found at the lower energies. The maximum of the reflected pattern shows only slight shift with energy; however, adding considerable quantities of nitrogen or carbon monoxide on the target surface results in wider distributions with higher backscattering and a shift in the maximum towards the surface. A saturation level of hydrogen appears not to change the scatter results from those obtained on a clean surface, probably due to the low activation energy for surface migration of hydrogen. At no time, even under conditions of high gas coverage in carbon monoxide, did the distributions approach that of a cosine law reflection: implications concerning the effect of physical parameters and the surface state on the scattering and accommodation are discussed.

TABLE OF CONTENTS

		Page
1.	INTRODUCTION	1
2.	DESCRIPTION OF EXPERIMENTAL APPARATUS	4
	2.1 Molecular Beam Facility	4
	2.2 Scattering Chamber	6
	2.2.1 Description of Scattering Chamber	6
	2.2.2 System Preparation	6
	2.2.3 Collimation Chamber	7
	2.3 Molecular Beam Detector	7
	2.3.1 General Design Considerations	7
	2.3.2 General Description of Detector	9
	2.3.3 Rotary Electrical Feedthrough	10
	2.3.4 Electron Multiplier	11
	2.4 Cryopump and Molecular Trap	12
	2.5 Target	14
	2.5.1 Target Surface	14
	2.5.2 Target Alignment	17
	2.5.3 Target Mount	17
	2.5.4 Target Cleaning	18
	2.5.5 Retarding Field Diode	19
3.	RESULTS	20
	3.1 Background Gas Environmental Study	20
	3.1.1 Mass Spectral Analysis	20
	3.1.2 Flash Desorption Results	21
	3.1.3 Retarding Field Diode Results	22
	3.2 Scattering Results	23
	3.2.1 Determination of Beam Properties and Scattered Flux Intensities	23
	3.2.2 Effect of Gaseous Monolayers on the Scattered Number Flux Distribution	26
	3.2.3 Effect of Incident Beam Energy on the Scattered Number Flux Distribution	29
	3.2.4 Comparison with Existing Experimental Lower Energy Work	29
	3.2.5 Comparison with the "Hard" Cube Model	31
4.	CONCLUSIONS	32
	REFERENCE LIST	34
	FIGURES	

1. INTRODUCTION

The momentum and energy transfer between a surface and a rarefied gas flow depend strongly on the individual particle interactions which occur at the surface. Physical states of the gas and of the surface determine the nature of these interactions and a precise knowledge of these states is required in any serious study of gas-surface interactions. One prime reason for studying these interactions is to allow calculation of the momentum and energy transfer in satellite aerodynamic studies. Another is the kinetic theory problem of flow through a tube, important for specific types of atmospheric sampling space probes. The transfer processes occuring during a gas-surface interaction are of course, of extreme interest to chemists in the study of many catalytic reactions.

The majority of existing work (theoretical and experimental momentum and energy accommodation measurements and beam reflection studies) has been performed in the thermal energy range (0.03 to 0.4 eV), and with the exception of a very few notable cases, on undefined surfaces. This paper presents some of the first data to be obtained for the higher beam energy (0.3 to 2.0 eV) range (approaching satellite velocity) and under well characterized surface conditions.

Theoretical models for the higher energy range are rapidly emerging which require experimental validification and it is hoped that this data will aid in the prediction of the form of the potential of interaction as well as permit calculation of parameters such as the well depth energy. In this regard, a carefully performed scattering study provides a sensitive test for any theory, and also is a means of obtaining the above parameters. For this reason, the present work is a study of the fundamental interaction problem of an inert gas on a single crystal surface. For later satellite aerodynamic studies, when the physical mechanisms of the interaction processes are better understood, more practical engineering surfaces and atmospheric gas beams will be used.

In investigating the kinetic interactions which take place between a beam of molecules and a surface, it has been generally observed that there is a significant spreading of the particle trajectories upon reflection. The terms diffuse, specular and lobular are used to describe this spreading effect. The first is usually equivocal with cosine law scattering in which it is assumed that there is total energy accommodation at the surface. In such a case, the gas is re-emitted with a Maxwellian distribution of velocities at the temperature of the surface. The term specular is used to describe the situation in which a narrow beam of particles, similar to the incident one, is reflected at the "mirror" angle. A reflection pattern intermediate between the two extremes described above is called lobular, and should this distribution be symmetric about the specular angle and of significant width, it is called quasi-specular. Concerning the mechanism of the redistribution, it is quite possible to obtain a so-called "multi-specular" interaction in which particles retain their initial speeds, but reflect quite randomly due to surface roughness. With such a mechanism, a diffuse reflection results with incomplete accommodation to the surface. Diffuse reflection is therefore not synonomous with total energy accommodation and the preparation of atomically smooth surfaces is of paramount importance in any basic investigation of scattering. Recent experiments employing time-of-flight detection methods (Refs. 1, 2 and 3) have given direct evidence of the very incomplete and varying accommodation

possible in different directions in the scattered flux distributions. These measurements were all made at near-thermal velocities and there is every reason to expect that this situation will be even more pronounced at the higher incident energies.

One experimental method of studying the interaction is to measure directly the momentum or energy exchange at the surface; however, detailed physical insight into the reasons for a condition of high or low momentum or energy accommodation is provided by a thorough knowledge of the reflected spatial distribution. The theoretical model of Schamberg (Ref. 4), although it contains the false assumption that all the particles are reflected with the same velocity, illustrates how the width and angular position of the reflected distribution affect the drag on a body in a rarefied flow. At the present time, theoreticians are for the most part relying on experimental scattering data to determine their approach to the prediction of gas-surface interaction problems. Influenced by this approach, experimenters are determining the parameters which most greatly affect the interaction. Variations in the scattering pattern have been found to result from changes in the relative temperature between gas and solid, gas species, kind of surface (i.e., type of material), surface condition (rough, smooth, single-crystal, polycrystalline, with or without adsorbed gas layers) and angle of incidence.

With the exception of some recent experimentation (Refs. 5, 6, 7, 8 and 9), the majority of work in the field of surface interactions (i.e. scattering experiments and thermal and momentum accommodation coefficient measurements) is difficult to interpret due to undefined surface conditions. The excellent early work by Knauer, Estermann and Stern (Refs. 10 and 11) reported a diffraction effect for the light gases (hydrogen, helium) from the alkali halides. Concurrent with this work and for the same gas-surface combination, workers such as Johnson and Kirschbaum (Refs. 12 and 13) reported no such effect. Present day experimenters are convinced that the failure to see diffraction phenomena was due to the existence of an "unclean" surface. The importance of surface preparation was evident in the early work of Zabel (Ref. 14) in which a degradation of the reflected signal at the specular and diffracted positions was observed upon exposure of the target to moist room air. Datz et al (Ref. 15) have illustrated the effect of a gaseous monolayer on the form of the scattering pattern. A quasi-specular lobe was effectively changed to a cosine-like distribution upon the adsorption of a saturation level of background gas. Hinchen and Foley (Ref. 16) have observed this effect as well. In both these references a relatively high background gas contamination level was required before a diffuse (cosine-like) reflection resulted. Smith and Saltsburg (Refs. 7 and 8) have used a continuously deposited metal film to maintain reproducible surface conditions without recourse to ultrahigh vacuum techniques. They have reported structural (diffraction-like) behaviour in helium, hydrogen and deuterium and lobular distributions for the heavier gases.

Almost all recent work has involved the fly-through detection method, in which reflected beam in-flight number density is the quantity recorded. A measure of the mean velocity of the reflected particles is then required to determine the actual spatial distribution (i.e. the number flux). Modulated beam techniques (Refs. 17 and 18) employing lock-in narrow band-pass amplifiers and phase sensitive detection have provided greatly improved signal-to-noise ratios plus an indication of the mean reflected velocities. They do not, however, provide a signal proportional to the total number flux in any

given direction because the signal contains no information about those molecules which have no coherence with the initial modulation, such as those trapped at the surface for appreciable times or those with widely different velocities from the mean for that direction. In the present work, we have elected to use the stagnation mode of operation in which the flux is determined directly from the signal. This flux measurement combined with a reflected velocity determination employing the time-of-flight method developed in this laboratory by Locke (Ref. 19) will be used in later work to determine the momentum and energy distribution of the reflected species. This information together with a measure of the total momentum and energy transfer (currently being investigated), will afford a rather complete analysis of the interaction. A knowledge of the flux distribution is specifically required when discussing any kinetic theory problem involving concave surface geometry.

It was the objective of the present work to obtain results with carefully determined surface conditions. Towards this end, a careful preparation of the surface was employed, the target was placed in an ultrahigh vacuum environment and surface gas coverage has been inferred in situ using the retarding field diode method to measure work function changes (Ref. 20). The choice of an inert gas beam (argon) avoided any complications resulting from the adsorption of the beam on the surface. Tungsten was chosen for the target material because of the facility of cleaning in ultrahigh vacuum and also because of the large amount of previous work available on adsorption, work function measurements and surface preparation. Electron miscroscopy and high energy (low angle of incidence) electron diffraction results are described which provide a detailed description of the test surface.

The present work also involved the use of a seeded nozzle beam (Refs. 21, 22, 23 and 24), allowing scattering studies to be performed with a nearly monoenergetic beam in the relatively unexplored energy range between thermal and satellite velocities (0.3 to 10 eV). With the exception of one recent investigation, all previously measured scattered distributions have been performed with thermal (0.03 to 0.4 eV) beams. Alcalay and Knuth (Ref. 25), using the continuously deposited film technique of Smith and Saltsburg to maintain reproducible surface conditions without recourse to ultrahigh vacuum methods, have measured the reflected spatial distribution of 1.2 eV argon atoms from silver. A comparison of the present results was not made with their work because they used a different angle of incidence as well as a different surface temperature ($560^{o}K$ in order to get epitaxial growth of (111) orientation in silver). Devienne et al (Ref. 26) have reported scattering experiments for several gas and surface combinations; however, their beam energy (a charge exchanged ion beam) extends from 100 to several thousand electron volts and the mechanism of the interaction for such energetic beams is grossly different from what is to be expected in the satellite velocity range, and thus this work will not be discussed further in this report.

In summary, this paper reports a scattering study of a high energy argon beam on a single crystal (100) tungsten surface, allowing a direct comparison with the high energy theoretical flux predictions of Jackson (Ref. 27) and Oman (Refs. 28 and 29). A description of surface preparation and characterization using electron microscopy and reflected high energy electron diffraction is included, together with the results of the auxillary surface work function measurements used to monitor surface gas adsorption during the scattering experiments. Direct comparison of the half width and position of the maximum of the reflected distributions is made with existing results at the lower end of the

energy range of the present results, and with the predictions of the hard cube model (Ref. 30). The position of the lobe maximum is predicted rather accurately; however, experimental distributions are found to be considerably wider than those calculated using the model. Implications concerning the effect of physical parameters and the surface state on the scattering and accommodation are discussed.

2. DESCRIPTION OF EXPERIMENTAL APPARATUS

2.1 Molecular Beam Facility

The UTIAS molecular beam facility is typical of the nozzle beams used by other workers in the study of particle-surface interactions and beam-beam collisional processes. There are several publications (Refs. 31 - 36) available which describe the design, construction and performance of these beams. Also contained in these references is an extensive bibliography on the work performed in nozzle beam research. For the particular beam system employed in this work, references 37, 38 and 39 should be consulted.

The present nozzle beam is equipped with a heated source (design temperature $\simeq$ 2500 degrees Kelvin) and employs the usual seeding technique to achieve increased velocities. A velocity analyser is presently being installed, but for the present work, calculated values of the velocity are used. Anderson and Fenn (Ref. 40) have investigated the velocity distributions in a nozzle beam under several conditions of skimmer interference. The parameter which best describes this so-called "interference" is the Knudsen number based on the skimmer orifice diameter. For Knudsen numbers up to 1.6 they found only small ($<$ 5 percent) discrepancies between the calculated and measured velocities. Becker and Henkes (Ref. 22), in an early investigation of seeded beams, performed a similar analysis in which they have shown that there is negligible velocity slip between the seed and carrier gases when the skimmer Knudsen number is 0.3 or greater. Later work by Abauf (Ref. 43) corroborated the work of Benker and Henkes for xenon-hydrogen mixtures and also showed that there was good agreement between calculating and measuring the velocity for argon in a helium-argon mixture. Table 2.1.1 is a comparison of the threshold conditions which the above workers have found, with two typical runs performed using the UTIAS facility. A brief look at the table will reveal that the present system is definitely in a region free from skimmer interference in so far as the prediction of the beam velocity distribution is concerned. A calculation of the velocity of the molecular beam from source values of temperature and composition is thus believed to introduce only small uncertainties. The present beam system is not free from skimmer interference as it pertains to the beam intensity, and centre-line fluxes are measured to be 1/5 of the calculated value as typically found by other workers (Ref. 44). A measured flux of 10^{14} argon atoms/cm^2 sec was found to be adequate for the present work. The choice of a skimmer source distance of 70 nozzle diameters was based on the work of Davis (Ref. 39) in which the flux was found to be maximum at this value. Table 2.1.1 also includes effective Mach number calculations for the seed gas assuming negligible slip conditions. Note that the carrier gas because of its high percentage, controls the flow, and thus no attempt has been made to calculate the parameters based on the flow of the seed gas alone. Also note that for the case of the argon-hydrogen mixture that rotational and vibrational relaxation was not considered since these modes freeze out quite rapidly in the flow (Ref. 36, especially Fig. 15), making the flow behave essentially as an inert gas after the first few nozzle diameters.

A skimmer geometry analysis similar to that reported by Hagena and Morton (Ref. 41)* was employed to achieve theoretical centre line beam fluxes. A brief summary of the analysis may be outlined as follows:

The centre line flux is written as G x F (molecules/cm^2sec) where G is the flow through the source orifice given by:

$$G = \left(\frac{2}{\gamma+1}\right)^{\frac{(\gamma+1)}{2(\gamma-1)}} \rho_o a_o A^* \qquad (1)$$

or measured experimentally by a flow meter.

The function denoted by F results from the above analysis and is written as:

$$F = 0.63121 \ \gamma M_f^2 \int_0^{\theta} \cos^4 \ x \cos^2 K \ x \sin x \ e^{\frac{-\gamma M_f^2 (\sin^2 x)}{2}} dx \qquad (2)$$

where M_f is the translatory freezing Mach number and θ is the angle contained between the axis of the free jet and the line drawn from the source to the point "P" on the quitting surface (illustrated in Fig. 2.1.1).

The quantity K is equivalent to the expression $\pi/2C$ where C is a free jet parameter which can be obtained from table I of Ref. 36.

Figure 2.1.2 shows the variation of the quantity F with respect to θ for various values of the freezing Mach number. In the present work, a choice of geometry was made to insure operation in the region of large Mach numbers and at optimum values of θ. Considering the pure argon run of Table 2.1.1 where the value of the freezing Mach number is 21.0, the choice of a 1.067 mm diameter skimmer (θ = 7.5 degrees) gives a value of F which is 99% that of F_{max}. Previous operation of the molecular beam was performed using a skimmer which gave an F value of 0.2. Thus a three fold increase in the centre line intensity was expected and later verified experimentally.

Although one essentially increases the size of the skimmer to achieve an increase in the centre-line flux, it is not advantageous to make the skimmer larger than the point at which F is maximum. Indeed beyond this point there is virtually no gain in signal and an undesireable increase in the background pressure in the region downstream of the skimmer results.

The low temperatures (typically as low as 10 degrees Kelvin) achieved in the free jet expansion lead to the direct possibility of agglomerates in the beam. The presence of an appreciable number of these agglomerates would greatly affect the beam reflection problem and so conditions which will give a condensed beam should be avoided. Milne and Greene (Ref. 42) have measured the mole fraction of argon clusters formed in a free jet and have found the majority of the nucleated species to be dimers. The operating pressure and temperature conditions of the present beam system for a pure argon expansion when

---

* Present analysis due to G.E. McMichael of this laboratory.

inserted in their results indicates the formation of a mole fraction of Ar_2 less than 10^{-4}. Also, it is expected that the use of such dilute mixtures of argon and helium in the present beam system (5% - 95%, 1% - 99% argon in helium) will not allow enough collisions between argon atoms to take place in the continuum expansion stage to form an appreciable number of condensed argon particles. For this reason, it is believed that the present system gives a true indication of the results for the reflection of single argon atoms.

2.2 Scattering Chamber

2.2.1 Description

A photograph of the molecular beam scattering chamber is shown in Fig. 2.2.1. The entire construction is of type 304 stainless steel and employs only metal gasket sealing. Small flanges use seals of the "conflat" design, while the large 24 inch diameter seals are made with OFHC copper wire. A General Electric triode getter ion pump (nominal pumping speed for air of 500 litres/sec) is used to maintain a low pressure ($\simeq 10^{-9}$ torr) in the chamber. The choice of a getter ion pump was made because of its inherent cleanliness. Bakeout to 350°C is achieved by thermostatically controlled heating elements located on the outside of the apparatus. Spun glass insulation and radiation shielding are used to assure more even heating of the entire assembly.

The scattering chamber is joined to the molecular beam collimation chamber by means of a stainless steel bellows. This flexible link allows one to position the entire experimental chamber with respect to the line-of-sight of the beam. Adjustment screws on the scattering chamber assembly aid in achieving this correct position. A bakeable straight-through valve (Granville Phillips type S) is used to isolate the experimental and collimation chambers.

2.2.2 System Preparation

For the initial pump down of the above assembly it was necessary to bake for three days at 350 degrees Centigrade while pumping with an extremely well trapped two stage mechanical pump. The pressure during this initial pump down time was about one micron. On the third day, the triode getter-ion pump was started and when the pressure reached about 5×10^{-7} torr, the bakeout was terminated. The next day, the total pressure was usually found to be $1 - 2 \times 10^{-9}$ torr (air) as measured by a Balzers IM 800 nude Bayard-Alpert gauge. System preparation became much easier after the initial pump down and a one day bake was found to be sufficient to achieve 10^{-9} torr when the system was later let up to atmospheric dry nitrogen for various experimental modifications. It should be mentioned that it was necessary in the bake-out procedure to bring the system up to temperature rather slowly to avoid having the large diameter (24 inch diameter copper wire gaskets) seals break open.

2.2.3 Collimation Chamber

The collimation region of the molecular beam system consists of a large mild steel chamber (shot blasted) pumped by means of an untrapped 32,000 litres/sec 5 stage fractionating oil diffusion pump employing a DC 704 fluid. The blank-off pressure of this chamber has been measured to be 10^{-7} torr by means of a cold cathode discharge gauge. Mass spectrometric analyses for untrapped fractionating diffusion pumps are difficult to obtain; however, the manufacturers' specification sheet for DC 704 lists mass numbers 39, 49, 50, 51, 52, 77, 78, 105, 137, 149 and 150 amu as the major species. Since the lowest mass number will represent the highest effusion rate into the scattering chamber, the assumption that 100% of the gaseous vapour over the pump has mass number 39 amu will be made. Based on the above assumption, the flow through the collimator orifice (2 mm diameter) between the collimation and scattering chambers is calculated to be 1.2×10^{-8} torr litres/sec. Assuming a moderate pumping speed of 100 litres/sec (actually very much greater than this due to the use of cryogenic pumping), the total pressure rise in the system due to the effusion of oil would be 1.2×10^{-10} torr. The number of these particles striking the surface can be calculated knowing the solid angle subtended by the target. Such a calculation reveals that it takes about 1.5 months to form a monolayer on the surface, assuming that there are 10^{14} lattice sites per cm^2 available for adsorption and that the sticking probability is unity.

It should be emphasized that the above calculations are conservative and that in actual fact the contamination will be less, due to the fact that the majority of the gaseous components in the collimation chamber are of a larger mass number and that the pumping speed for these oil fractions is considerably higher due to the use of liquid nitrogen and helium pumping. Except for the component of the gas which diffuses straight on to the target surface along the line-of-sight of the beam, the cryogenic shroud (described in Sec. 2.4) will prevent all other oil particles from reaching the target. The retarding field diode results of section 3.1 verify this experimentally. It should be mentioned at this point that the total pressure measured in the collimation chamber with the beam on was $2\text{-}3 \times 10^{-6}$ torr; however, since only inert gas beams were used in this series of experiments, the contamination rate at the surface due to effusion from the collimation chamber remains the same as calculated above.

2.3 Molecular Beam Detector

2.3.1 General Design Considerations

For the present experiment, a detector must not only be capable of measuring the extremely low signals of the reflected beam, but must as well, be compatable with the conditions of ultrahigh vacuum and 400°C bakeout. The requirement on the signal capabilities was initially found by calculating the flux which would have to be detected if an incident beam flux of 10^{14} particles/cm^2sec (typically the flux of the present beam system) was scattered into a cosine distribution. The result indicated that, at the centre of this distribution (the maximum), signals down from the incident flux by a factor of 1/10,000 would have to be detected. This was confirmed experimentally by the actual signal levels recorded (see section 3.2). For the typical flux assumed above, this means that the detection of a reflected signal equivalent to

1×10^{-11} torr must be realized in those regions of the distributions where the signal falls off from the peak intensity (the backscattered direction).

Although the use of a total pressure measuring device is a possibility, a mass spectrometer has the advantage of being able to measure these small signals more easily and as well discriminate between gases in the system. This is particularly important in the detection of mixed beams in which the carrier gas cannot be entirely removed from the beam, especially for the dilute mixtures (i.e. 1% - 99%). Also in employing a mass spectrometer one necessarily gains an increase in signal-to-noise ratio for those situations in which certain background gases cannot be removed adequately by the pumping system. A case in point would be a high background of helium gas which cannot be pumped adequately by either a getter pump or a liquid helium cryopump. Since the helium does not present a surface contamination problem, it is best, from a financial point of view, to make use of a mass spectrometer rather than invest in an exotic pumping system such as a cryosorption array. The presence of large amounts of hydrogen, on the other hand, requires the use of either the above array or a sublimation pump. A mass spectrometer of course allows a thorough knowledge of the environment surrounding the surface and is paramount in any serious study of gas-surface interactions.

In considering the signal-to-noise problem of the detection of reflected argon, it is now evident from the experimental results that the background pressure level in the scattering chamber with the beam on and using only ion pumping, is about 3×10^{-9} torr (argon), and thus a signal-to-noise ratio of 1/300 is typical for signals in the backscattered direction. One popular method for increasing the signal-to-noise ratio in molecular beam experiments has been the modulated beam lock-in-amplifier (Refs. 17 and 18) technique. Such a technique, in general, requires a gauge with a relatively fast time response since chopping frequencies of the order of 300 cps are routinely used. The fly-through mode of operation, in which the beam flies through the ionization detector, displays a time response compatable with the above requirements. For this reason, the fly-through method (signal proportional to number density) has been the most popular in beam experiments to date. A hundred fold increase in signal-to-noise is typically obtained using the above technique.

In the present system, we have elected to use the stagnation mode of operation (signal proportional to flux) and improve signal-to-noise by decreasing the beam gas background pressure level using liquid helium cryopumping in the region of the target. This method has the advantage that it gives the flux directly (the quantity most useful in a discussion of satellite aerodynamics) and at the same time the cryopump reduces the possible background gas contamination of the target surface to a negligible level. A possible limitation of the stagnation method is that it may not be well suited to the detection of a chemisorbable gas beam. Having the walls of the gauge act as a source or sink for the beam gas would result in much longer effective gauge response times. On the other hand, if the adsorption-desorption rates are either small or large compared with the time required for the measurement of a step function change in density, then the detection of a chemisorbable gas beam is a possibility. It is difficult to obtain estimates of these rates for a material such as stainless steel, however, some data suggest that the problem will not be severe since the sticking probability for most adsorbent-adsorbate combinations is extremely small after the first monolayer. This suggests that once the gauge volume possesses an adsorbed monolayer, that the kinetics of the multilayers

are such as to allow the detection of chemisorbable beams. These qualitative arguments can only be verified by an experimental study. Certainly the use of inert gas beams presents no problem in this regard since physisorption is not appreciable at room temperature. This was verified experimentally for the case of argon because the pressure level of argon in the gauge volume is found to drop to an extremely low level ($< 10^{-12}$ torr) in a short period of time (15 sec) when the beam is shut off.

2.3.2 General Description of Detector

A General Electric model 22PT121 mass spectrometer is used as the reflected beam detector. Figure 2.3.1 is a photograph of the above unit in its position on the traversing gear assembly. The detector is essentially a stagnation (closed volume) device with a sensing probe attached to the ionization region (Figs. 2.3.2 and 2.3.3). This probe is located 9.6 cm from the target surface and has an angular resolution of 1.8 degrees. Beam molecules entering the probe orifice are scattered randomly inside the entire gauge volume and are recorded as a density change in the mass spectrometer. At equilibrium (assuming negligible pumping due to the mass spectrometer itself) the flux entering the gauge volume is equal to the flux which leaves. An accurately machined orifice (0.3086 cm) in a thin walled (0.005") section of the probe (Fig. 2.3.3) allows the use of the simple kinetic calculation $\frac{1}{4}n\bar{c}$ for the flux, provided one assumes that the molecules in the gauge volume are completely accommodated to the gauge wall temperature. The present choice of geometry in which the molecules are forced to suffer a large number of collisions with the walls of the detector before entering the ionization region makes this a good assumption. A cone positioned at the rear wall of the probe and directly behind the orifice prevents high velocity particles, such as those encountered in the primary beam, from being reflected straight back out the hole on the first collision. Note that the assumption made in this paragraph about the negligible pumping speed of the mass spectrometer is generally true; these pumping speeds are usually much smaller than Bayard-Alpert total pressure gauges which are typically 0.01 litres/sec for normal operating conditions.

The detector is mounted on a large (18 inch diameter) gear, fabricated from stainless steel, and rotated by a means of a worm. Oppositely machined "V" grooves in the gear and gear support flange (Fig. 2.3.2) comprise a race for the 200 stainless steel balls upon which the gear turns. To avoid sticking and possible cold welding in ultra-high vacuum, these ball bearings were gold plated. The choice of gold was made after reference to a recent article on bearing performance in ultra-high vacuum (Ref. 45). At no time during the bakeout cycle or during normal operation did this vital part of the apparatus stick or become jammed.

A Varian vacuum rotary feed-through was used to supply leak tight linkage between a variable speed (5 rpm to 300 rpm) DC motor and the inside worm. The gear ratio between outside drive and inner gear is 1/338 so that for the lowest motor speed, the detector can be rotated at a rate equivalent to 1/100 rev/min. Since the time response of the gauge volume is about 5 seconds and the detector advances only 1/3 of a degree in this time interval it is possible to accurately record the scattered beam signal concurrently with the detector rotation. Although not used in the present work for reasons given in Section 3.2.1, the use of a properly geared down multi-turn linear

potentiometer could be used to obtain plots on an x - y recorder of the type shown in Section 3.2. Further, sophistication would be required to obtain a normalized signal readout on the y axis.

Because of the difficulties in designing target or detector articulation in the bakeable chamber, the detector scans only in the so-called "incident" (i.e., the plane contained by the incident beam and the normal to the surface) plane. This has been the normal procedure of most other workers in the field of molecular scattering. Enough travel is provided in the detector rotation to allow the detection of the incident beam once the target has been retracted. In this manner it was possible by recording the incident signal before and after a run to normalize all scattering data by the incident flux value, and this was always done.

2.3.3 Rotary Electrical Feedthrough

The unavailability of bakeable (350°C, low outgassing) and flexible organic wire insulation necessitated the design of a rotating device which would provide noise-free electrical connections to the molecular beam detector (mass spectrometer). The method employed in the present experiment was to connect a copper strip (0.015" x 0.1875" x 18") to a stainless steel centre post, spirally wind it around this post in the manner of a clock spring, and connect it to an outer concentric ring (Fig. 2.3.4). Since the present experiment required only a maximum of 300 degrees rotation, it was possible by fixing the centre post to the gear assembly and the outside ring to the inside top of the scattering chamber to maintain electrical continuity as the copper strip was wound or unwound. The copper strip allows flexibility along the radius from the inner to the outer contact points, but possesses good rigidity in the plane of the feedthrough. A number of these units (total of 15) were stacked one on top of the other and insulated from one another by means of boron nitride standoffs. Electrical connections were made to each of the rotating units by bare copper wires insulated from one another and from the other stacked units by glass tubing placed in holes drilled in the inner and outer contact rings. To prevent the copper spring from coming out of the rotation plane and touching another stack, a thin (0.015") piece of stainless steel sheet was placed between each unit. This piece of stainless steel sheet represented a resistance of the order of 8×10^{-5} Ω in parallel with the copper strip (resistance = 0.004Ω). Each feedthrough was designed to take a current of 5 amperes without overheating and a voltage of 5 kV without breakdown; under actual operation there was no evidence of the existence of either of these problems. A resistance measurement made on a test stack using a Wheatstone bridge revealed that the resistance for the unit (0.034Ω) was about 10 times greater than the calculated value (0.004Ω) for the copper strip; the higher resistance has been ascribed to the contact resistance between the copper strip and the stainless steel terminal posts. The greatest change recorded in the resistance, between having the spiral fully wound or fully unwound, was 5% of the measured value. The effective mass spectrometer filament circuit resistance (nominally 1.0Ω) change due to the above 5% variation was calculated to be 0.2% making the system acceptable for the present application. Smaller variations in the resistance could have been achieved by assuring better electrical contact between the strip and ring, by means of welding or brazing instead of the mechanical method (screw fastener) which was used in this design.

The low current measuring levels of the electron multiplier output (typically 10^{-10} amperes) required that a flexible and bakeable shielded

cable connection be made within the vacuum system. A rigid coaxial connection at the electron multiplier was constructed from stainless steel tubing with the central bare wire conductor insulated from the tube by boron nitride spacers. This connection terminated in a hermetically sealed electrical feedthrough (ceramic sealed) welded to a flexible bellows link ($\frac{1}{2}$" diameter x 15" long) to the wall of the vacuum chamber. A specially designed bakeable knife edge seal at the vacuum wall made it possible to remove the bellows with the detector assembly when the top lid was lifted (Fig. 2.3.1). A low noise conventional miniature coaxial cable was placed in a teflon tube on one end of which was installed a push-fit connector. By sliding the teflon tube and cable into the bellows assembly from outside the vacuum chamber it was possible to make contact with the hermetically sealed connection inside. A spring loading device on the teflon tube assured noise-free electrical contact as the detector was rotated about the target for a measure of the reflected flux. The cable and teflon tube assembly was withdrawn each time a 350°C bake was conducted.

Bakeable glass sealed resistors were spot welded to the multiplier structure in order to provide the voltage dividing chain between dynodes. This meant that only two connections to the multiplier from outside the vacuum chamber had to be made, namely the multiplier high voltage (2 KV) which was supplied through the rotary device described above, and the signal readout which was carried to the outside by means of the flexible bellows link. The connections to the mass spectrometer ionizer, thermocouple junctions and detector outgassing oven were all made through the rotary unit.

2.3.4 Electron Multiplier

The General Electric mass spectrometer is equipped with a Dumont type 241-199 silver-magnesium electron multiplier. This unit consists of nine dynode stages with a nominal gain of 10^6. Difficulty has been experienced with high residual background current leakage ($\simeq 10^{-7}$ amperes) after system bakeout. This has also been the experience of other workers using the same instrument*. Effective removal of this leakage current was achieved by back filling the entire vacuum chamber to about 100 microns pressure of pure hydrogen (Ref. 46) and then initiating a glow discharge in the electron multiplier region. Following this procedure, residual background currents were reduced to less than 10^{-12} amperes with no detrimental effects to the multiplier gain. The addition of such large amounts of hydrogen did, however, affect the absolute background pressure level in the system. Before the introduction of hydrogen, blank off pressures of the order of 2×10^{-10} torr (with liquid nitrogen pumping) were routinely achieved, but after treatment, 10^{-9} torr was recorded. The mass spectrometer data of section 3.1, indicates that 95 percent of this background is hydrogen. Such a treatment had the significant effect of eventually affecting the ultimate goal of the experiment since it was impossible to remove this hydrogen by any of the pumps existing in the system and consequently the cleanest possible state achievable at room temperature was a hydrogen covered surface. For reasons to be discussed later, the presence of this saturation level of hydrogen on the surface does not affect the position or signal of the scattered flux distribution. This was inferred by flashing the target to 2000°C and monitoring simultaneously the reflected argon signal at various points in the reflected

---

* Gosselin C., Midwest Research Institute, (private communication)

distribution. The above dilemma could be resolved by the replacement of the present electron multiplier with a now available bakeable version of the Bendix resistive strip multiplier which is extremely insensitive to the contamination experienced when the system is outgassed (baked). Also the addition of a sublimation pump for the fast removal of hydrogen in the region of the target is suggested.

2.4 Cryopump and Molecular Trap

Removal of the background gases in the region surrounding the target serves two purposes. Firstly, it increases the signal-to-background pressure ratio of the reflected beam measurement and secondly, it decreases the contamination of the surface by the background gases. Early design considerations centred around the use of liquid helium cryopumping since it appeared capable of fulfilling both these requirements very effectively. A drum-shaped cryogenic pump region was designed and built to surround the target. It consists of a liquid helium stainless steel dewar (9.5" in diameter by 3.75" deep) completely surrounded by a larger but similarily constructed vessel of liquid nitrogen (Fig. 2.3.2). Since it was expected that some of the atoms reflected from the surface would retain a high percentage of their initial energy (1 to 10eV), and that these particles would not have very large sticking coefficients, even on a 4.2^{o}Kelvin surface, a molecular trap surface was designed. This consisted of machined fins on the inside wall of the liquid helium vessel skewed at an angle to the radius vector from the target centre (Fig. 2.4.1). In such a case, molecular reflections typical of the high energy particles (lobular) would be in towards the fin cavity, and such particles would suffer multiple collisions with the 4.2^{o}Kelvin surface. A cosine distribution (presumably resulting from slow moving particles) at the tip of a fin would represent the most severe case of the reflection of unwanted gas into the target region; however, such slow moving particles are most likely to be trapped at the 4.2^{o} Kelvin wall, and so do not present a problem. The effectiveness of the cryotrap is illustrated experimentally since the argon background pressure level measured when the detector was behind the target and not looking at the reflected signal was typically $< 5 \times 10^{-12}$ torr for liquid helium vapour (20^{o}K) cooled walls implying that virtually all false signals into the detector (resulting from internal reflections in the target region) were removed.

The above "serrated" wall was constructed as follows. Machined from flat stainless steel stock on an end mill and leaving a 0.010" wall at the root (Fig. 2.4.2), the unit was rolled into the proper diameter and then welded into the inner section of the helium dewar (Fig. 2.4.3). Note that support struts in the interior of the annulus allow light-weight construction with appropriate strength, and as well, results in better use of the liquid helium vapour for cooling. Figure 2.4.4 is a photograph of the liquid helium dewar with fill and vent tubes installed. The fill tube was placed to the bottom of the dewar and the vent at the top on the opposite side. This also aids in making full use of the cooling capacity of the liquid and gaseous helium. The entire dewar assembly was highly polished to decrease the radiative heat load from the surroundings. A slot in the top of the vessel allows the mass spectrometer probe to traverse around the target in the so-called "incident" plane, and a circular hole at the bottom centre allows one to position the target in the beam or retract it into the open region of the scattering chamber for target heating (cleaning). The liquid helium vessel weighs 7.75 lbs, requiring a calculated value of about 1 litre of liquid helium for cool down from 77^{o}K to

$4.2^{o}K$. This presupposes that the vessel is precooled by liquid nitrogen and that the heat capacity of the helium gas is utilized fully. Note also that this is the estimated amount of liquid helium required merely to cool down the vessel and does not take into account the radiative and conductive heat loads present in this initial filling period. An initial estimate of the equilibrium heat load on the system was calculated to be 0.4 watts, resulting in a liquid helium usage of about 2 litres per hour. A value of 6 litres/hour was realized experimentally and the difference is believed to be due to an error in estimating the surface emissivity values (assumed 0.1) as well as not having proper radiation shielding on both, the fill tubes and the detector slot. It has been calculated that the detector slot itself is responsible for about 30% of the total radiative heat load and modifications are to be made in the near future, involving the use of a radiation shield attached to the detector probe and rotated with it.

In order to maintain uniform temperatures on all sides of the cavity, the liquid helium vessel was constructed with hollow regions at the top and bottom. To achieve argon partial pressures below 10^{-12} torr it was found that the use of liquid helium vapour at 20°Kelvin was sufficient.

The liquid nitrogen vessel was constructed similarily to the liquid helium tank except that solid OFHC copper thermal conduction members were used both for the top and bottom (Fig. 2.4.5). The calculated temperature distribution on these members indicated that the temperature at the centre was typically about 10 to 20°Kelvin higher than at the actual annular reservoir. Since liquid nitrogen is relatively inexpensive compared to liquid helium, not as much care was taken in making the vessel of light-weight construction. Estimated values for the liquid nitrogen consumption indicated that there would be a boil off of four litres in the cool down stage and a loss of 3 litres/hour under operating conditions. Experimentally measured values and these estimates were not very different.

The top and bottom conduction members make good thermal contact with the annular reservoir through a retaining ring attached by a number of closely spaced bolts on the circumference. This construction allows easy removal of the liquid nitrogen top and bottom for repair on the inner vessel should this be required.

Both vessels are supported by long, small cross-section rods to avoid large heat leaks. The helium vessel is supported from the liquid N_2 vessel ($77^{o}K$) as shown in Fig. 2.4.5 and the latter in turn is supported from the main body of the chamber ($300^{o}K$) as in Fig. 2.4.6. Carefully aligned holes in opposite sides of the pumping cavity allow the beam to enter the molecular trap region and the above supports have degrees of freedom which allow alignment of these holes with respect to the beam axis. A conventional ultra-high vacuum viewing port placed on the beam axis makes it possible to replace the beam source with a point source of light and align the system optically. Further refinements to this alignment are arrived at by positioning the system for the detection of maximum beam signal.

The effect of a 4.2^{o} Kelvin cavity on the temperatures of the detector probe and target was investigated both theoretically and experimentally. Theoretical considerations indicated that heat conduction to these components from their respective supports was sufficient to maintain them nearly at room temperature. Thermocouples both on the detector probe and on the target indi-

cated this to be the case. If there had been any gross change in the temperature of the probe an accurate value of the beam flux could still have been calculated based on the thermal transpiration between the ionization cavity at T_1 and the probe orifice at T_2. Also since the target is supplied with electron-bombardment heating, it is possible to maintain this surface at any desired value of temperature from 25° to 2000°Centigrade. Raising the temperature too high, however, will result in an excessive loss of liquid helium. All the scattering work presented in this paper was performed on a room temperature surface.

The theoretical pumping speed of a cryogenic pump is $3.638\ S(T/M)^{\frac{1}{2}}$ litres/cm^{2}sec, where T is the temperature of the pumping surface and S and M are the sticking coefficient and molecular weight respectively of the gas being trapped. Assuming a sticking coefficient for argon of unity at the finned surface and knowing the projected area to be 1300 cm^2, the pumping speed of the cryotrap is $\simeq$ 10,000 litres/sec at 4.2°Kelvin. A liberal estimate of the leak rate of condensable gases into the trap region from the 10^{-9} torr environment of the scattering chamber, indicates a predicted pressure of about 10^{-12} torr.

The background pressure of the beam gas cannot be calculated on the basis of the above formula since the beam being a one dimensional gas and having direction into the liquid helium cooled walls either before or after reflection, means that the theoretical pumping speed is infinite for a sticking coefficient of unity. This limit, of course, can never be obtained in practice, and as stated previously, background pressures of 5×10^{-12} torr were typically found for helium vapour cooled walls (20°K) when the high energy argon beam was entering the cavity at a flow of 3×10^{-7} torr litres/sec. The use of actual liquid helium (4.2°K) would presumably increase the sticking probability of the energetic argon atoms and result in a lower argon pressure; however, the use of the helium vapour was sufficient in the present work to increase the signal-to-noise ratio of the argon beam signal to argon background to a workable level, at which the remaining noise was due to other causes such as electron multiplier variation.

2.5 Target

2.5.1 Target Surface

A true understanding of the kinetic interactions which occur when a beam of gas particles strikes a target, only becomes a possibility when the atomic arrangement of the surface is known. For this reason a single crystal target of known orientation was used in the present work. Tungsten was chosen for the target material because of the facility with which it can be cleaned in ultrahigh vacuum and because of the large amount of previous work available on adsorption, work function measurements and general surface preparation. For direct comparison with the theoretical interaction models of Oman (Refs. 28 and 29) and Jackson (Ref. 27), a single crystal surface of (100) orientation was used. An important consideration in the choice of a (100) single crystal tungsten surface was its inherent stability (no microfaceting) even after prolonged heating in vacuum (Ref. 47).

The target button (6 mm diameter x 2 mm thick) was spark cut from a zone refined rod of tungsten and mechanically polished using the technique described by Samuels (Ref. 48) and used successfully by Sewell (Ref. 49). The above polishing does work-harden the surface of the crystal to many lattice

layers deep. This is illustrated by the rather large and diffuse reflection spots in the Laue back-reflected x-ray photograph shown in Fig. 2.5.1, taken before high temperature annealing. Figure 2.5.2 is a Laue taken after the crystal was heated repeatedly to 2000°C in an ultrahigh vacuum environment. The spots are much less diffuse in this case, implying that most of the work hardening has been removed. The above photographs were taken employing tungsten white radiation with electron voltages and currents of 25 KV and 20 ma, respectively. Laue photographs taken using higher voltages (40 KV) did not reveal the presence of work-hardening; this is thought to be due to the fact that the more energetic x-rays penetrate deeper into the crystal thus resulting in the Laues being less sensitive to the localized work-hardened region near the surface.

Another result of the polishing technique described above is the presence of polishing marks (scratches) on the surface. These scratches normally disappear for the materials in which there is a high degree of mobility of the surface atoms (e.g., platinum, nickel and iron) at high annealing temperatures (Ref. 49). For the present surface, the tungsten atoms did not display a high enough degree of mobility at the annealing temperature of 2000°C and as a result, traces of the polishing marks remain. Figure 2.5.3 is an optical photograph of the surface in bright field taken at 140 power in which only the deepest scratches are resolved. The estimated width of the scratches is 10^5Å and they cover an estimated 5% of the total surface area. Such a coverage of the surface is not expected to change the reflected distributions considerably since particles reflected from these parts of the surface will be randomly distributed over the entire reflection region and thus add only a small percentage to the signal near the maximum direction.

An optical phase contrast microscope accentuates these polishing marks (Fig. 2.5.4) and as well shows a greater number of features at the surface than for the bright field. It is to be noted that the appearance of the surface is deceiving if interpreted as an ordinary shadow-relief picture. A half wave shift in the vertical direction of 2600Å would result in a variation from maximum brightness to maximum darkness. Thus the worst scratches (those seen in bright field) are less than 2600Å in depth, and a very large percentage of the surface has a height variation considerably less than this, as estimated from the moderate brightness variation. The surface is thus in reality very flat. The ripple-like structure covering most of the surface in between the larger scratch marks represent a waviness in the surface for which it has been estimated that the distance between crests is typically 10^5Å with a roughly estimated depth of several hundred Angstroms. This gentle rolling would not be expected to affect the scattering results to any great degree because from the electron diffraction results (to be discussed), it is concluded that the slopes of these contours are not smooth but stepped in highly ordered (100) flat areas. The effect of this on the molecular scattering is that only about 2% of the molecules could be involved in striking the steps between the order (100) faces. Since the resulting distribution for molecules striking these steps is almost certainly expected to be diffuse and distributed randomly over the entire reflection region above the surface, the distributions found in the present work will not be greatly affected because of their narrowness. The appearance of highly ordered but stepped single crystal faces has also been the finding for similarly constructed surfaces using electron microscope techniques (Ref. 49). The above considerations suggest that a surface which appears relatively featureless in a bright field (ordinary optical microscope) can possess structure which is revealed when viewed with a phase contrast microscope, suggesting that the

former technique should be used with discretion when inferring the smoothness of surfaces.

The optical phase microscope was used to study the surface contour of the crystal. Figure 2.5.5 indicates that the surface was found to be higher at the centre than near the edge as is the common finding for most surfaces polished by grinding. The extent of this surface displacement is such as to result in an angular deviation between the normals to the surface at the centre and at the edge of the crystal of less than 0.006 degrees. Certainly no errors in the experimental results are expected because of this slight curvature.

Reflected high energy electron diffraction techniques (Ref. 49) were used to characterize the surface further*. Figure 2.5.6 illustrates 2 electron reflection patterns taken for two different azimuthal angles before the crystal was installed in the experimental chamber. The history of the surface to this point was as follows: surface mechanically polished to within one degree of the (100) orientation, surface annealed in ultrahigh vacuum at 1150°C for 30 minutes, further anneal to 1150°C in 10^{-6} torr hydrogen and annealed again in ultrahigh vaccum to 1700°C for a total of 20 hours. Electron reflection studies taken at each step in the above procedure indicated that a well constructed surface of (100) orientation was formed after annealing. The exposure to hydrogen resulted in neither an improvementnor a degradation of the surface, indicating that there would be little or no effect when the target was exposed to the relatively low concentration of hydrogen (95% of the total pressure) in the ultrahigh vacuum environment of the scattering chamber. Figure 2.5.7 is from a RHEED study performed after the scattering experiments, during which the surface was exposed to the high bombardment rates of the argon beam and flashed to 2000°C repeatedly (about 30-40 times) both during bombardment and without. At one point a nitrogen beam was used for comparison purposes and the target was also exposed to its high bombardment rate. As indicated by the above RHEED photographs, the crystal still retained its ordered structure and no microfaceting to orientations other than (100) were recorded. Also found from these results was the absence of carbon growth at the surface, implying that the crystal did not contain a high percentage of carbon as impurity. The quoted distributors' carbon concentration was 9 ppm. There was also no evidence that thorium from the retarding field diode filament had contributed to a reconstruction of the surface (see section 2.5.5). This result was anticipated since the thorium emitter was not heated above 1300°K and the evaporation rate at this temperature is low. Equilibrium evaporation data taken from Chapter 10 of Ref. 50 was used to calculate a lower limit on the time required for a monolayer coverage of thorium on the target surface. Such an estimate revealed that it would take of the order of 10 years assuming 10^{14} lattice sites available for adsorption. Estrup et al (Ref. 51) have measured the adsorption of thorium on a (100) single crystal face of tungsten and have concluded that the entire amount of the thorium is removed from such a surface by heating to 1900°C; their LEED studies also indicated that the surface had not changed structurally in any way due to the existence of these atoms at the surface. For a detailed discussion of how to interpret reflection electron diffraction data for infering the presence of microfaceting or carbon growth, the

---

* RHEED work performed by P. Sewell, National Research Council of Canada.

reader is advised to consult Ref. 49.

2.5.2 Target Alignment

An identification of the azimuthal directions in the crystal was made by taking a Laue x-ray photograph and identifying the poles using the method described in Refs. 52 and 53. The identification of these poles also verified that the centre pole was that of the (100) orientation. Figure 2.5.1 is a Laue photograph taken after the crystal was orientated (using previously photographed x-ray diffraction patterns) so that the [010] direction was in the beam detector plane. Figure 2.5.2 is a Laue taken after the experiment was performed, and indicates that the [010] direction has rotated 8-10 degrees from the detector plane. The rotation was ascribed to a deformation of the tungsten support pins (see description in section 2.5.3) upon heating. This misalignment occurred before the experimental data taking and so the entire amount of reflection work is for this orientation. A slight change in the position of the pins was noticed when the crystal was first heated, but a rotation of the amount recorded above was not anticipated. The initial azimuthal orientation was made in order to make easy comparison with the existing theoretical models (Refs. 27, 28 and 29). Jackson has looked at the effect of changing the azimuthal angle from zero to 8 degrees and has found a negligible difference in the position and width of the maximum of the reflected distribution as predicted by his model. Based on this result and on the fact that the experimental distributions are typically 10 degrees wide at 90% of maximum, it is expected that the above misalignment will not affect the results materially.

Figure 2.5.2 was taken after careful optical alignment of the surface normal to within $\frac{1}{2}^{o}$ of the incident x-ray beam direction. The skewness of the pattern affords a good estimate of the degree of misalignment of the (100) crystal direction with the normal to the surface. Using the above technique, the angular deviation between the above two directions has been found to be within 1 - 2 degrees.

The actual position of the crystal once in the scattering chamber was measured in situ (using laser optical techniques) after the tungsten pins had stress relieved. These measurements gave an angle of incidence of $45^{o} \pm 1^{o}$, but revealed that the plane containing the incident beam and the normal to the crystal was about 3^{o} from the detector plane at the angular position of the maximum of the distributions. Again using the same arguments as in the previous paragraph, the width of the experimentally measured distributions is about 10 degrees at 90% of maximum and the above misalignment problem is not expected to affect the results appreciably.

2.5.3 Target Mount

A complete view of the target mast assembly is illustrated in Fig. 2.5.8. The target button is supported by three right angle pins (0.020" diameter) each of which is set in a spark etched hole (0.010" diameter) positioned at 120 degree intervals in the side of the target disc (Fig. 2.5.9). One of these pins is pure tungsten and the other two are tungsten-5% rhenium; two unlike pins paired together form a thermocouple for measuring the target temperature. Figure 2.5.10 is a plot of the temperature profile for heating to $2000^{o}C$. Note that in the cooling portion of the curve that 17 seconds are required for the temperature to reach $120^{o}C$.

The target support pins are mounted on a boron nitride insulator which is in turn mounted on a stainless steel disc which is inserted into a hole in the target mast. Rotation of this disc allows one to set the azimuth angle of the target once the orientation has been found using Laue back-reflection methods (section 2.5.2). A set screw locks the above disc in place once the correct orientation has been located. The mast assembly is mounted on a base which can be raised or lowered by means of a linear feedthrough device in the side of the vacuum chamber. In this manner it is possible to either place the target up into the line-of-sight of the beam or lower it into the main body of the scattering chamber for heating to 2000°C and subsequent cleaning. When the target is intercepting the beam, a baffle on the mast (Figure 2.5.8) reduces the leak rate of the gas coming in from the 10^{-9} torr environment and also the radiative heat load from the room temperature surroundings of the chamber. Provision is made at the base of the holder for varying the angle of incidence of the target, but due to the difficulty of designing target articulation in ultrahigh bakeable vacuum systems, the vacuum has to be broken in order to make this change, or a change in the azimuth angle.

The motion feedthrough device used to move the target in or out of the beam position is an integral part of the target mount and consists of a flexible stainless steel bellows link on the outside of the vacuum chamber allowing a rotation (pivot at point A) of the driving rod (Fig. 2.5.11). A rod located parallel to this main rod and pivoted as well at the vacuum wall (point B) maintains the vertical orientation of the target mast over its entire travel. A small lateral motion ($\frac{1}{2}$" over 4" of vertical travel as designed for the present application) of the mast results from such a design; however, it is straight-forward to determine when the centre of the target is in the detector plane and at the centre of the detector measuring circle. An indicator on the outside of the vacuum chamber allows one to set the required position of the target precisely, and a lock screw retains the desired position.

2.5.4 Target Cleaning

Target heating is accomplished by means of electron bombardment from the back face, and temperatures of 2000°C are easily achieved. Heating to this temperature is the standard procedure in the field of gaseous adsorption (Ref . 54, p.22)and desorption of curves obtained by flash filament techniques for the common gases indicate that heating to the above temperature removes the majority of the adsorbed species (Refs. 55, 56 and 57).

The electron bombardment filament is shown clearly in Fig. 2.5.9. For the instantaneous application of 120 watts of heating it was found to take about 7 seconds to reach 2000°C (see heating curve Figure 2.5.10). As noted previously in section 2.5.3, the cooling portion of this same curve shows that it takes about 17 seconds to return to a surface temperature of 120°C.

2.5.5 Retarding Field Diode

The retarding field diode method for the measurement of the change in surface work function due to the adsorption of a gas on the surface has been frequently used (Refs. 20, 58 and 59) in surface studies. Figure 2.5.12 is a circuit diagram of the diode as it was used in the present work. Such a circuit can be used in two different modes. With the mode switch in position No. 1, the circuit can display the entire i-V characteristic of the diode as shown in Fig. 2.5.13. A sweep voltage from a suitable oscillator supplies the biasing voltage on the anode (target) and is recorded on the x axis of an x-y recorder. The voltage drop across a 2KΩ resistor is supplied to the y-axis and is proportional to the current of the diode. The adsorption of a gas on the surface will cause a shift in the entire characteristic as shown in Fig. 2.5.14 for the adsorption of nitrogen on (100) tungsten. In method No. 2, a specific value of the current is chosen at which to run the diode, and the variation in V_a upon the adsorption of gas is recorded by a Keithley 610B electrometer and displayed on an x-t plot as shown in Fig. 2.5.15. The background gas of the scattering chamber at the time of this particular work function analysis did not contain as large an amount of hydrogen as in the experiments that followed after electron multiplier treatment (section 2.3.4). Consequently the adsorption of nitrogen on the surface is more complete and a larger change in work function (730 mV) is recorded for saturation in nitrogen. This change is relatively close to the work function change (650 mV) recorded by Estrup and Anderson (Ref. 67) for a clean tungsten (100) surface. Results obtained for the adsorption of nitrogen on a hydrogen saturated surface will be discussed later in Section 3.1.3. The controlling equations for the circuit as derived in Ref. 20, are listed in Fig. 2.5.12. Note that when the temperature of the cathode is held constant (i.e. current i_a = constant) and $V_L \gg kT/e$, any change in the anode voltage is recorded by the electrometer and is equal to the change in the surface work function and this is generally true for any diode provided $i_a = f(\phi_a - V_a)$. A further advantage is the independence of variations in the cathode work function (Ref. 60) on the measurements. The method as described above has been found to be sensitive to a fraction (1/100)of a monolayer coverage making it ideally suited to its present function in this work. The DC millivoltmeter in Fig. 2.5.12 is used to record the target temperature (thermocouple output) during the cleaning period. The TC record position is for the use of a more accurate meter (higher input impedance) for measuring this temperature. A calibration of the DC millivoltmeter was made against a Keithley voltmeter (input impedance $\simeq 10^6\Omega$) at the lower temperatures (up to as high an electron bombardment voltage as the Keithley 610B could be floated).

The retarding field diode filament is mounted in front of the crystal in a plane parallel to the incident plane but displaced from it by a small distance 2 mm. This has been done to allow the beam to impinge on the surface with no interference from this 0.005" wire; a negligible number of reflected particles have their trajectories affected by the presence of the wire. To reduce the chemical conversion of gases at the hot filament to a negligible level, the retarding field diode filament was catephoretically coated with a layer of pure thorium oxide to allow the same yield of electrons at a lower temperature than that of a pure tungsten filament. Also, the deposited thorium oxide was localized near the centre of the filament in order to avoid the false indication of target work function change that could result if the target mount and its structure were involved.

3. RESULTS

3.1 Background Gas Environmental Study

3.1.1 Mass Spectral Analysis

A mass spectral analysis of the background gas in the molecular beam scattering chamber was performed using a GE 22PT121 mass spectrograph. Figure 3.1.1 is a mass spectrum over the total mass scan from 2 to 70 amu of residual gas without the use of cryopumping in the scattering chamber. The use of the 3 kilogauss permanent magnet did not allow higher mass numbers to be focussed and the control on the ion focussing voltage did not extend high enough to obtain the mass 1 amu (H atom) peak. Figure 3.1.2 is an enlarged mass spectra from 12 to 70 amu in which it is possible to distinguish some of the lower intensity peaks.

The relationship of the above mass spectrum to actual partial pressures existing in the scattering chamber is not straightforward since the mass spectrometer is essentially in a closed volume except for a 1 litre/sec conductance (through the orifice) to the 10^{-9} torr region of the scattering chamber. It has been found that outgassing products from the walls of the gauge interior take between 1 - 2 hours to achieve their equilibrium pressure levels after the filament of the detector has been turned on. All peaks (including H_2) decrease in approximately the same ratio except for mass 16.33 amu which remains relatively constant throughout the filament outgassing operation. The presence of this non-integral satellite peak of 16 amu is a common occurrence in mass spectra taken using a single-focussing mass spectrometer and has been discussed by Robins (Ref. 61). It is due to the electronic desorption of oxygen atoms from their adsorbed phase on the ion source electrodes. Such desorbed atoms possess a kinetic energy of about 6 eV in addition to the focussing voltage and are focussed at a different point on the spectrum. Applying the standard cracking ratios one finds the presence of water vapour, ammonia, methane, carbon dioxide, oxygen, nitrogen and carbon monoxide. A quantitative analysis on the amount of each of these gases has not been performed since the large outgassing source within the gauge volume itself has masked the actual situation existing in the main body of the scattering chamber. The use of cryopumping in the region surrounding the gauge orifice had very little effect on the mass spectra. A 10% decrease in peak height was recorded for mass 28 when cryopumping was added, implying that the dector was in part sensing the environment outside the gauge volume. The failure for even liquid nitrogen pumping to remove water vapour was indicative that this peak was due to an outgassing phenomenon within the gauge volume. Qualitatively the data suggest that the prime gaseous components in the scattering system are hydrogen, nitrogen and carbon monoxide in order of decreasing concentration. The hydrogen was found to account for 80 to 90% of the total pressure, with the majority of the remaining gas being nitrogen and carbon monoxide. The retarding field diode results of Section 3.1.3 support the above inferences. Note that the argon peak at 40 amu is of significant abundance, contrary to the levels observed in most bakeable stainless steel systems of this type. This is due to the fact that the system had experienced a large amount of argon pumping and ion pumps are known to have a "memory" for the inert gases (Ref. 62); that is to say that continuous pumping of other gases after exposure to argon will result in re-evolution of the latter. When liquid helium cryopumping was employed in the region surrounding the detector, the argon pressure level within the gauge volume fell quickly to a new low level ($\approx 10^{-12}$ torr) because of the weak adsorption (physisorption) of argon on the room temperature surfaces within the detector volume. This very low pressure level in argon allowed the detection of the reflected beam since reflected flux signal levels were typically 10 times this value. It is not possible with the

present system to detect a beam composed of a gas having a long outgassing time constant in the gauge volume.

An increase in the total pressure ($\Delta P_{tot} \simeq 3 \times 10^{-9}$ torr) was recorded in the scattering chamber when the isolation valve (in bellows link section, Fig. 2.2.1) at the collimation chamber was opened. A study of the mass spectrum indicated that the only peak which increased after opening this valve was hydrogen. The re-emission effects found by Rozgonyi (Ref. 63) and verified by this experiment, suggest that this rise in hydrogen may be due to an evolution from the pump and the chamber walls upon the admittance of a gas with a higher mass such as typically found in the diffusion pump environment as discussed in Section 2.2.3. In the present system, nitrogen and argon have both been shown to cause large increases in the ambient hydrogen pressure when admitted. Evolution of carbon monoxide has also been observed upon the addition of nitrogen. The interplay between gases makes it difficult to calibrate the mass spectrometer against total pressure changes recorded by the Bayard-Alpert ionization gauge when such gases are admitted. Hydrogen was not found to be effective in re-emitting other gases. Masses 36 and 38 amu have been observed by Rozgonyi to appear upon the addition of argon to an ion pumped system; this was also observed in the present system, as well as an increase in mass 28 and hydrogen.

3.1.2 Flash Desorption Results

The time required for saturation of hydrogen at the surface was determined by flashing the target to 2000°C at time zero and then allowing the gas from the scattering chamber (no cryopumping) to adsorb for a time "t"; the target was then flashed again to 2000°C and the peak height growth recorded as proportional to the amount of gas adsorbed. Figure 3.1.3 is a plot of the hydrogen gas coverage as a function of time after flash for both a polycrystalline (electron bombardment filament) tungsten surface and the target (tungsten (100) single crystal). The first result is that the saturation time for hydrogen is reached more rapidly for the single crystal than for the polycrystalline tungsten. This corroborates the comparison between the results obtained with single crystals by Estrup and Anderson (Ref. 64) and those obtained with polycrystalline tungsten reported in Ref. 65. The second result is that a replacement phenomena involving carbon monoxide (Ref. 66) is occurring which tends to deplete the quantity of hydrogen at the surface after several minutes. Included in Fig. 3.1.3 is the curve for the amount of mass 28 on the polycrystalline tungsten surface versus the adsorption time. The saturation level has been obtained from data taken out to several hours in which it has been found that a leveling off to saturation begins to occur after 3 hours. An estimate of the time required for saturation was then made, and the data plotted in Fig. 3.1.3 with a normalization to unity as for the case of the hydrogen curves.

The results of section 3.1.3 (to be discussed) verify that replacement of the hydrogen by carbon monoxide is occurring at the surface, but that concurrent with this replacement is an adsorption of nitrogen in the vacant lattice sites left by the hydrogen. It suffices to say here that the replacement process is more complex than anticipated from the results of this section and that the growth of the mass 28 peak is due to adsorption of both nitrogen and carbon monoxide.

3.1.3 Retarding Field Diode Results

Background Gas Analysis

The retarding field diode method, as discussed in Section 2.5.5, was used to infer the amount of gas coverage at the surface. In a background gas analysis of the scattering chamber (no cryopumping, no beam entering the chamber) the work function change recorded as a function of time after flashing was first negative then positive (curve A, Fig. 3.1.4). By admitting nitrogen gas to the system ($\Delta P_{N_2} \simeq 1 \times 10^{-8}$ torr), curve B was obtained. It appears from the latter curve that we have accelerated the adsorption process for two different gases. Liquid nitrogen pumping was then used and the result was a depletion of the gas causing the positive change. A gas which is pumped readily by liquid nitrogen and gives a positive change in work function (Ref. 66) and is a prime constituent in the background gas is carbon monoxide. Adding liquid helium pumping removed the negative variation as well (see Fig. 3.1.4), implying that this gas was nitrogen since Estrup and Anderson (Ref. 67) have found nitrogen to give a negative change on (100) tungsten. In testing the effect on the work function of the large amount of hydrogen gas present in the system, the diode level showed no change upon adding greater amounts ($\Delta P_{H_2} \simeq 10^{-8}$ torr). This implies that saturation in hydrogen is indeed reached rapidly as suggested by the data of the flash filament desorption study (Section 3.1.2). A thermal effect which exists after the target is flashed (typically of 2 minutes duration) masks the changes in work function due to gas adsorption during this interval. Figure 3.1.4 is thus a variation in the work function after thermal effects have become negligible and necessarily after hydrogen saturation has taken place.

The complex situation created by the simultaneous adsorption of three gases at the surface prevents a quantitative comparison with the work of Estrup and Anderson. The subsequent adsorption of nitrogen on a polycrystalline tungsten surface which has been saturated with hydrogen has been studied by Rigby (Ref. 68) in which he has found that 20% of the surface remains available for nitrogen adsorption. Assuming this to be the case for (100) tungsten and using the work function change corresponding to nitrogen saturation ($\Delta\phi$ = - 650 mv) as found by Estrup and Anderson, the change expected in the present case would be 130 mv. Curve B (obtained with liquid nitrogen pumping) of Fig. 3.1.4 shows that the saturation level for nitrogen is close to this value. The adsorption of the carbon monoxide is a complex problem in the present situation since replacement of the hydrogen can occur, as found in the studies of Robins (Ref. 69) and Rigby (Ref. 68). Rigby has also shown in another study (Ref. 70) that carbon monoxide can adsorb appreciably on a nitrogen saturated polycrystalline tungsten surface and the same result has also been observed by Estrup and Anderson (Ref. 67) for (100) tungsten. The change in work function for CO adsorption on clean (100) tungsten found by Estrup and Anderson is + 430 mv. Curve B (nitrogen gas admitted) of Fig. 3.1.4 shows that, for the present work, the change with CO is about of this magnitude. Note that, in adding nitrogen to the system, the amount of CO increased due to re-emission from the ion pump. A mass spectral analysis (Section 3.1.1) indicated that hydrogen was also evolved upon admitting nitrogen thus assuring that a saturation level in hydrogen was reached even more rapidly. The effects on the argon beam scattering results of this saturation level of hydrogen will be discussed in Section 3.2.2.

Beam Analysis

A check on the impurity level in the beam was made under normal reflected flux measuring conditions. Liquid helium vapour pumping in the region

surrounding the target prevented contamination of the target by nitrogen, carbon monoxide and any other background gas condensable at 20°K. The only gases not pumped were hydrogen (main constituent in the background) and helium (molecular beam seed gas). Helium is not expected to affect the gas-surface interaction since it is an inert gas and does not physisorb appreciably on a room temperature surface. The effect of the hydrogen on the scattered flux distribution will be discussed in Section 3.2.2.

Figure 3.1.5 illustrates the change in the work function which occurs when an argon beam at 0.25 eV is incident on the surface. A slight change (1/50 of nitrogen saturation) in the work function after 20 minutes is in the negative direction and suggests that there is a nitrogen contaminant in the beam and/or the hydrogen is being removed by the impinging beam particles. The bombardment rate of the hydrogen gas on the target surface from the background pressure environment of the scattering chamber ($P_{H_2} \simeq 6 \times 10^{-9}$ torr) was calculated to be 10^{13} hydrogen molecules/cm^{2}sec. This is a bombardment rate not much different from that of the beam and so it is unlikely that the beam will be effective in removing the adsorbed hydrogen. The slight change in the work function for the argon beam on the surface is thus believed to be due to a nitrogen contaminant in the beam possibly due to an air leak in the gas supply line. The target was flashed to 2000°C every 20 minutes during the course of a scattering experiment to remove any possible effect of this slight adsorption.

The change in work function for a nitrogen beam formed by the same source conditions as for the argon beam but of energy 0.18 eV, is also shown in the above figure. Under these conditions the hydrogen covered surface reaches saturation ($\simeq$ 100 mv) in nitrogen in about 30 minutes. With a typical flux of 5×10^{13} nitrogen molecules/cm^{2}sec (typically measured for a pure nitrogen beam) at the surface, the sticking probability of 0.18 eV nitrogen on clean (100) tungsten is estimated to be 0.001. This has been calculated following the assumption that the nitrogen adsorbs only on 20% of the surface covered in hydrogen and that 4×10^{14} lattice sites/cm^2 are available for adsorption in the clean state (from Estrup and Anderson, Ref. 67 and corroborated in this experiment). The sticking probability quoted by the above workers for the adsorption of 300°K nitrogen on clean (100) tungsten is 0.55. To the best of the author's knowledge an estimate of the sticking probability of a beam at this energy on any surface has not been reported to date.

3.2 Scattering Results

3.2.1 Determination of Beam Properties and Scattered Flux Intensities

Molecular beam source conditions for a particular mixture ratio and stagnation temperature were set by a sequence of steps, from which the beam velocity was inferred. First, the source conditions were set with the beam source temperature at room value and with the maximum source flow condition (restricted by the pumping throughput of the pumping system). In particular, it was the second stage of pumping (collimation chamber) which was limited, since 200 microns in the backing line of the 32,000 litre/sec diffusion pump was the maximum pressure permissible. The mass flow through the source is proportional to $P_o/(T_o)^{\frac{1}{2}} d_*^2$ where P_o is the source stagnation pressure, T_o the source temperature and d_* the effective diameter of the source. For a required argon beam energy a plot such as in Fig. 3.2.1 (derived from the equations for a seeded nozzle beam (Ref. 36)) permits choosing a mixture and source temperature to obtain this energy. This mix-

ture was then set on the flow meters provided on the gas supply line to the beam source and each component of flow increased (with the source at room temperature) until the pumping limitation was reached. The pressure at this point ($P_{o_{RT}}$) was recorded along with the room temperature value ($T_{o_{RT}}$). The source was then heated maintaining the flows for the two gas species (seed and carrier gases) constant until P_{o_H} was reached as determined by the quantity $P_{o_{RT}} (T_{o_H}/T_{o_{RT}})^{\frac{1}{2}}(d_{*_{RT}}/d_{*_H})^2$. At this point it is known that the a priori determined value of the temperature T_{o_H} has been reached. The ratio $(d_{*_{RT}}/d_{*_H})^2$ has been determined by Davis (Ref. 39) through Reynolds number considerations and is 1.0147 for $T_{o_H} = 1000^oK$. This was the highest temperature used throughout these runs since higher temperatures evolved considerable quantities of contaminants from the oven to cause the impurity level of the beam to be in doubt. The measurement of P_o was made on a Heise gauge of sufficient accuracy to allow a determination of the temperature to within 5%. The use of calculated values of energy such as those plotted in Fig. 3.2.1 has been discussed in Section 2.1 and as stated there, there is evidence available in the literature to show that the calculation of velocities and energies from source values introduces very little error (< 5%) provided certain conditions are met at the skimming position in the free jet. The beam system was operated well outside the conditions causing appreciable slip between seed and carrier gases or serious skimmer interference with its attendant wide velocity distributions. Figure 3.2.2 is a plot of the molecular beam velocity determined by the same procedure as for the energy. For a satellite, the orbital velocity is typically 8×10^5 cm/sec, while the maximum velocity of argon achieved with the present source conditions ($T_o = 1000^oK$, 1%A-99%He) is about one third of this value.

At the start of a run the scattered flux detector was rotated into the incident beam position and the target retracted, allowing the incident beam to enter the detector directly. The geometry was such that the detector orifice (0.3 cm diameter) was larger than the beam size (0.2 cm diameter) resulting in the detector "swallowing" the incident beam completely. In the equilibrium situation (flux into detector = flux out of detector) this means that the flux incident into the detector is $\frac{1}{4}n\bar{c}\, A_{det}/A_{beam}$ where "n" is the number density in the detector caused by the stagnated beam, "$\bar{c}$" is the mean molecular velocity of the stagnated gas and A_{det} and A_{beam} are the detector orifice and beam areas respectively. In principle, the absolute value of the incident beam flux could be calculated from this expression if the mass spectrometer calibration required to link the peak height to the density "n" were known. However, it became obvious that with the re-emission problems (Section 3.1.1) encountered with the ion pump, that a change in total density as recorded by the Bayard-Alpert gauge (which acts as a secondary reference standard when calibrated at higher pressures against a McLeod gauge) could be due to a large percentage of gas other than the beam gas. An absolute flux calibration was obtained by measuring the Bayard-Alpert pressure rise when argon was admitted to the system, and recording the large increase in the hydrogen which evolved due to re-emission from the pump. Even under conditions in which a large amount of argon ($\simeq 10^{-8}$ torr) was admitted to the system, the increase in the amount of hydrogen was large enough to still account for 90 to 95% of the total pressure. Based on this fact, the mass spectrometer output was calibrated for hydrogen and the sensitivity (amps/torr) calculated for argon by using the appropriate ionization cross-sections available in Ref. 71. Secondary electron ejection probabilities of a silver-magnesium surface for hydrogen and argon ion bombardment do not differ appreciably at 2kV (the potential supplied to the first dynode of the electron multiplier) as shown by Ref. 72 and thus this correction was not included. Incident flux measurements made using the above method were typically 10^{13} to 10^{14} argon atoms/cm^{2}sec depending on the source conditions used.

With the difficulty of obtaining absolute flux levels in the present system the following procedure, when measuring scattered number flux distributions, was adopted. The argon peak height (in amperes) due to stagnation of the incident beam was recorded before and after the experimental run. This value (corrected for the fact that the detector "swallowed" the incident beam entirely) was used to normalize the reflected signals (peak heights also proportional to flux) found as the detector was rotated about the target. The result was a normalized flux (I_R/I_o) which when combined with the known dimensions of the detection system (distance of detector orifice from the target = 9.6 cm, incident beam diameter = 0.2 cm) gives the probability of being scattered into the given angular direction. The ratio of the number of particles per second per steradian (ψ) reflected at the angle θ_R to the total flow incident (N_o) is obtained from the expression $\psi/N_o = 2.94 \times 10^3 I_R/I_o$. For convenience this conversion is included at the bottom of each figure displaying scattered number flux distributions. It is noted that most previous work display flux and in-flight number density distributions in arbitrary units, making it difficult to compare, for example, the trends in peak intensity with energy to a given theory. The present method of plotting should be much more convenient for this purpose. For a typical experiment (1 to 2 hours duration) the two values of I_o before and after a run usually remained within 10% of each other.

When a run was to be performed, the beam was let into the scattering chamber and allowed to strike the target. The detector was first positioned behind the target and thus sensed any increase in argon background pressure due to the beam. Helium vapour at 20°K was then let into the dewar surrounding the target and the argon background pressure (peak height) monitored as pumping began. Once the partial pressure level of argon reached a value which was 1/10th or less of the expected reflected signal level, the target was removed from the dewar, flashed several times in the 10^{-9} torr environment of the ion pump, then heated for 10 minutes at 1500°C in the same environment, and then raised while still hot into the dewar and the beam. It was then allowed to cool in the contaminant free (except for hydrogen) environment of the cryopump. The reason for keeping the target hot while raising the target into the dewar was to try and prevent possible contamination from the nitrogen and carbon monoxide gases outside the cryopumped region. Before the measurements were begun, the target was once again flashed to 2000°C and then allowed to cool. The target was also flashed to 2000°C in the cryopumped region every 20 minutes during the course of an experiment. No discernible change was noticed in the argon background ($< 10^{-12}$ torr) of the cryopump region when the target was flashed once; however, 4 or 5 flashes in succession caused an appreciable change, but pump-down to the original pressure level was rapid after cesation of the last flash.

When a flux distribution was measured, 30 or more points on the distribution both in the clockwise direction of detector rotation and in the counterclockwise direction were taken. Agreement between points taken in one or the other direction was good, with about the same amount of scatter for each as found for successive points and attributed to electronic noise in the electron multiplier. At various times during the measurements, surface and beam conditions were repeated and corresponding reflected distributions obtained; results were found to be quite reproducible.

The manner of recording the scattered flux distribution was to move the detector to the desired measuring position (usually in 5 degree increments) and record the reflected signal (peak height of argon) at the position for several sweeps of the ion focussing voltage. It was not possible to position the instru-

ment on the peak maximum and record a DC readout with detector position since the stability of the high voltage supply provided with the detector was not adequate. It is believed that the use of a stable high voltage supply would accomplish this and make data taking much easier. This is therefore a recommended modification to be made on the present system.

By sweeping the ion focussing voltage over several volts and recording the argon peak height repeatedly, it became obvious that some type of electronic noise was causing the peak height to change by about 5%. This was attributed to either electronic noise within the electron multiplier or charging effects on the ion focussing lens due to gaseous contamination. The procedure was to take several of these peak heights and average; this is the quantity which is plotted on the ordinate of the scattered flux distributions after normalization by the incident flux. Note that the electronic noise problem was not recorded in the case of the incident flux since signal levels were of the order of 10^4 times greater than for the reflected flux. The residual background current of the electron multiplier increased slowly throughout the experimental runs due to contamination in the multiplier region. Accompanying this residual current increase was an increase in the electronic noise level, making it difficult to obtain accurate readings of the scattered number fluxes. When this noise level became significant (usually a month after reactivation), the multiplier was reactivated with hydrogen employing the technique discussed in Section 2.3.4. This was done several times without detrimental effect to the multiplier. A slight decrease in the multiplier gain was observed over the same period of time, but was not a severe limitation on the measurements. For a particular experimental run (running time 1 - 2 hours) the condition of the multiplier remained relatively unchanged.

Another limitation which made itself manifest was the fact that the CO_2 peak at 44 amu was a large outgassing product in the mass spectrometer which could not be removed by the liquid helium pumping in the region surrounding the target. The presence of this peak adjacent to mass 40 meant that the sweep time had to be long in order to resolve the two peaks. The result was that a fast scan over only the mass 40 peak with the detector moving simultaneously was not a possibility, and data had to be taken point-by-point as described above. The removal of the CO_2 by baking the mass spectrometer to 300°C by means of the small oven surrounding the ionization and electron multiplier regions was unsuccessful.

In the sections to follow, the experimentally measured scattered flux distributions will be discussed in detail. Results have been obtained for an argon beam at 45 degrees incidence and under varying conditions of gas surface coverage and incident beam energy. A room temperature surface was maintained throughout the flux measurements, as determined by a thermocouple attached to the target edge.

3.2.2 The Effect of Gaseous Monolayers on the Scattered Number Flux Distribution

The effect of gaseous monolayers on the scattered number flux distribution for a 1.35 eV incident argon beam is shown in Fig. 3.2.3. Run No. 3 (the cleanest state) was obtained by making sure that the residual gases (mainly CO and N_2) from the 10^{-9} torr region of the ion pump did not adsorb appreciably at the surface. This state was achieved by raising the target hot (1500°C) into the low-contaminant region of the cryopump and flashing to 2000°C when up in this region. From previous evidence the surface was then free of all gases except a saturation coverage of hydrogen. There is direct evidence that the presence of this saturation level in hydrogen (which was verified by the flash desorption

experiments and retarding field diode tests) does not change the shape or position of the maximum of the distribution from that obtained with a completely gas-free surface. This important and somewhat surprising result was obtained by heating the target to 2000°C and monitoring simultaneously the reflected flux at several parts on the distribution including the maximum position. Not only did the adsorption of the hydrogen have no effect on the distributions, but also the variation in target temperature between 2000°C and room temperature had no effect at these beam energies. These studies were performed for all the distributions measured and with the same result. It is suggested that the former result is due to the facility with which hydrogen adatoms are moved from one site to another on the surface. Rideal and Sweett (Ref. 73) have measured the activation energy for the migration of hydrogen adatoms on a saturated nickel surface and have found under such conditions, that 88% of the adsorbed particles are highly mobile with an activation energy for surface migration of 0.02eV. On the other hand, the energy required to break the chemical bond (desorption energy) for hydrogen atoms on such a saturated surface has been found to be 0.2 eV by the same workers. (The often-quoted value for the desorption energy of a hydrogen atom in a dilute layer on a tungsten adsorbent is 2-3eV compared to 0.7 eV for the activation energy for migration (Ref. 74).). Since the conditions of the present experiment are closely related to the saturated levels used by Rideal and Sweett, it is likely that the low value of 0.02 eV for the activation energy of migration will prevail. It seems likely that energetic particles such as are employed in this experiment would be effective in moving the adsorbed hydrogen from the collision site. Using a typical bombardment rate of the beam on the surface (10^{14} particles/cm^{2}sec), it has been calculated that every lattice site is struck once per second, thus allowing the surface to recover from one collision in time for another. Thus it is suggested that hydrogen adatoms are moved from one site to another without the surface becoming depleted in hydrogen. There is also evidence from the work of Datz et al (Ref. 15) that a saturation level of hydrogen on a platinum surface did not affect the reflection of either helium or deuterium. (Adsorbed oxygen had a marked effect, to the extent that it rendered the scattered distribution to that of a cosine-law reflection.)

The fact that the results were not affected by the increase in the surface temperature is most likely due to the fact that at these beam energy levels the effect of thermal motion of the lattice on the scattering is not very important (i.e. the ratio of thermal agitation velocities in the lattice to beam velocities at these relatively high beam energies is quite small). The "hard" cube model (Section 3.2.5), which depends totally on the effect of the thermal motion of the lattice to produce spreading of the reflected particle trajectories, will verify that thermal velocities cannot be important. The surface was not heated continuously during a run since the increased radiative heat load on the liquid helium consumption would be intolerable. Instead, temperature effects were studied by flashing the target to 2000°C for 15 seconds and then allowing the temperature to fall back to room value (Sec. 3.2.1).

Run No. 6 of Fig. 3.2.3 was obtained for a partial coverage of carbon monoxide and nitrogen on the hydrogen-covered surface. This partial coverage was obtained by allowing the target to remain in the 10^{-9} torr environment of the scattering chamber for 30 minutes before raising it into the cryopumped region. Because of the interactions taking place between the adsorbing gases, it is difficult to say exactly how much nitrogen and carbon monoxide has adsorbed, as well as how much hydrogen has been desorbed. Run No. 4 was obtained by allowing the background gases in the scattering chamber to adsorb on the surface over a period of 3 days. Robins and Rigby (Refs. 69 and 70) have found that after a

period of hours that only 30% of the surface remains covered in hydrogen after exposure to carbon monoxide and that a large amount of carbon monoxide can adsorb in this same time interval on a surface already covered in nitrogen. In view of these results, the state of the surface for run No. 4 is believed to almost be entirely covered in carbon monoxide with a small quantity of hydrogen and nitrogen still remaining. It is interesting to note that carbon monoxide is immobile at the surface (Ref. 74) and thus the beam is not expected to be effective in removing it from the bombardment site since it takes about 4 eV to desorb it.

It can be seen from Figure 3.2.3 that the addition of relatively small quantities of the adsorbed species CO and N_2 does not affect the position of the maximum greatly; however, there are fewer atoms scattered in the direction of the maximum reflected flux and more scattered back into the incoming beam quadrant (backscattered direction). Adding a large percentage of CO to the surface (Run No. 4) had the effect of both widening the distribution as for Run No. 6, but also shifting the maximum towards the surface. This shift towards the surface can be understood if the reflection process is, to the first order, governed by the mechanics of simple binary collisions between the gas atom and one surface atom. When the lighter adsorbent atoms become the collision partner, the resulting leaving vector for the reflected argon will be still further below the specular angle. In fact, Jackson's model (Ref. 27), which includes hard sphere scattering, an attractive potential, and multiple collisions with several surface atoms when these occur, suggests that under the present experimental conditions that the majority of the molecules are reflected after only one collision. The model, for increasing mass ratio of gas to surface atom, predicts a shift in the distribution maximum towards the surface as found here experimentally. Although the addition of an adsorbed gaseous layer onto a surface is not strictly equivalent to changing the mass ratio, it is believed that the trend predicted will be the same. This shift in the maximum (due to gas coverage) towards the surface is contrary to the trend found at the lower energies (Refs. 7 and 15).

An important result of Fig. 3.2.3 is that at no time, even under conditions of extreme surface contamination (Run No. 4), did the form of the distribution follow the cosine law. A cosine distribution calculated from the incident beam flow for these experiments and normalized on the same scale as Figure 3.2.3 would have a maximum value of $I_R/I_o \times 10^4 \simeq 1$ at θ_R = zero degrees. An estimate of the number of argon atoms contained in the central peak of the distribution for Run No. 3 of Fig. 3.2.3 was made by considering the distribution to be a body of revolution about the maximum position and symmetric for 20 degrees on either side of maximum. The normalized flux scale on the ordinate was converted to the number of argon atoms/sec striking the detector position at angle θ_R divided by the total incident flow. By dividing the distribution into 2 degree segments and weighing the signal at the centre of each by the corresponding angle, 70% of the incident particles were accounted for. As suggested by Jackson's theoretical considerations, most of the reflected particles in this relatively narrow distribution have velocities resulting from binary collisions at the surface and hence are very incompletely accommodated.

Figure 3.2.4 presents similar results to those in Fig. 3.2.3 except for a lower incident argon beam energy (0.25 eV). The same general behaviour is noted for partial coverages of carbon monoxide and nitrogen, with very little shift in the maximum, but a reduction of the signal at this position and an increase in the backscattered direction.

3.2.3 The Effect of Incident Beam Energy on the Scattered Number Flux Distributions

Figure 3.2.5 is a plot of the scattered number flux distribution showing the effect of incident beam energy, for partial coverage in CO and N_2 on a hydrogen saturated surface. There is very little shift in the maximum position with increasing energy and the tendency is for the higher energy distributions to be narrower. In becoming narrower, there is an increase in the signal near maximum and a reduction in the backscattered direction.

Figure 3.2.6 is a similar study to that of Fig. 3.2.5 except for a surface condition of hydrogen saturation only. As discussed previously in Sec. 3.2.2 this represents the cleanest state achievable in the present system for a room temperature target, and the experimental results showed that this state is equivalent to a gas free tungsten surface in so far as scattering of high energy argon is concerned. The trend with energy is identical to that found in the case where there was partial coverage of CO and N_2, except that the distributions are narrower and the signal at the maximum position is significantly greater. Figure 3.2.7 illustrates the variation of this maximum signal with incident beam energy.

One will notice that Run No. 2 of Fig. 3.2.6 has considerably more scatter in it than any of the other distributions measured. This scatter arose from an electrical noise problem in the electron multiplier which could not be rectified by means of the hydrogen treatment discussed in Sec. 2.3.4. It was thought that possibly this data (taken for the cleanest surface state) was displaying some structure near the maximum, but the above noise problem prevented any definite verification of this. It is hoped that replacement of the multiplier and improved baking of the detector gauge volume will result in clarification of this speculative point. For the present results, a smooth curve has been drawn through the points; it was not believed that usual curve fitting procedures were warranted for this one distribution.

3.2.4 Comparison with Existing Experimental Lower Energy Work

Figure 3.2.8 is a comparison of the scattered number flux distribution obtained in the present work using a 0.25 eV incident beam, with that found by Hinchen et al (Ref. 18) for 0.15 eV incident argon on a (110) platinum surface. This is the best comparison with lower energy work available since both experiments were performed for the same angle of incidence and surface temperature. Also, both experiments have used a single crystal surface and the ratios of the gas particle mass to the surface atom mass are almost identical. Comparison has been made by making the peak heights the same.

From the comparison between the two results of Fig. 3.2.8 it is found that the present distribution does not lie as far below the specular angle and is narrower. The use of a monoenergetic beam in the present experiment, on such well cleaned surfaces as described, would suggest the opposite to that observed in the comparison. The reason for the discrepancy is believed to be due to the following: Hinchen et al have used a chopped beam system with lock-in narrow band-pass amplification and phase sensitive detection to measure the in-flight number density of the reflected beam. The technique is to adjust the phase of the detector along each reflection direction until the signal is a maximum. The resulting signals contain no information about those molecules which have no coherence with the initial modulation such as those trapped at the surface for appreciable times, or those with widely different velocities from the mean for that direction. The present detector on the other hand, since it measures

the total reflected number flux in each direction, will detect all re-emitted particles including those trapped at the surface and re-emitted later. Thus it is expected that the distributions measured in this manner will differ from those using the modulation technique. The fact that the discrepancy is largest in the backscattered direction is consistent with the idea that the velocity distribution in this direction is much broader (i.e. the accommodation is more complete). Interpreted in this manner, the discrepancy lends support to the variation in mean velocity with scattering direction found by Hinchen et al (Ref. 1) where the mean velocity was found to be greatest along the surface and least in the direction of the surface normal.

Figure 3.2.9 presents a plot of the deviation of the position of the distribution maximum from the specular position ($\theta_i - \theta_{max}$) as a function of the normalized beam energy ($E_{beam}/k\ T_s$), where T_s is the surface temperature and k is the Boltzmann constant. The normalization is a convenient way of comparing the present room temperature results with the widely varying surface temperature results of previously performed lower energy experiments. In some cases it was necessary to heat the surface in order to assure cleaner surfaces and in others (Notably Refs. B, C and D) elevated temperatures were used to obtain epitaxial single crystal growth when vapour depositing the surface films. The lower energy points display considerable scattering, suggesting differences in the actual surface conditions used. Present results show a smooth extension to slightly more negative $\theta_i - \theta_{max}$ values at the higher beam energies, with considerably less scatter in the data points. Note that the position of the maximum for these higher energy results is not very different whether measured for a "clean" surface state (H_2 covered) or with partial coverage of carbon monoxide and nitrogen. The data point for the one distribution taken for large coverage in carbon monoxide is displaced appreciably from the rest of the data in the higher energy range. In Section 3.2.2 the displacement of the maximum towards the surface for this one experimental run was discussed in detail, with the conclusion that the mechanics of the interaction was controlled primarily by binary collisions between the incoming beam particles and the surface atoms. A study of the position of the distribution maximum for argon on platinum was obtained by Hichen et al (Ref. 18) and is included on this same plot and shows that they have obtained distribution maxima closer to the surface for the lower energies than those found with the higher energy beams of these experiments. As suggested by the data of the present work, their distribution maxima may lie lower due to the presence of surface gas coverage. A discussion of the theoretical curves plotted in Fig. 3.2.9 will follow in Section 3.2.5.

Figure 3.2.10 shows a plot of the width at one half maximum of the distribution ($\Delta\theta_{\frac{1}{2}}$) for various gas-surface combinations as a function of normalized beam energy^2 ($E_{beam}/k\ T_s$). The width at one half maximum is a rough measure of the narrowness or broadness of a scatter pattern. For a particular surface state, the present results show a definite trend with increasing energy, i.e. the distribution becomes wider with decreasing energy. The effect of adding gaseous monolayers to the surface is also to widen the distribution but notice that the highest energies are least affected. The lower energy work appears to be an extension of the results of the cleanest state found in the present work although there is considerably more scatter. Part of the variation is due to the fact that a variety of surfaces were used in the correlation, and part of it may be due to unspecified variation in the surface condition. Oman (Ref. 29) has suggested from his theoretical considerations that the width of the distribution may be expected to decrease with increasing energy up to a point and then become

wider again due to significant overlapping of the potential fields of the incident particles and the surface atoms. The results of this experiment indicate that the minimum-width point has not been reached up to the energies achieved (2 eV).

3.2.5 Comparison with the "Hard" Cube Model

A comparison of the present experimental results with the predictions of the "hard" cube model (Ref. 30) was made, and as shown in Fig. 3.2.9, the agreement between the position of the maximum as predicted by the theory and these experiments is good. Due to the simplicity of the model and its failure to predict other aspects of the gas-surface interaction problem, such as the reflected velocity distribution, the above agreement may be to some extent fortuitous. However, it may be that the position of the maximum of the distribution is controlled primarily by the mechanics of a single binary collision between incoming gas particle and surface atom. There is evidence from Jackson's work (Ref. 27) that under the present experimental conditions, that the majority of particles (70 - 80%) do reflect in this manner. Further, the flat surface elements used in the "hard" cube model, to some extent, average out the directional scattering that the actual spherocity of the surface atoms would cause. Taken together, these facts may help to account for the observed agreement. Note that models for the monoenergetic and Maxwellian incident beams become asymptotically close in the prediction of $(\theta_i - \theta_{max})$ at the higher energies.

The cube model has been derived for lower energy beams where the thermal motion of the lattice atoms is a controlling factor in the scattering; however, as suggested in Ref. 30, it may be instructive to apply it to higher energy work and this has been the approach in this report. Since the model does not have a surface trapping mechanism and depends on the thermal vibration of the atoms at the surface to produce distribution width, it is not expected to be successful in predicting the parameter $\Delta\theta_{\frac{1}{2}}$ (the width at one half maximum) for incident energies which are much greater than thermal. Figure 3.2.11 is a comparison of the distribution calculated from the "hard" cube model (monoenergetic incident beam) and our experimental result at 0.25 eV. The theory predicts a considerably narrower distribution, and the discrepancy becomes even more accentuated at the higher energies as shown in Fig. 3.2.12 for 1.35 eV. The fact that the "hard" cube model contains no mechanism to permit out-of-plane scattering means that absolute flux levels cannot be obtained, and that comparison with the present results has to be made by adjusting peak height levels to be the same.

An improved model based on the above simple classical theory and called the "soft" cube model has recently been reported (Ref. 75). The new model still incorporates the assumption that the tangential component of the velocity is unchanged in the interaction process (i.e. the tangential momentum accommodation is zero); however, it includes a "step" interaction potential which tends to widen the reflected distribution and also includes a total trapping mechanism. Also included is an attempt at describing out-of-plane scattering by allowing the surface to assume a roughness described by a roughness parameter. Using realistic values of the adjustable parameters, Logan and Keck (Ref. 75) have had some success in fitting the lower energy distributions (argon on gold, argon on silver); however, the model is not amenable to easy comparison with the present results since their computer program has to be reproduced in order to do so.

4. CONCLUSIONS

The main objective of the present work was to provide reliable data on the scattering of fast argon atoms from well characterized surfaces for comparison with concurrent theoretical models appropriate for the energy range and commensurate with satellite flight. The present fundamental study of the reflection of a monoenergetic inert gas beam from a well characterized single crystal surface will allow this to be done with a good measure of confidence. It is anticipated that the above theories will be able to infer from these results both the energy and momentum accommodation coefficients so greatly desired for gas-surface interactions in this energy range.

The multiple requirements of producing a pure monoenergetic high energy beam and known surface conditions necessitated the development of a combination of experimental techniques. From the results obtained, it may be concluded that the use of heated seeded nozzle beams affords an excellent method of achieving the required conditions, and that the use of an inert gas beam was successful in eliminating, almost entirely, the contamination at the test surface due to the beam gas. The use of gaseous helium cryopumping at 20°K around the interaction region has been shown to be extremely effective in maintaining a clean target surface and in permitting the measurement of small reflected molecular fluxes using a simple stagnation detector (for the inert gases at least). The use of the retarding field diode surface work function monitor has been shown to be compatable with the simultaneous beam scattering studies, and to afford a convenient and very useful method of inferring gas coverage at the surface, especially when combined with mass spectrographic and flash desorption techniques.

The scattering results themselves, which are the first obtained in this high energy range (0.25 to 2.0 eV) under such well characterized beam and surface conditions, show the following: Firstly, the deviation of the distribution maximum from the specular angle ($\theta_i - \theta_{max}$) is always negative and only slightly varying in this energy range. Secondly the narrowness of the distribution, as roughly determined by the parameter $\Delta\theta_{\frac{1}{2}}$ (the width at one half maximum) is still increasing with energy at least up to the extent of this energy range. Thirdly, adsorbed layers of hydrogen on the surface, even to the extent of saturation coverage, have not changed in any way, the form of the scattering from that for a clean (bare) surface, implying that higher energy inert beam scattering results, equivalent to reflection from a clean surface, can be obtained using a hydrogen carrier gas in a seeded nozzle beam with the same mixture ratios and source conditions as in the present case. The effect of other gases, namely nitrogen and carbon monoxide was to broaden the distribution considerably and shift the maximum of the distribution towards the surface. An important conclusion of the present work is that at no time in this energy range, even under cases of extreme surface gas coverage in the heavier gases, did the form of the distribution approach cosine law. The use of such a scattering law for the prediction of satellite drag or flow through a tube, even under conditions of extreme gas coverage, in this energy range, is therefore, not advised.

Qualitatively, the narrowness of the present reflected distributions combined with the calculation that there are 70-80% of the reflected particles in the lobe, suggest that the reflection mechanism at the surface is that of a binary collision and that the reflected particle velocities are not much different from those in the incident beam. Hence, the conclusion that the energy and momentum accommodation are significantly incomplete even for the gas covered surfaces.

The use of the present results to infer the reflection properties of other gas beams from other surfaces is a reality if theory can accurately predict the form, position of the maximum,and absolute flux values of the scattered number flux distributions obtained in these experiments. A theory is said to be suitable if in predicting one distribution by a best fit analysis, it can predict all the other distributions by retaining the same fitting parameters and varying only the physical parameters (e.g. angle of incidence, incident beam energy, etc.). In principle, such a theory could not only be used to develop the gas-surface interaction results for other single crystal surfaces, but could also, by proper averaging procedures, obtain results for polycrystalline surfaces (more engineering-like). This represents the more tedious approach and it is suggested instead, that once the fundamental principles of scattering are resolved more fully by experiments such as reported here, that results be obtained with the present equipment using atmospheric gas beams and surfaces more appropriate to satellite construction.

TEXT REFERENCES

1. Hinchen, J.J. Malloy, E.S. — Velocity of Molecular Beam Molecules Scattered by Platinum Surfaces. The Fundamentals of Gas-Surface Interactions, (ed. Saltsburg, H., Smith, J.N. Jr., Rogers M.), pp. 448-460, Academic Press, N.Y., 1967.

2. Moran, J.P. Wachman, H.Y. Trilling, L. — Time of Flight Measurements in an Argon Beam Deflected by a Heated Platinum Target. The Fundamentals of Gas-Surface Interactions, (ed. Saltsburg, H., Smith, J.N. Jr., Rogers M.), pp. 461-479, Academic Press, N.Y.,1967.

3. Wilmoth, R.G. Hagena, O.F. — Scattering of Argon and Nitrogen Off Polycrystalline Nickel. Univ. of Virginia Eng. Report No. AEEP-4038-105-67U, August, 1967.

4. Schamberg, R. — A New Analytic Representation of Surface Interactions for Hyperthermal Free Molecular Flow with Application to Neutral Particle Drag Estimates of Satellites. Rand Corporation Research Memorandum No. 2313, 1959.

5. Hinchen, J.J. Foley, W.M. — Scattering of Molecular Beams by Metallic Surfaces. in Rarefied Gas Dynamics, 4th Inter. Symp., (ed. J.H. deLeeuw), pp 505-517, Academic Press, N.Y., 1966.

6. Hinchen, J.J. Shepherd, E.F. — Molecular Beam Scattering from Surfaces of Various Metals. in Rarefied Gas Dynamics, 5th Inter. Symp., (ed. C.L. Brudin), pp. 239-252, Academic Press, N.Y., 1966.

7. Smith, J.N. Jr. Saltsburg, H. — Recent Studies of Molecular Beam Scattering from Continuously Deposited Gold Film. in Rarefied Gas Dynamics, 4th Inter. Symp., (ed. J.H. de Leeuw), pp. 491-504, Academic Press, N.Y., 1966.

8. Saltsburg, H. Smith, J.N.,Jr. Palmer, R.L. — Scattering of Helium, Deuterium and Hydrogen from the (111) Plane of Silver. in Rarefied Gas Dynamics, 5th Inter. Symp. (ed. C.L. Brudin), pp. 223-238, Academic Press, N.Y., 1966.

9. Smith, J.N. Jr. Saltsburg, H. — Molecular Beam Scattering from Solid Surfaces. The Fundamentals of Gas-Surface Interactions, (ed. Saltsburg, H., Smith, J.N. Jr., Rogers, M.), pp. 370-391, Academic Press, N.Y., 1967.

10. Knauer, F. Stern, O. — Zeitschrift fur Physik, 53, p. 779, 1929.

11. Estermann,I. Stern, O. — Beugung von Molekularstrahlen. Zeitschrift fur Physik, 61, p. 95, 1930.

12. Johnson, T.H. — J. Franklin Inst., 206, p. 301, 1928.

13. Kirschbaum, H. — Ann. d. Physik, 2, p. 213, 1929.

14. Zabel, R.M. — The Reflection of Atomic Beams from Sodium Chloride Crystals. Phys. Rev.,Vol. 42, pp. 218-228, 1932.

15. Datz, S.
Moore, G.E.
Taylor, E.H.
The Reflection of Modulated Helium and Deuterium Molecular Beams from Platinum Surfaces. in Rarefied Gas Dynamics, 3rd Inter. Symp., (ed. J.A. Laurmann), pp. 347-361, Academic Press, N.Y., 1963.

16. Hinchen, J.J.
Foley, W.M.
Scattering of Thermal Energy Gas Beams by Metallic Surfaces. United Aircraft Report No. D910245-7, Aug.1965.

17. Smith, J.N. Jr.
Fite, W.L.
Recent Investigations of Gas-Surface Interactions using Modulated Atomic Beam Techniques. in Rarefied Gas Dynamics, 3rd Inter. Symp. (ed. J.A. Laurmann), pp. 430-453, Academic Press, N.Y. 1963.

18. Hinchen, J.J.
Malloy, E.S.
Carroll, J.B.
Scattering of Thermal Energy Gas Beams by Metallic Surfaces 11. United Aircraft Report No. F910439-7,1967.

19. French, J.B.
Locke, J.W.
A Time-of-Flight Velocity Analyser using Metastable Molecules. in Rarefied Gas Dynamics, 5th Inter. Symp., (ed. C.L. Brudin), pp. 1461-1468, Academic Press, N.Y., 1966.

20. Redhead, P.A.
Chemisorption of Metals under Ultra High Vacuum Conditions. Paper presented at Symposium on Electronic and Vacuum Physics, Balalonfoldvar, Hungary, 1962.

21. Becker, E.W.
Bier, K.
Die Trennduse (Ein neues Element zur Gas-und Istopentrennung), Z. Naturforschg, Band 10a, Heft 7, pp 565-572, 1955. (Separation in the Nozzle, a New Method for the Separation of Gas and Isotopes).

22. Becker, E.W.
Henkes, W.
Geschwindigkeeitsanalyse von Laval-Strahlen. Zeitschrift fur Physik, Band 146, pp 320-332, 1956. (Velocity Analysis of Beams Formed from Laval Nozzles).

23. Klingelhofer, R.
Lohse, P.
Production of Fast Molecular Beams using Gaseous Mixtures. Physics of Fluids, Vol. 7, pp. 379-381, 1964.

24. Valleau, J.P.
Deckers, J.
Supersonic Molecular Beams 11. Theory of the Formation of Supersonic Molecular Beams. Can. J. Chem., Vol. 43, pp. 6-17, 1965.

25. Alcalay, J.A.
Knuth, E.L.
Experimental Study of Scattering in Particle Surface Collisions with Particle Energies of the Order of 1 eV. in Rarefied Gas Dynamics, 5th Inter. Symp., (ed. C.L. Brudin), pp. 253-268, Academic Press, N.Y., 1966.

26. Devienne, F.M.
Souquet, J.
Roustan, J.C.
Study of the Scattering of High Energy Molecules by Various Surfaces. in Rarefied Gas Dynamics, 4th Inter. Symp. (ed. J.H. deLeeuw), p. 584, Academic Press, N.Y. 1966.

27. Jackson, D.P.
(Ph.D. Thesis to be published)

28. Oman, R.A.
Bogan, A.
Weiser, C.
Li, C.H.
Interactions of Gas Molecules with an Ideal Crystal Surface. AIAA J., Vol. 2, No. 10, pp.1722-30, Oct. 1964.

29. Qman, R.A.
Research on Gas-Surface Interactions 1966-67. Part II. Numerical Experiments on Scattering of Noble Gases from Single Crystal Silver. Grumman Report No. 306, Nov. 1967.

30. Stickney, R.E.
Logan, R.M.
Yamamoto, S.
Keck, J.C.
Simple Classical Model for the Scattering of Gas Atoms from a Solid Surface. III Analysis for Monoenergetic Beams and Lock-in Detector Signals. in Fundamentals of Gas-Surface Interactions (ed. Saltsburg H., Smith, J.N., Jr., Rogers, M.), Academic Press, N.Y. 1967.

31. Kantrowitz, A.
Grey, J.
A High Intensity Source for the Molecular Beam. Rev. Sci. Inst., Vol. 22, pp. 328-332, 1951.

32. Anderson, J.B.
High Intensity and High Energy Molecular Beams. in Advances in Atomic and Molecular Physics, (ed. D.R. Bates), Vol. 1, Academic Press, N.Y., 1965.

33. Fenn, J.B.
Deckers, J.
Molecular Beams from Nozzle Sources. in Rarefied Gas Dynamics, 3rd. Inter. Symp., (ed. J.A. Laurmann), pp. 497-515, Academic Press, N.Y., 1963.

34. Scott, J.E.,Jr.
Drewry, J.E.
Characteristics of Aerodynamic Molecular Beams, in Rarefied Gas Dynamics, 3rd. Inter. Symp., (ed. J.A. Laurmann), pp. 516-538, Academic Press, N.Y., 1963.

35. French, J.B.
Continuum Source Molecular Beams. AIAA J., p. 994, June 1965.

36. French, J.B.
Molecular Beams for Rarefied Gasdynamic Research. AGARDograph 112, April 1966.

37. O'Keefe, D.R.
Initial Performance Study of the UTIAS Molecular Beam Facility, UTIAS Tech. Note No. 75, August 1964.

38. French, J.B.
O'Keefe, D.R.
Omegatron Studies of a Skimmed Beam System. in Rarefied Gas Dynamics, 4th, Inter. Symp., (ed. J.H. deLeeuw), pp. 299-310, Academic Press, N.Y., 1966.

39. Davis, J.H., Jr.
(Ph.D. Thesis to be published).

40. Anderson, J.B.
Andres, R.P.
Fenn, J.B.
Maise, G.
Studies of Low Density Supersonic Jets. in Rarefied Gas Dynamics, 4th Inter. Symp. (ed. J.H. deLeeuw) Academic Press, N.Y., 1966.

41. Hagena, O.F.
Morton, H.S. Jr.
Analysis of Intensity and Speed Distribution of a Molecular Beam from a Nozzle Source, in Rarefied Gas Dynamics, 5th Inter. Symp. (ed. C.L. Brudin), pp. 1369-1384, Academic Press, N.Y., 1966.

42. Milne, T.
Greene, F.T.
Mass Spectrometric Observation of Argon Clusters in Nozzle Beams. General Behaviour and Equilibrium Dimer Concentrations. Midwest Research Inst. Rept., Aug. 1966.

43. Abuaf, N.
Anderson, J.B.
Andres, R.P.
Fenn, J.B.
Miller, D.R.
Studies of Low Density Supersonic Jets. in Rarefied Gas Dynamics, 5th Inter. Symp., (ed. C.L. Brudin), pp. 1317-1336, Academic Press, N.Y., 1966.

44. Deckers, J.
Fenn, J.B.
High Intensity Molecular Beam Apparatus, Rev. Sci. Inst., Vol. 34, pp. 96-100, 1963.

45. Spalvins, T.
Buckley, D.H.
Vapor Deposited Gold Thin Films as Lubricants in Vacuum (10^{-11} mm Hg). The Journal of Vacuum Science and Technology, Vol. 3, No. 3, pp. 107-113, 1966.

46. Salser, G.E.
Rejuvenation of Electron Multipliers Used in Mass Spectrometers. Rev. Sci. Inst., Vol. 37, No. 5, p. 674, 1966.

47. Anderson, J.
Danforth, W.E.
Low Energy Electron Diffraction Study of the Adsorption of Oxygen on a (100) Tungsten Surface. J. Franklin Inst., Vol. 279, No. 3, pp. 160-168, 1965.

48. Samuels, L.E.
Sanders, J.V.
The Nature of Mechanically Polished Metal Surfaces: An Electron Diffraction Examination of Polished Silver Surfaces. J. Inst.Metals, V, 87, p. 129, 1958.

49. Sewell, P.B.
Cohen, M.
Mitchell, D.F.
Electron Optical Characteristics of Metal Surfaces. Surfaces and Interfaces , Vol. 1, Chemical and Physical Characteristics (ed. J.J. Burke, N.L. Reid, V. Weiss), Syracuse University Press, Syracuse, N.Y., 1967.

50. Dushman, S.
Lafferty, J.
Scientific Foundations of Vacuum Technique, John Wiley and Sons, Inc., N.Y., 1962.

51. Estrup, P.J.
Anderson, J.
Danforth,W.E.
LEED Studies of Thorium Adsorption on Tungsten. Surface Science, 4, pp. 286-298, 1966.

52. Cullity, B.D.
The Elements of X-ray Diffraction. Addison-Wesley Pub., Co., 1956.

53. Barrett, C.S.
The Structure of Metals. McGraw-Hill Publ. Co., 1952.

54. Hayward, D.O.
Trapnell, B.M.W.
Chemisorption. (2nd edition), Butterworths Publ. Co., London, 1964.

55. Redhead, P.A.
Trans. Faraday Soc., 57, p. 641, 1961.

56. Ehrlich, G.
Low Temperature Chemisorption. II Flash Desorption of Nitrogen, J. Chem. Phys., 34, p. 29, 1961.

57. Ehrlich, G. — Low Temperature Chemisorption. II Flash Desorption of Carbon Monoxide. J. Chem. Phys., 34, p. 39, 1961.

58. Jones, P.L. Pethica, B.A. — Proc. Roy. Soc., A256, p. 454, 1960.

59. Mignolet, J.C.P. — Disc. Faraday Soc., 8, p. 326, 1950.

60. Gysae, B. Wagener, S. — Z. Tech. Physik, 19, p. 264, 1938. Z. Physik, 115, p. 296, 1940.

61. Robins, J.L. — Mass Peaks from Adsorbed Gases in a Single-Focussing Mass Spectrometer. Can. J. Phys., 41, p. 1385, 1963.

62. Bance, U.R. Craig, R.D. — Some Characteristics of Triode Ion Pumps. Vacuum, Vol. 16, No. 12, pp. 647-652, 1966.

63. Rozgonyi, G.A. — Increase of Residual Background Gases During Ultrahigh Vacuum Mass Spectroscopic Analysis. J. Vac.Sci. Tech., Vol. 3, No. 4, pp. 187-191, 1965.

64. Estrup, P.J. Anderson, J. — Chemisorption of Hydrogen on Tungsten (100). J. Chem. Phys. Vol. 45, No. 6, pp. 2254-2260, 1966.

65. Moore, G.E. Unterwald, F.C. — Adsorption-Desorption of Hydrogen on Tungsten and Molybdenum. J. Chem. Phys.,Vol. 40, No. 9, pp. 2626-2638,1964.

66. Anderson, J. Estrup, P.J. — Adsorption of CO on a Tungsten (100) Surface. J. Chem. Phys., Vol. 46, No. 2, pp. 563-567, 1967.

67. Estrup, P.J. Anderson, J. — LEED Studies of the Adsorption Systems W(100) + N_2 and W(100) + N_2 + CO. J. Chem. Phys., Vol. 46, No. 2, pp. 567-570, 1967.

68. Rigby, L.J. — The Adsorption and Replacement of Hydrogen on Polycrystalline Tungsten. Can. J. Phys., 43, p. 1020, 1965.

69. Robins, J.L. — Replacement of Chemisorbed Gases on Tungsten. Trans. of 9th Vac. Symp. of the A.V.S. (ed. G.H. Bancroft), Pergamon Press, N.Y., p. 510, 1963.

70. Rigby, L.J. — The Interactions of Nitrogen and Carbon Monoxide on Polycrystalline Tungsten. Can. J. Phys.,42, p. 1256,1964.

71. Brown, S.C. — The Basic Data of Plasma Physics, 1966. The M.I.T. Press, Cambridge, Mass., U.S.A., 1967.

72. Higatsberger,M.J. Demorest, H.L. — Secondary Emission from Nichrome V, CuBe and AgMg Alloy Targets Due to Positive Ion Bombardment. J. Appl. Phys., Vol. 25, No. 7, p. 883, 1954.

73. Rideal, E.K. Sweett,F. — The Chemisorption of Hydrogen on Nickel. Proc. Roy. Soc. London, A. 257, p. 291, 1960.

74. Ehrlich, G. — Molecular Processes in Adsorption on Metals. Trans. of 8th Vac. Symp. of AVS (ed. L.E. Preuss), Pergamon Press, N.Y., p. 126, 1962.

75. Logan, R.M. Keck, J.C. — Classical Theory for the Interaction of Gas Atoms with Solid Surfaces. M.I.T. Fluid Mechanics Lab. Rept. No. 67-8, Oct. 1967.

FIGURE REFERENCE LIST

A.	Smith, J.N. Jr.	Scattering of Atomic Beams by Polycrystalline Nickel. J. Chem. Phys., Vol. 40, No. 9, pp. 2520-2527, 1964.
B.	Smith, J.N. Jr. Saltsburg, H.	Atomic Beam Scattering From Epitaxially Grown Gold Films. General Atomic Report No. GA-4947, April 1964.
C.	Smith, J.N., Jr. Saltsburg, H.	Recent Studies of Molecular Beam Scattering From Continuously Deposited Gold Films. General Atomic Report No. GA-5356, June 1964.
D.	Saltsburg, H. Smith, J.N., Jr.	Molecular Beam Scattering from the (111) Plane of Silver. General Atomic Report No. GA-6740, Dec. 1965.

PARAMETER	Becker & Henkes Ref. 22		Anderson & Fenn Ref. 40	U.T.I.A.S. Run No. 7		U.T.I.A.S. Run No. 1
BEAM GAS	2% A, 98% H_2		Pure Argon	1% A, 99% He		Pure Argon
	Argon	Hydrogen		Argon	Helium	
Source Press. P_o	0.6 Torr	29.4 Torr	10 Torr	15 Torr	1485 Torr	923 Torr
Source Temp. T_o	298 °K	298 °K	298 °K	1000 °K	1000 °K	1000 °K
Source Knudsen Number Kn_o		0.0064	0.0068		0.0013	0.0008
Trans. Freezing Mach Number M_f		8.9	9.0		16.9	21.0
Eff. Mach No. of Seed Gas (slip=0)	28.4			42.0		
Quitting Surface Pos'n (nozzle dia.)		4.5	4.7		11.5	16.0
Nozzle Skimmer Dist. (nozzle dia.)		2.0	8.3		70.0	70.0
Skimmer Knudsen Number Kn_s		0.335	1.56		9.4	5.46
Trans. Freezing Temperature T_f		10.5 °K	10.6 °K		10.0 °K	6.7 °K
% of Escape Speed Acheived		98.5	98.5		99.5	99.8

TABLE 2.1.1 TYPICAL OPERATING CONDITIONS FOR NOZZLE BEAMS

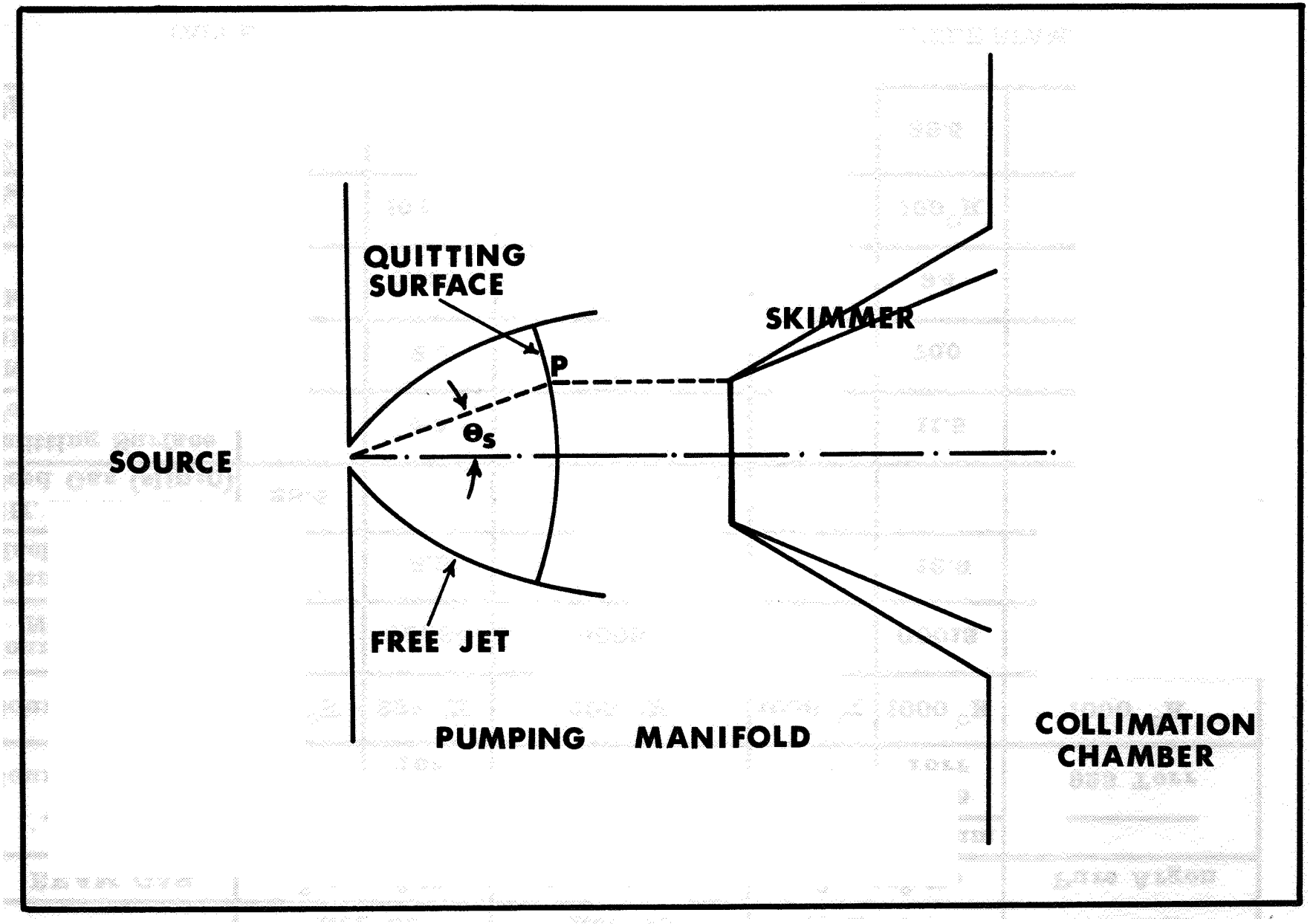
QUITTING
SURFACE
SKIMMER
P
θ_s
SOURCE
FREE JET
PUMPING MANIFOLD
COLLIMATION
CHAMBER

FIG. 2.1.1

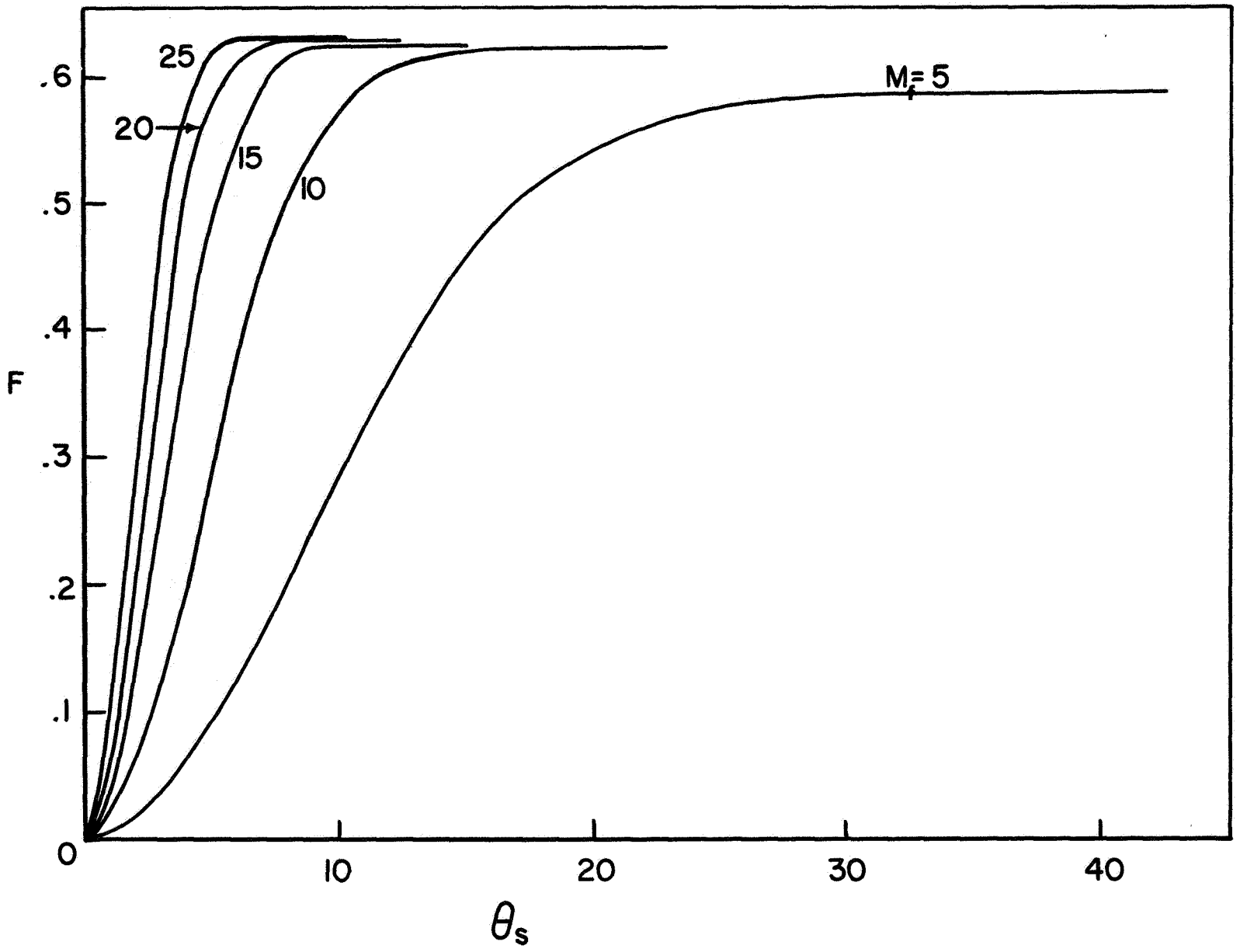

FIG. 2.1.2

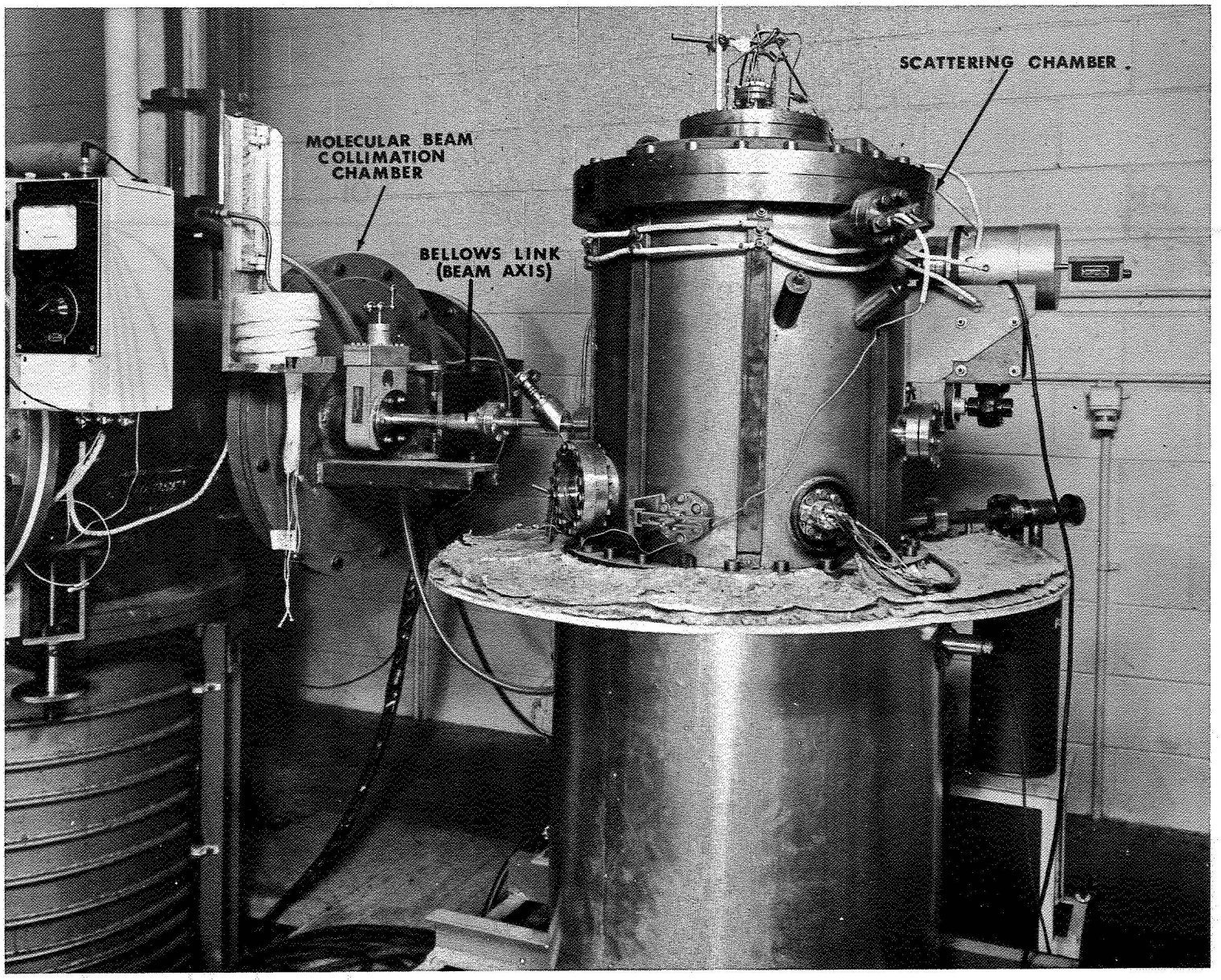

FIG. 2.2.1 MOLECULAR BEAM SCATTERING CHAMBER

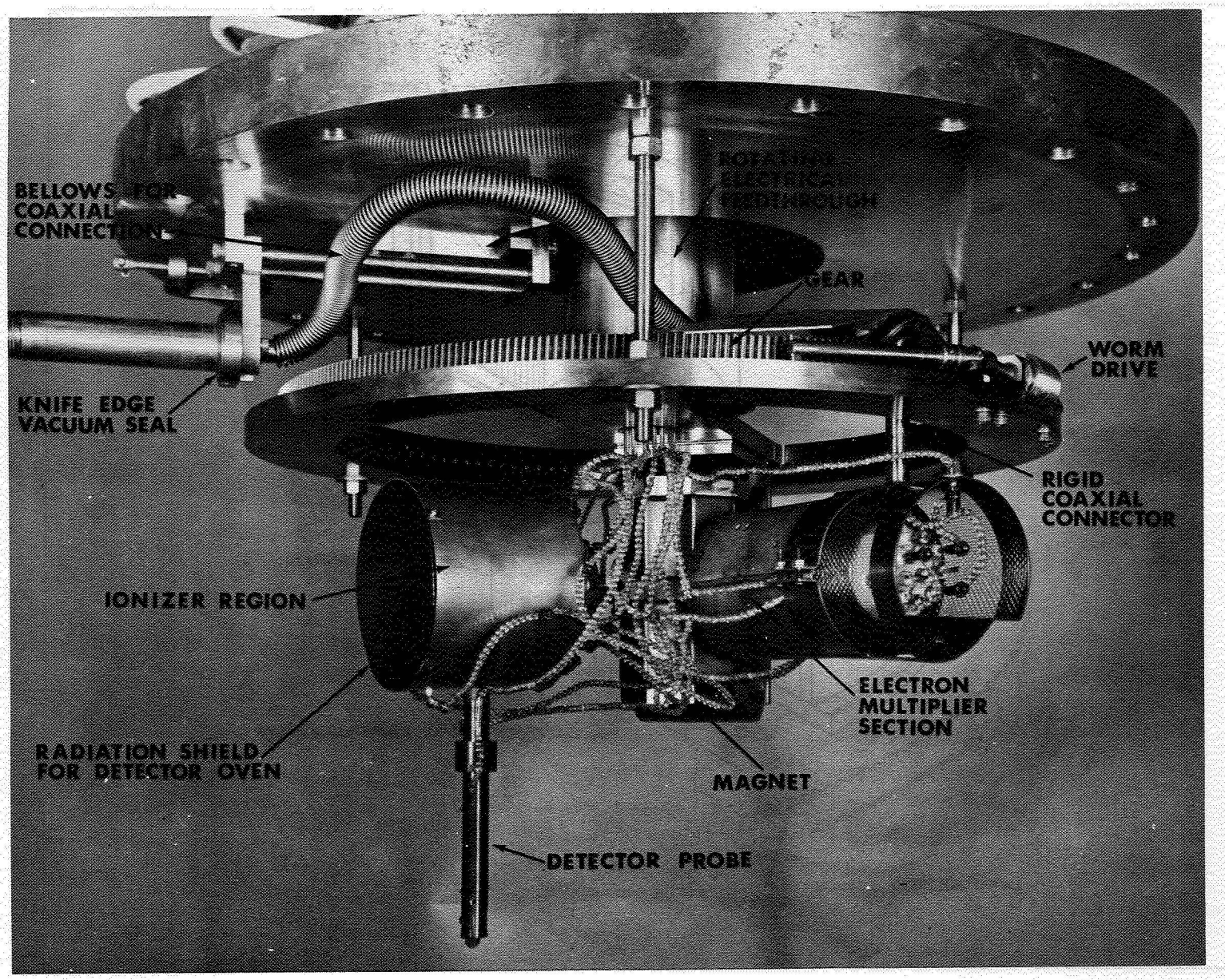

FIG. 2.3.1 MOLECULAR BEAM DETECTOR ASSEMBLY

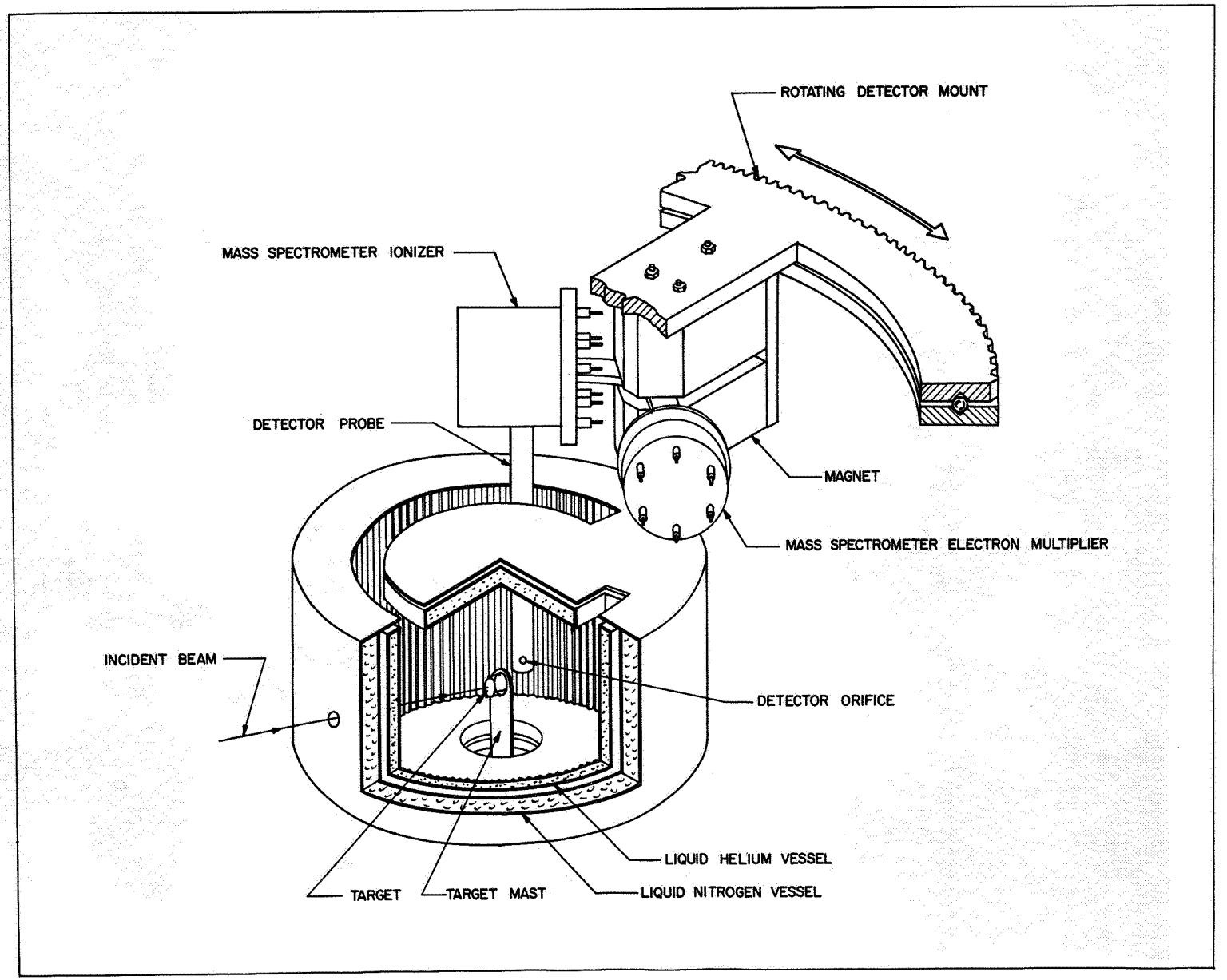

FIG. 2.3.2 SCHEMATIC OF MOLECULAR BEAM SCATTERING APPARATUS

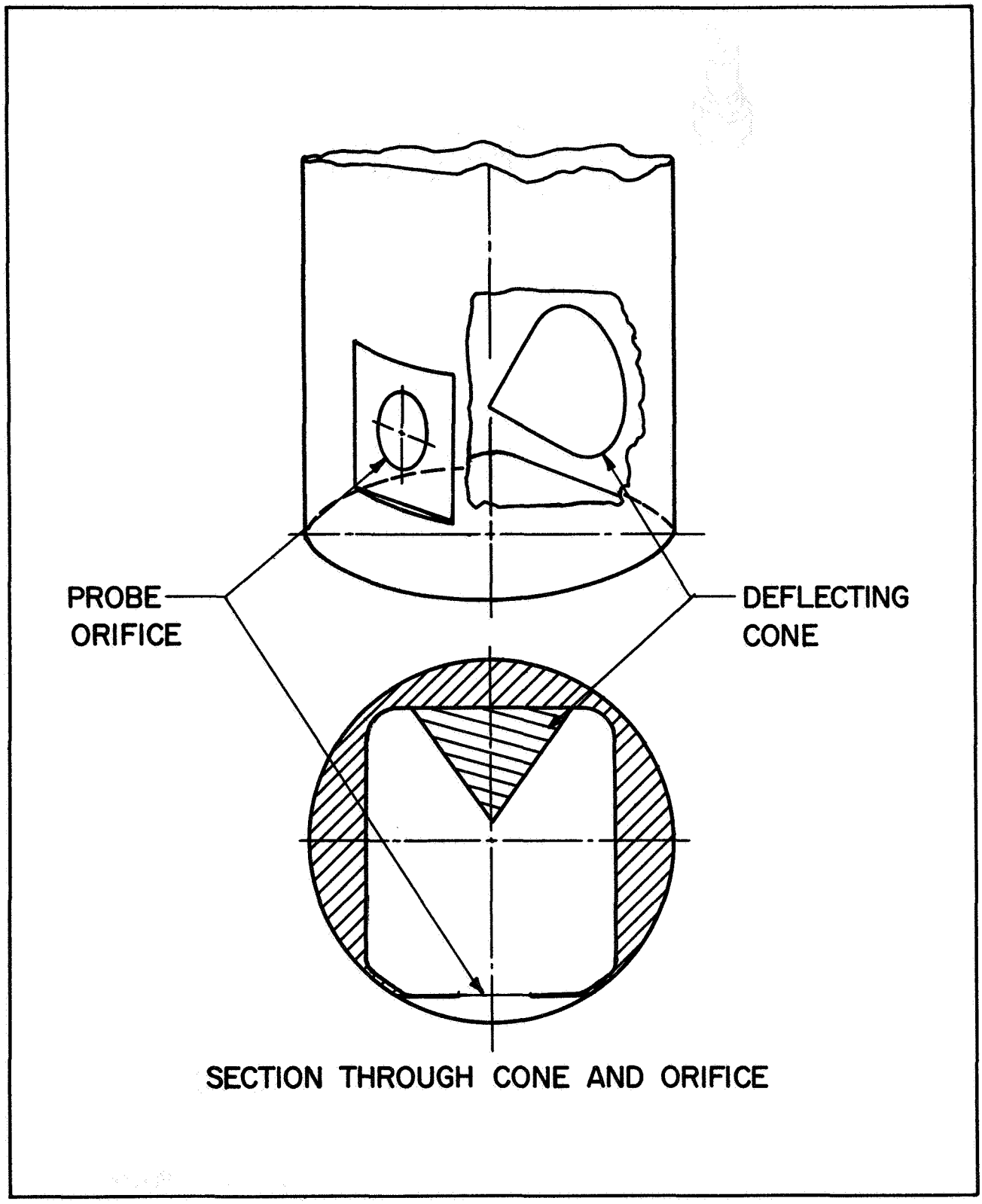

FIG. 2.3.3 SCHEMATIC OF DETECTOR PROBE ASSEMBLY

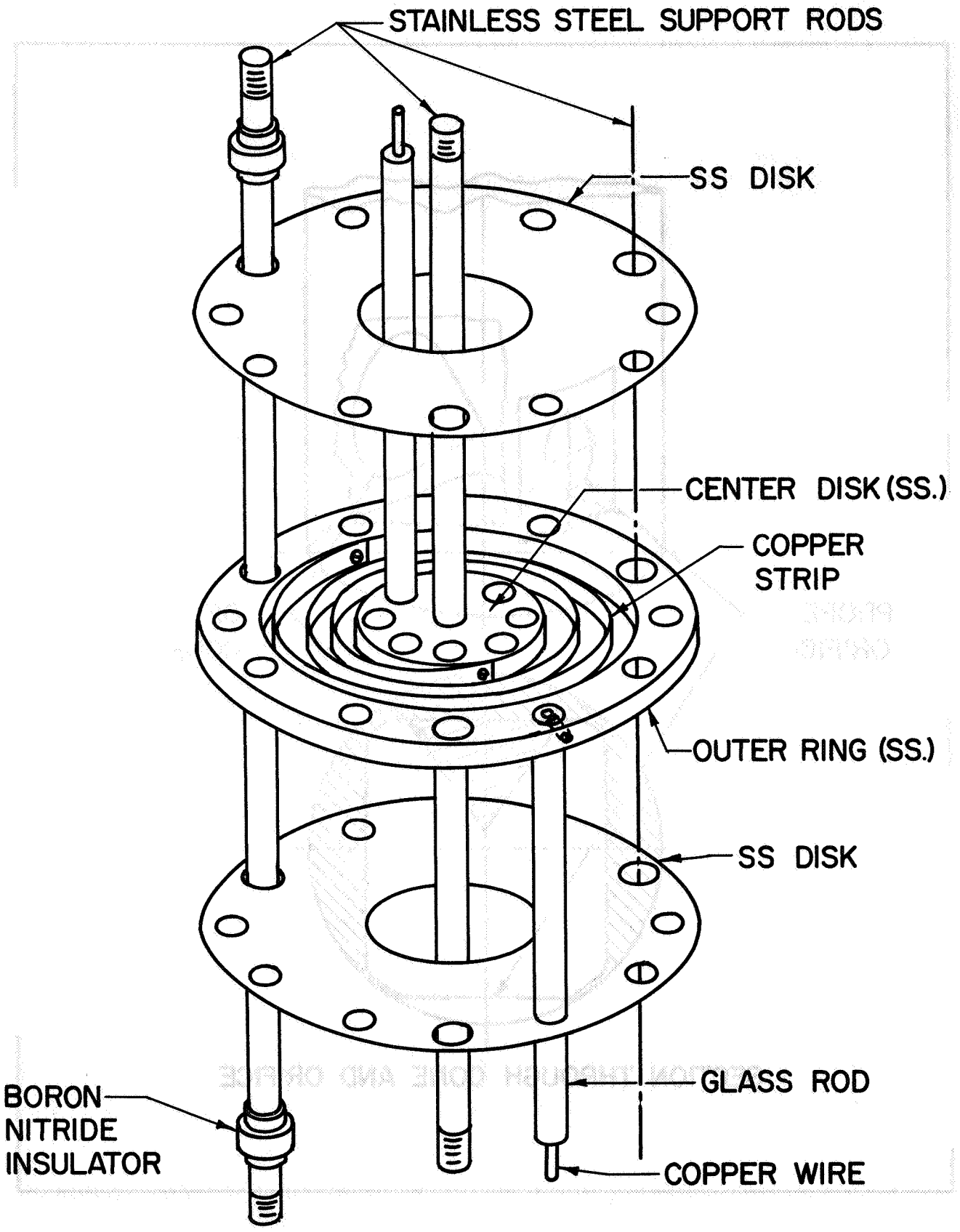

FIG. 2.3.4 SCHEMATIC OF ROTATING ELECTRICAL FEEDTHROUGH

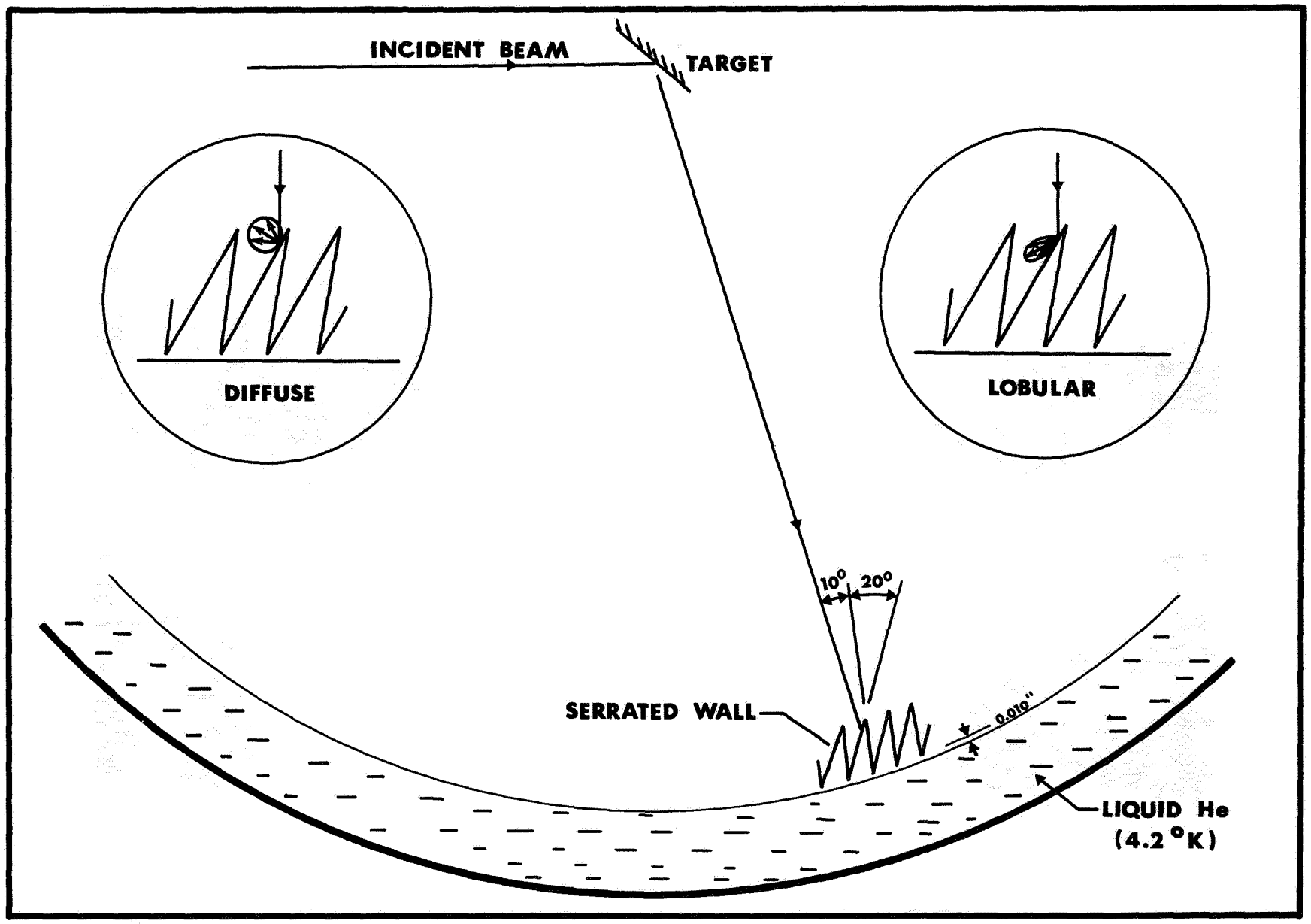

FIG. 2.4.1 SCHEMATIC OF MOLECULAR BEAM CRYOTRAP

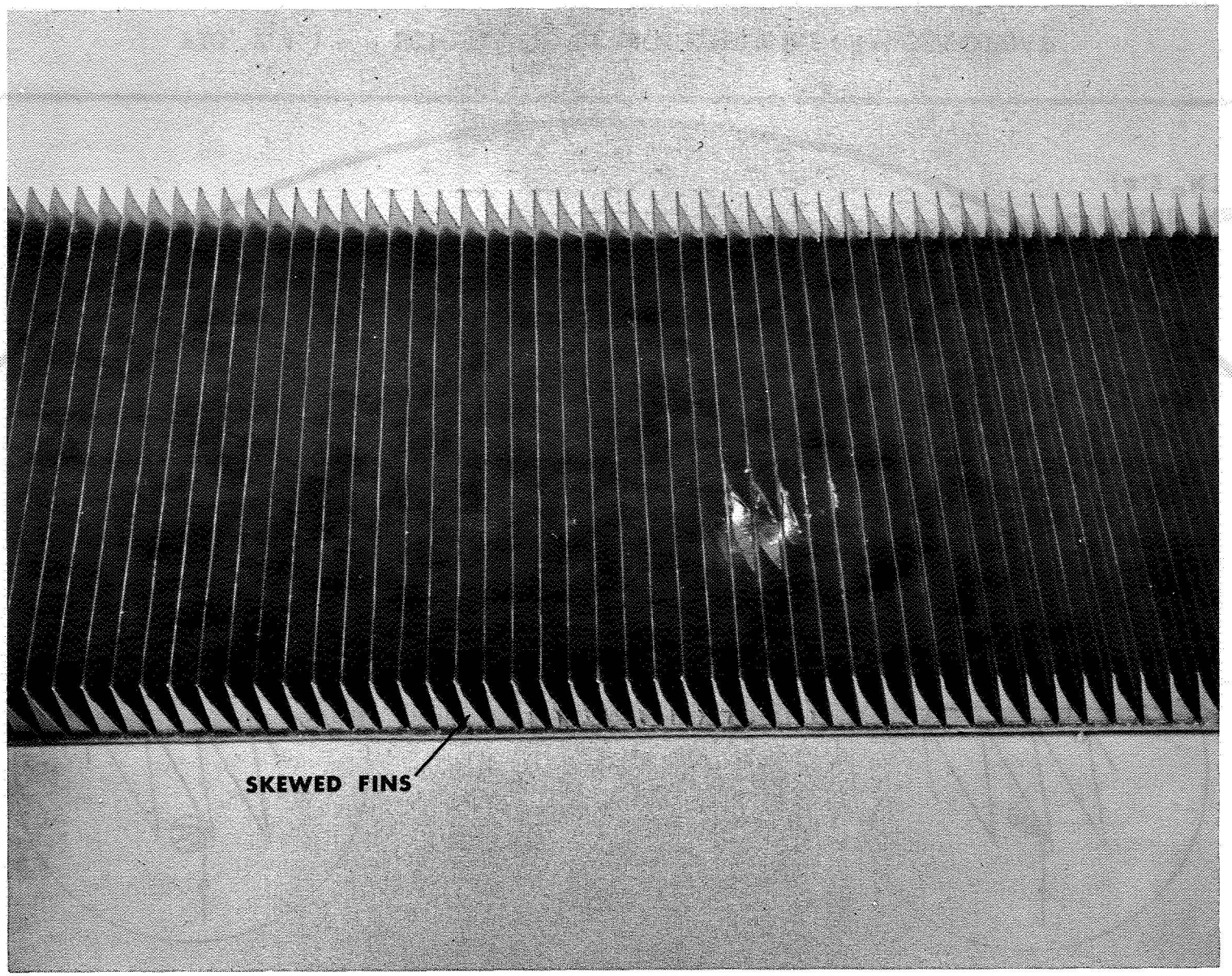

FIG. 2.4.2 SERRATED WALL OF MOLECULAR BEAM CRYOTRAP

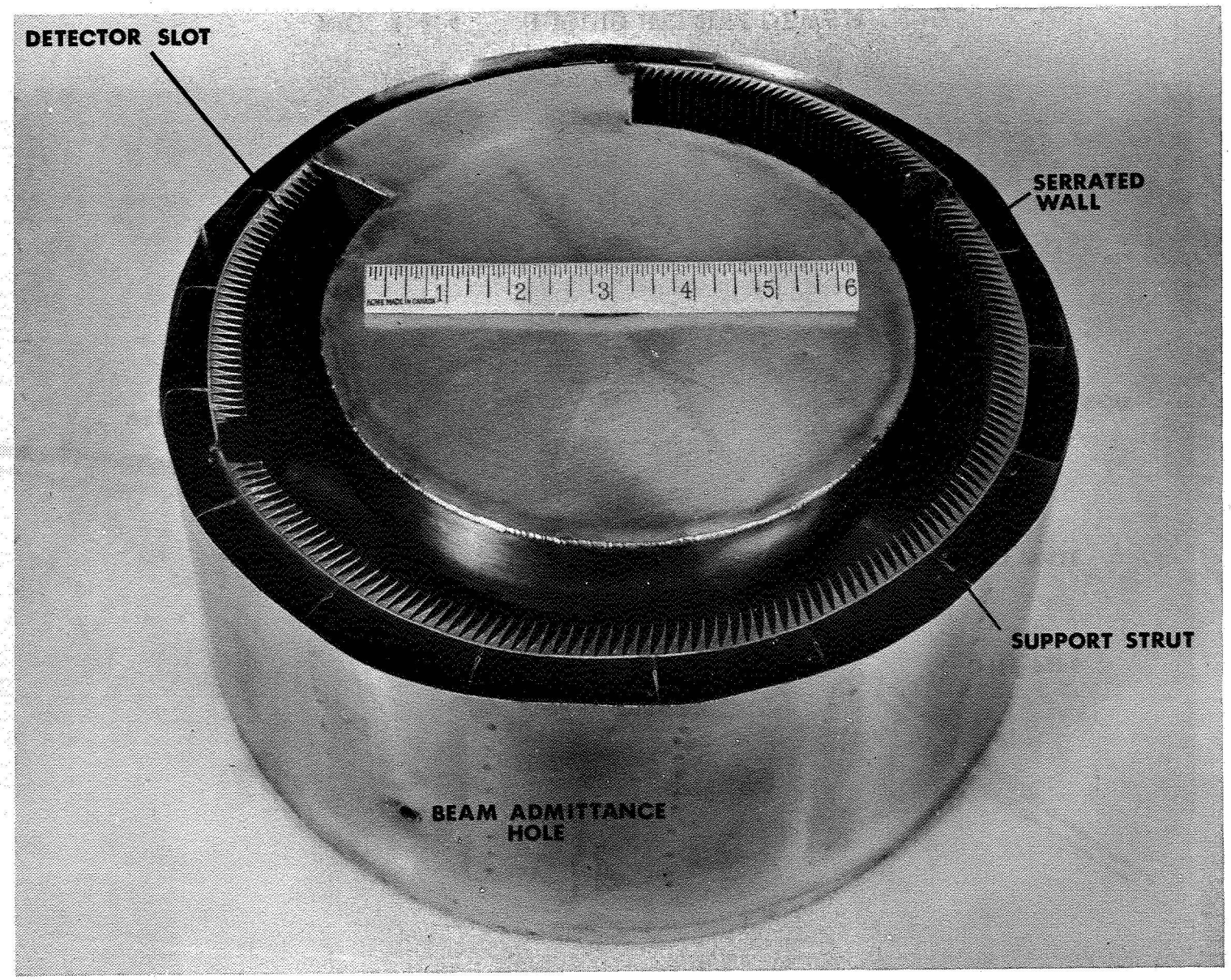

FIG. 2.4.3 LIQUID HELIUM DEWAR SHOWING INNER CONSTRUCTION

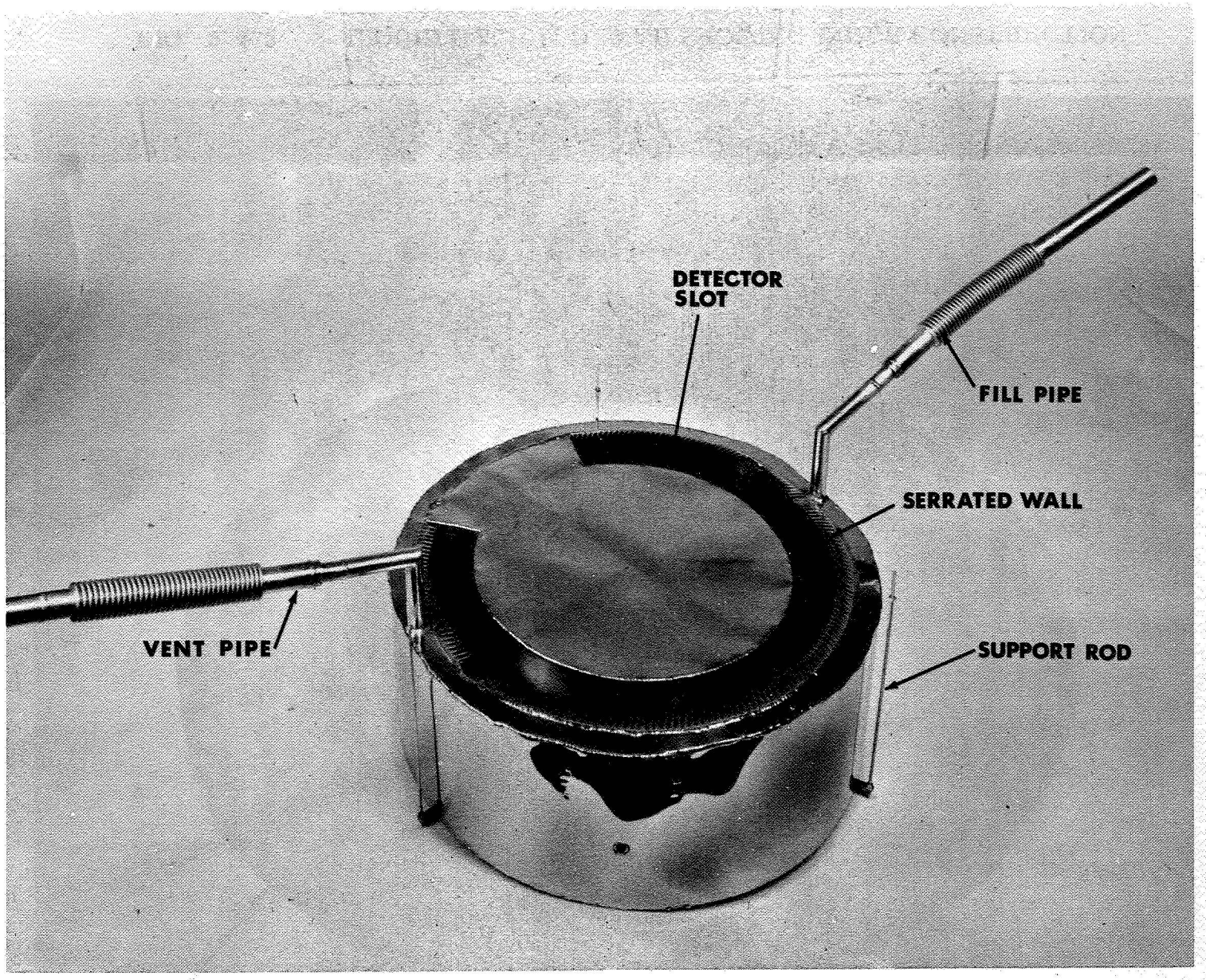

FIG. 2.4.4 LIQUID HELIUM DEWAR

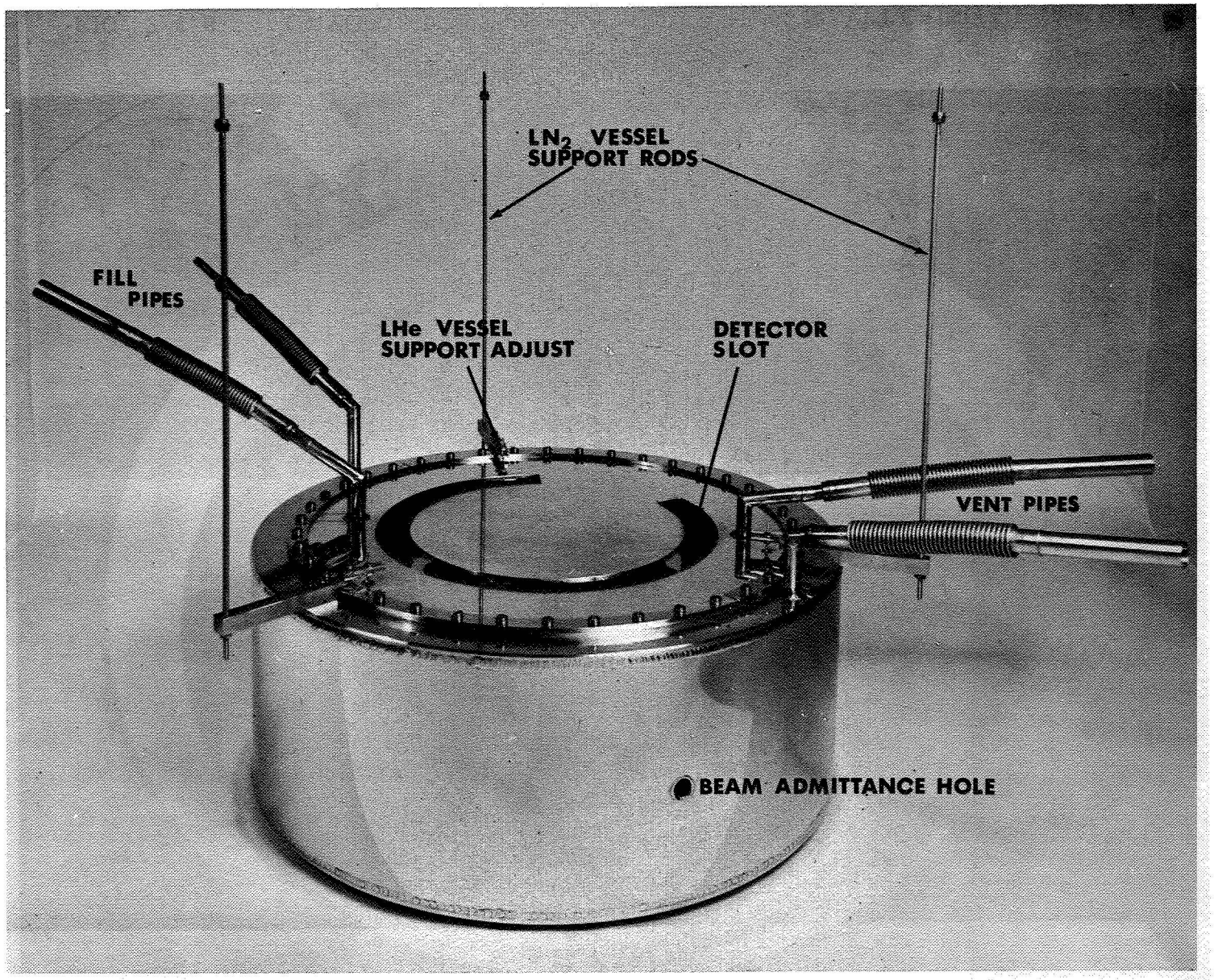

FIG. 2.4.5 LIQUID NITROGEN DEWAR

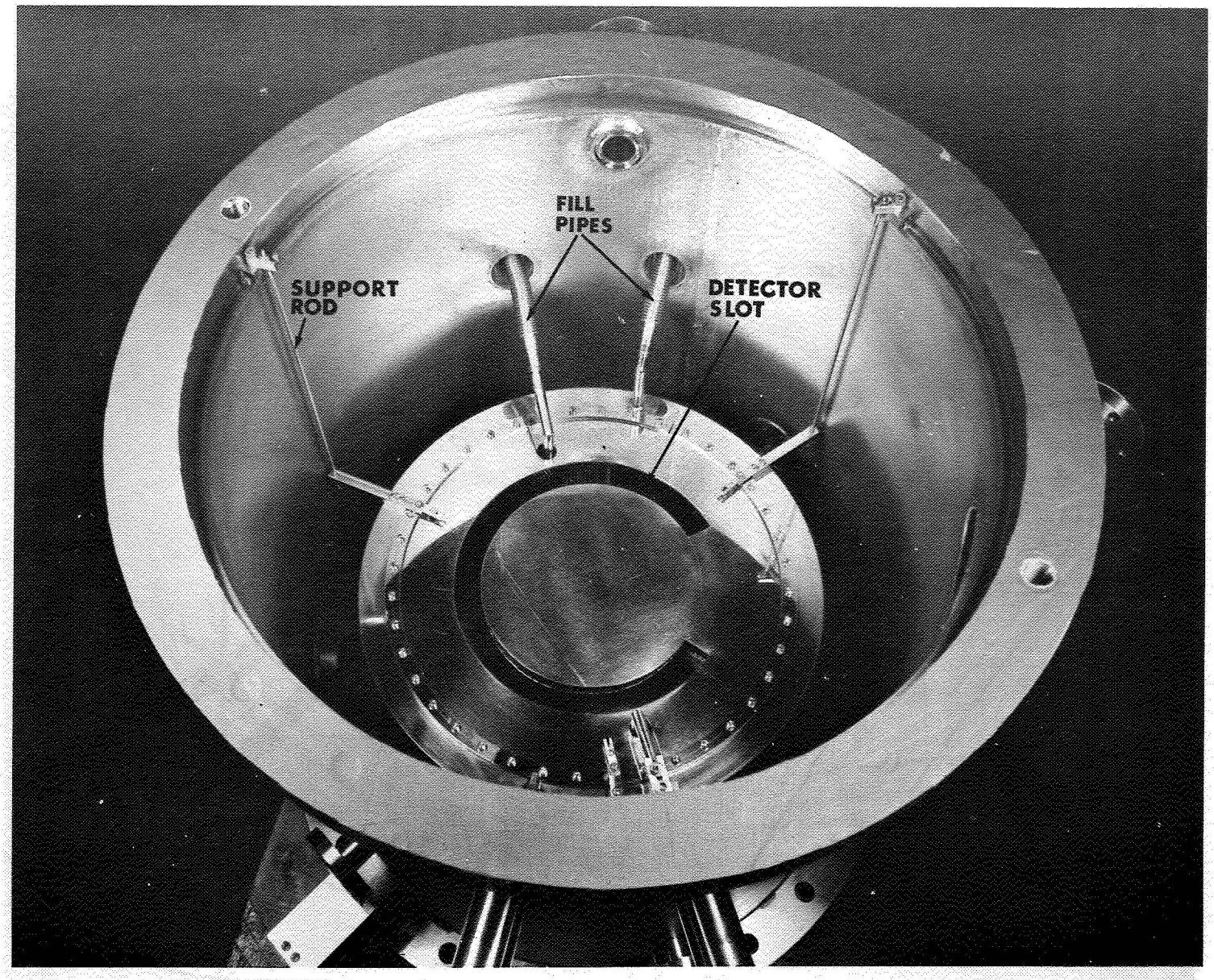

FIG. 2.4.6 CRYOGENIC ASSEMBLY IN PLACE IN SCATTERING CHAMBER

FIGURE 2.5.1

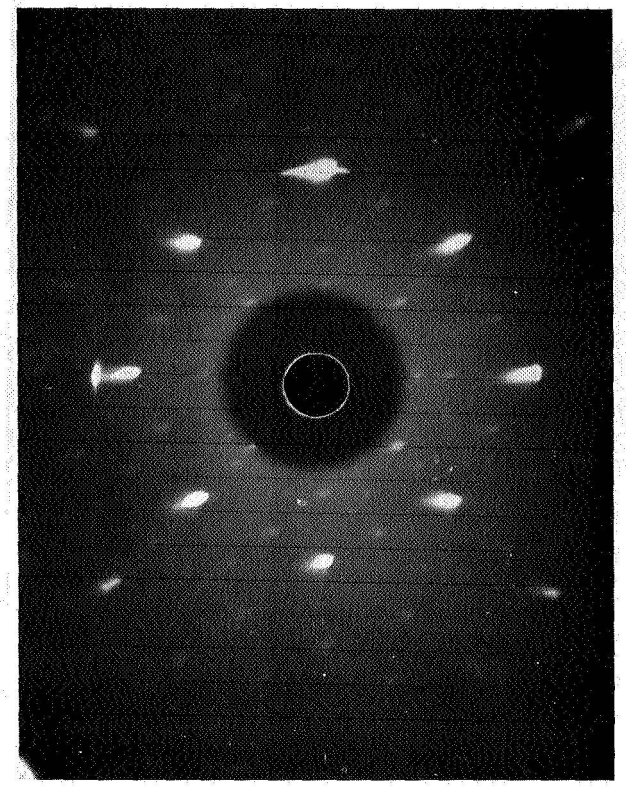

[010] DIRECTION

NORMAL TO INCIDENT PLANE

BEFORE ANNEAL

FIGURE 2.5.2

[010] DIRECTION

NORMAL TO INCIDENT PLANE

AFTER ANNEAL

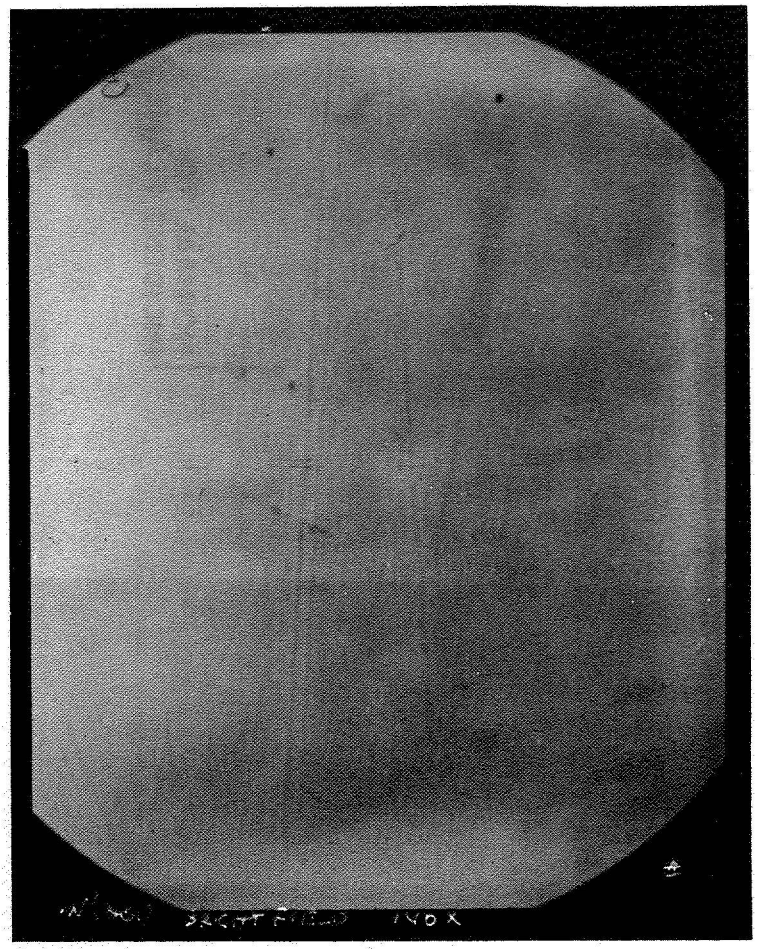

FIG. 2.5.3
BRIGHT FIELD

FIG. 2.5.4
PHASE CONTRAST

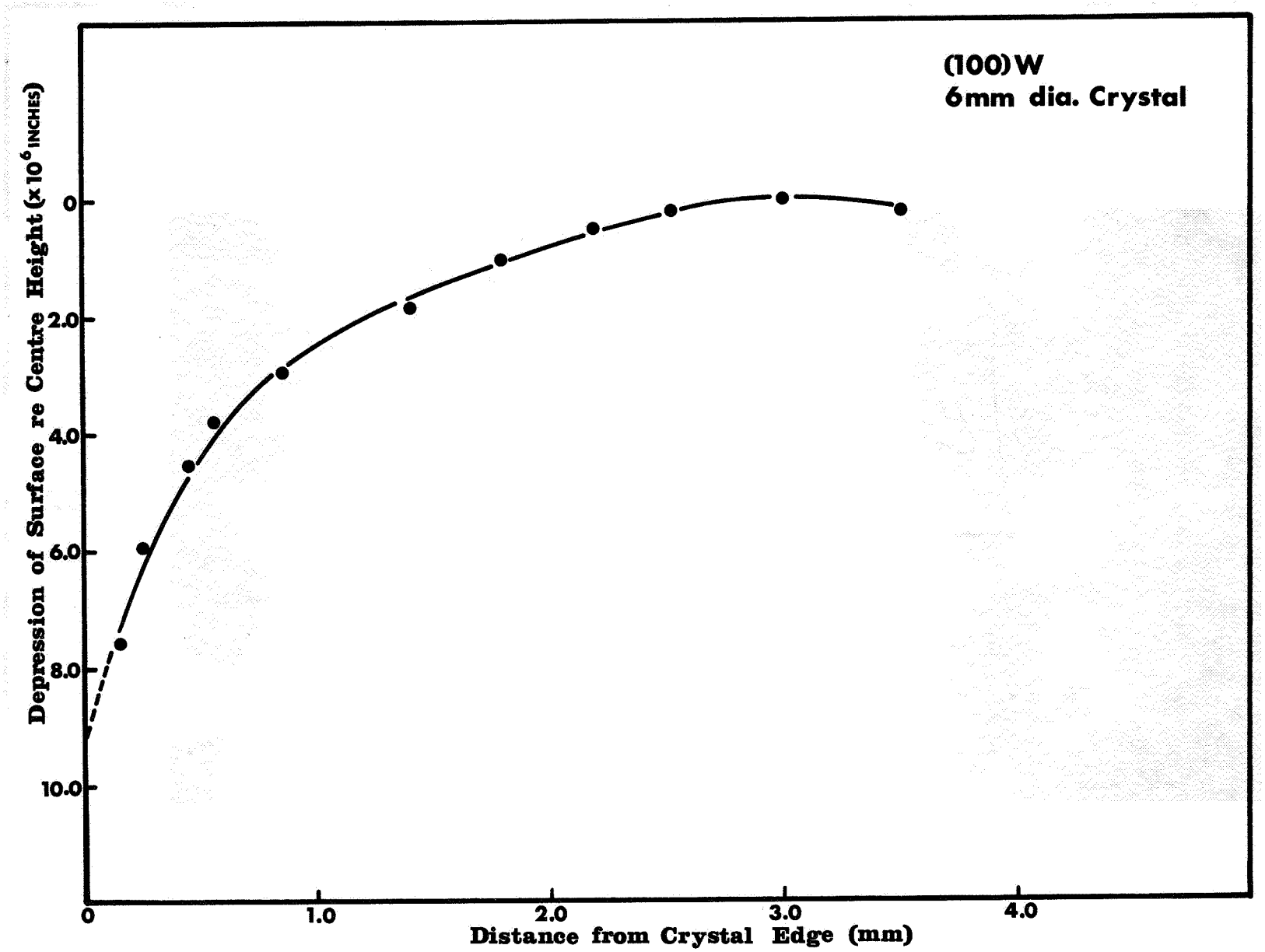

FIG. 2.5.5 SURFACE CONTOUR OF CRYSTAL

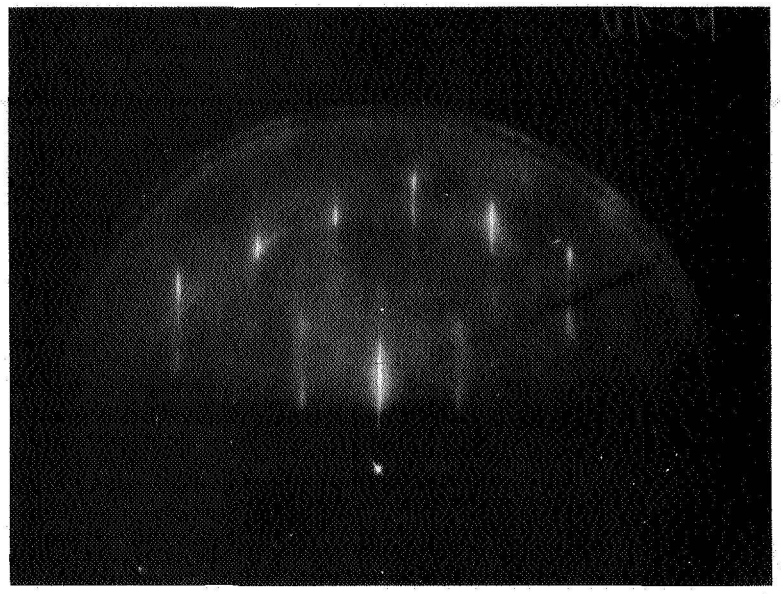

[021]

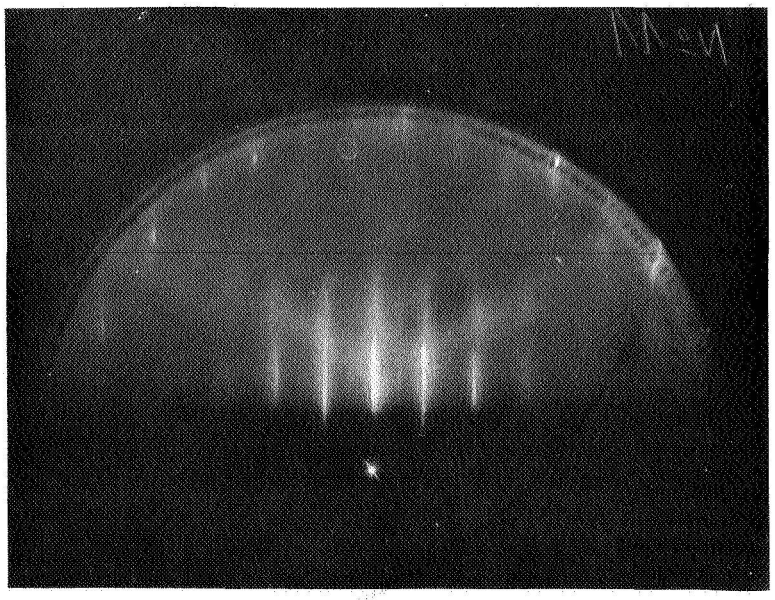

[011]

FIG. 2.5.6 REFLECTED HIGH ENERGY ELECTRON DIFFRACTION PATTERNS FOR TWO AZIMUTH DIRECTIONS (BEFORE PERFORMANCE OF EXPERIMENT)

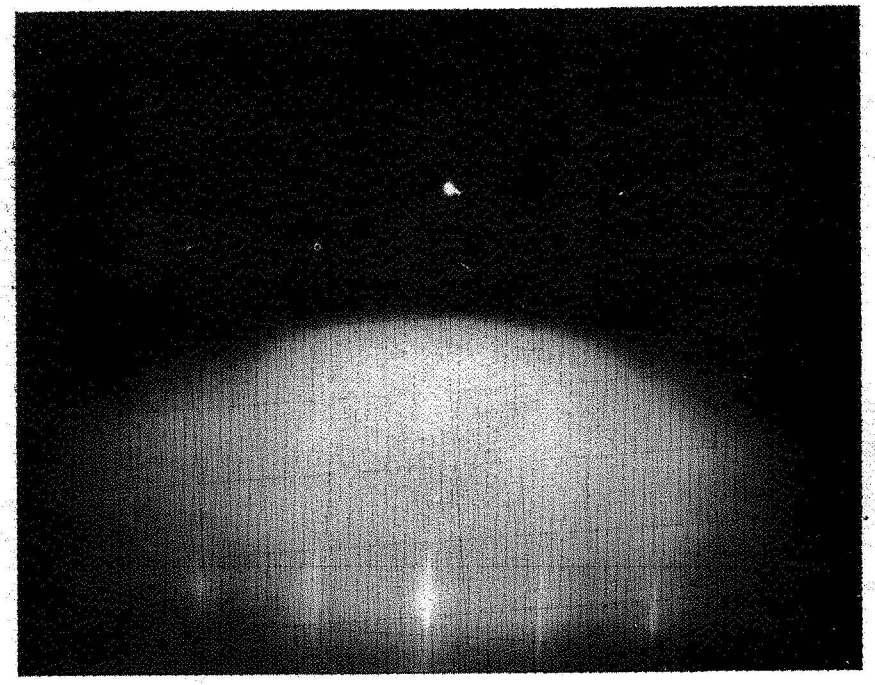

FIG. 2.5.7 REFLECTION HIGH ENERGY ELECTRON DIFFRACTION PATTERN AFTER PERFORMANCE OF EXPERIMENT TAKEN IN 011 AZIMUTH DIRECTION. DIFFUSE BACKGROUND DUE TO SURFACE ADSORPTIVE LAYER OF GAS FROM EXPOSURE TO ROOM AIR.

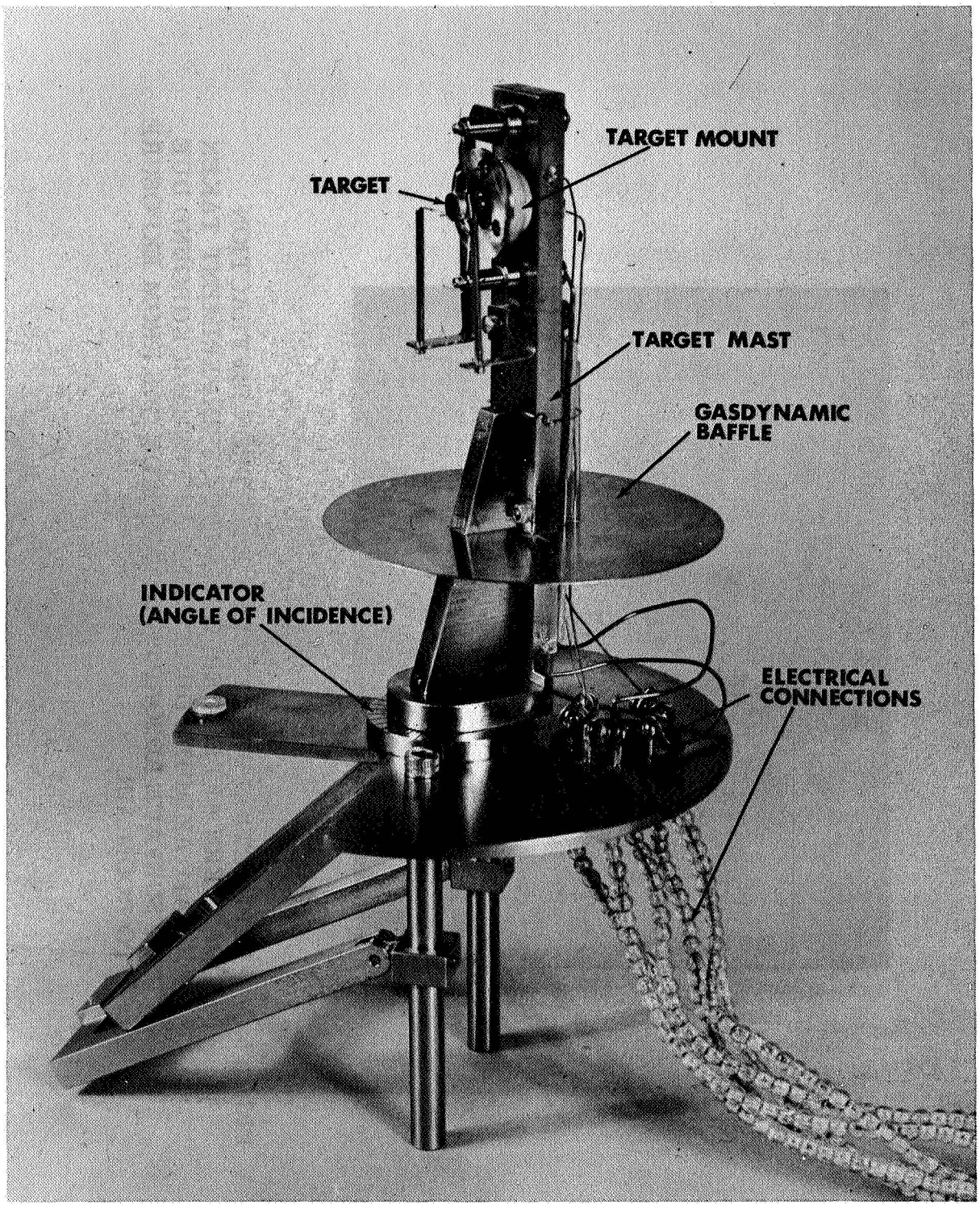

FIG. 2.5.8 TARGET MAST ASSEMBLY

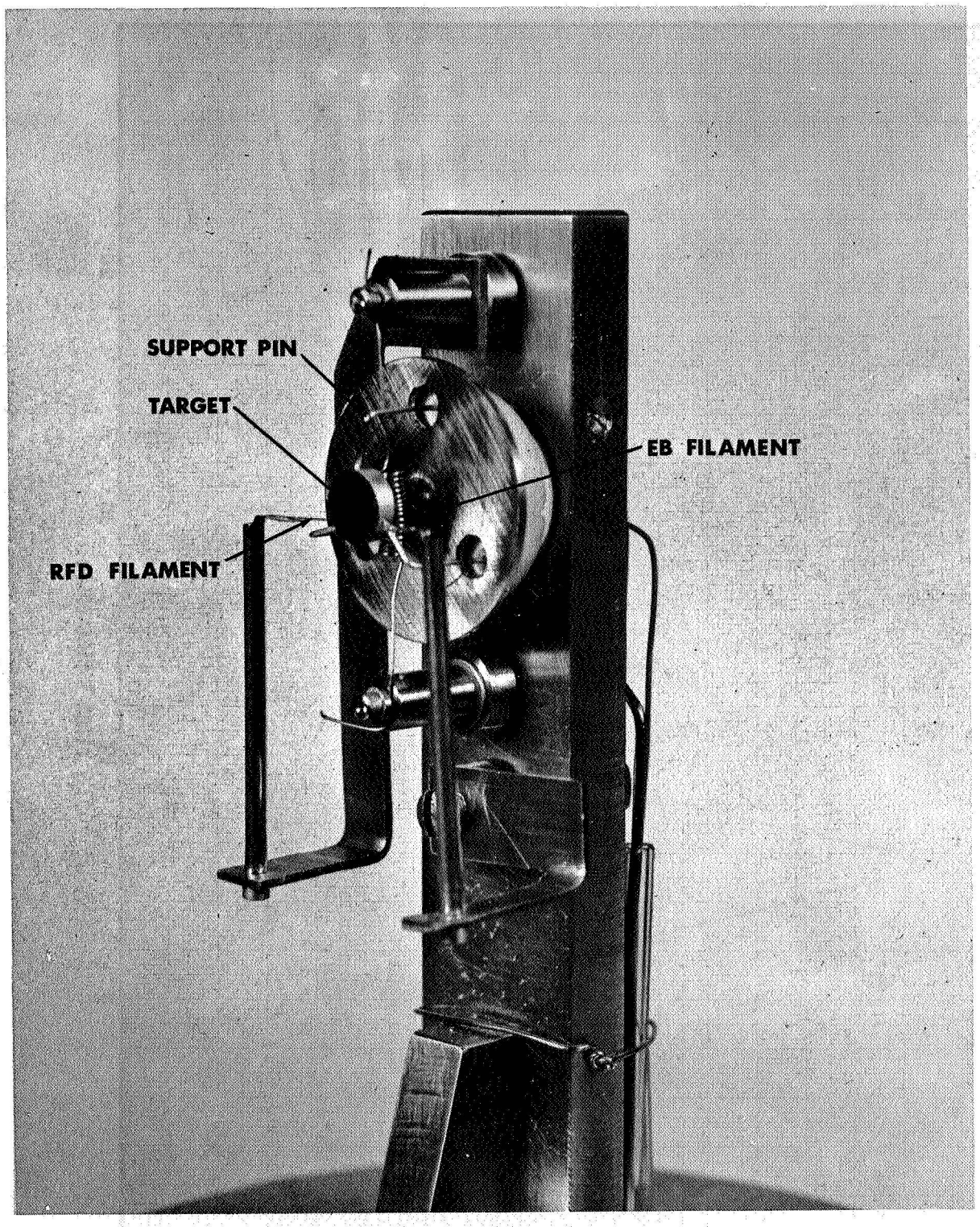

FIG. 2.5.9 TARGET MOUNT

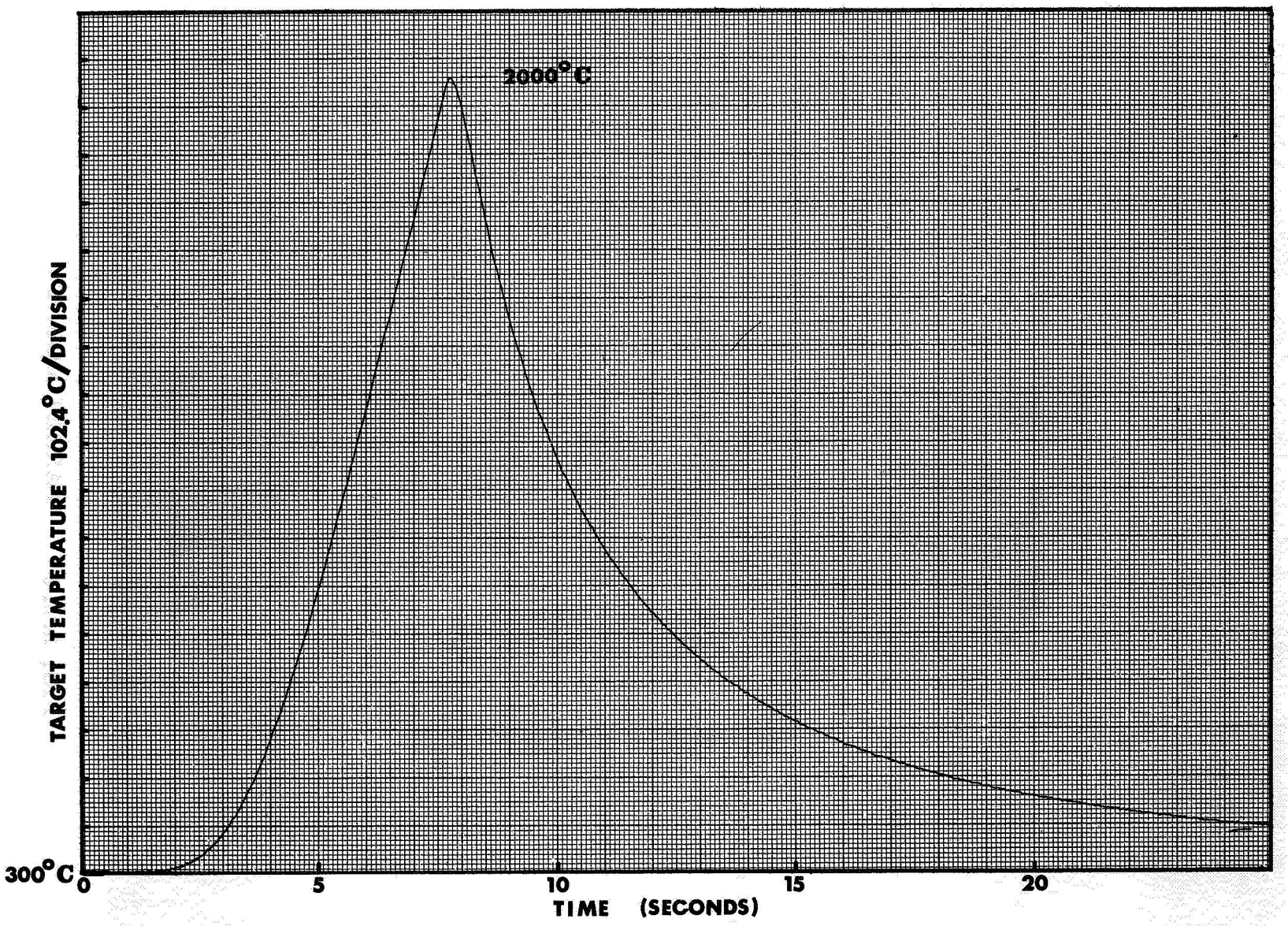

FIG. 2.5.10 TARGET HEATING PROFILE

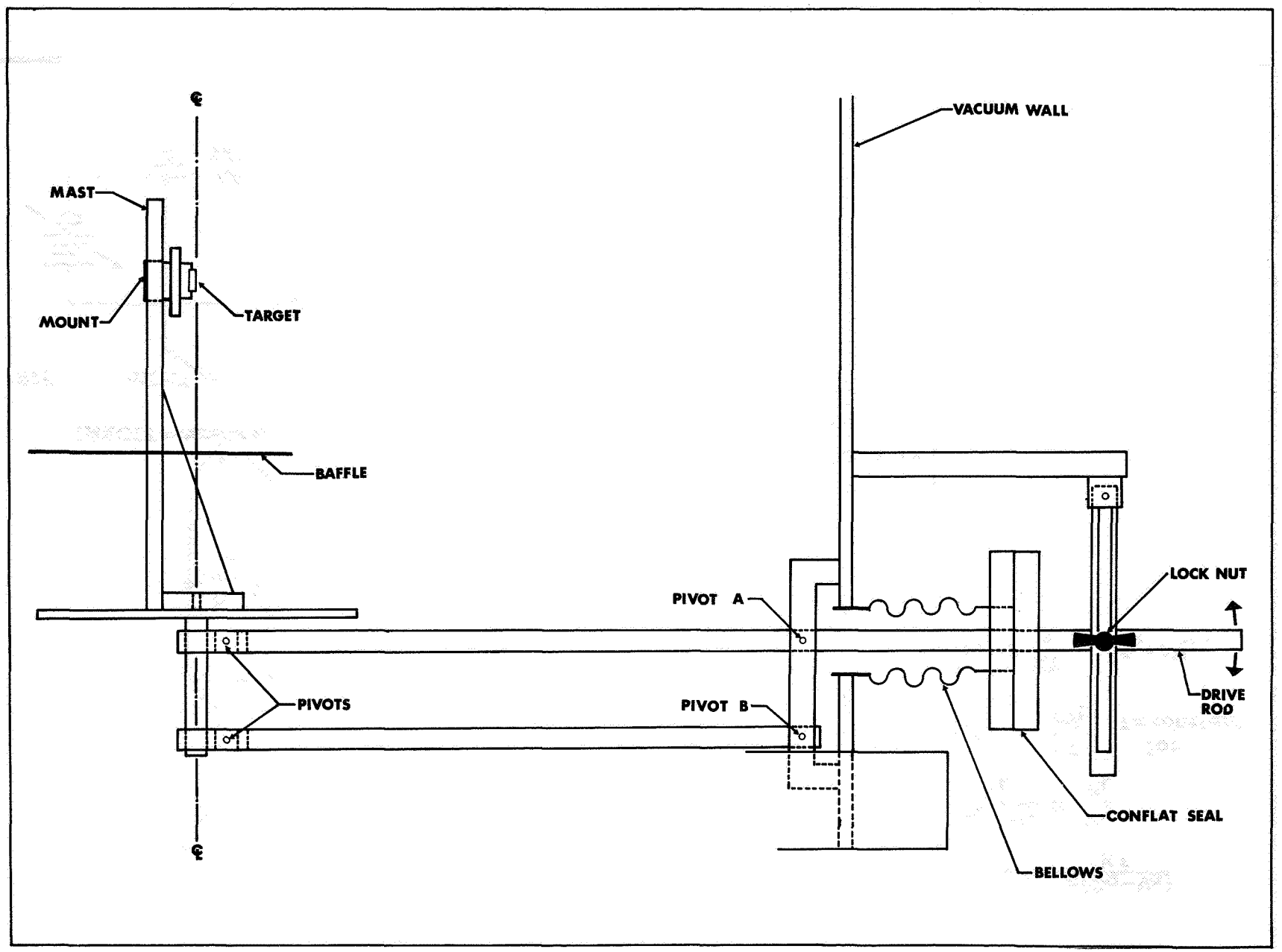

FIG. 2.5.11 TARGET LINEAR MOTION ACTUATOR

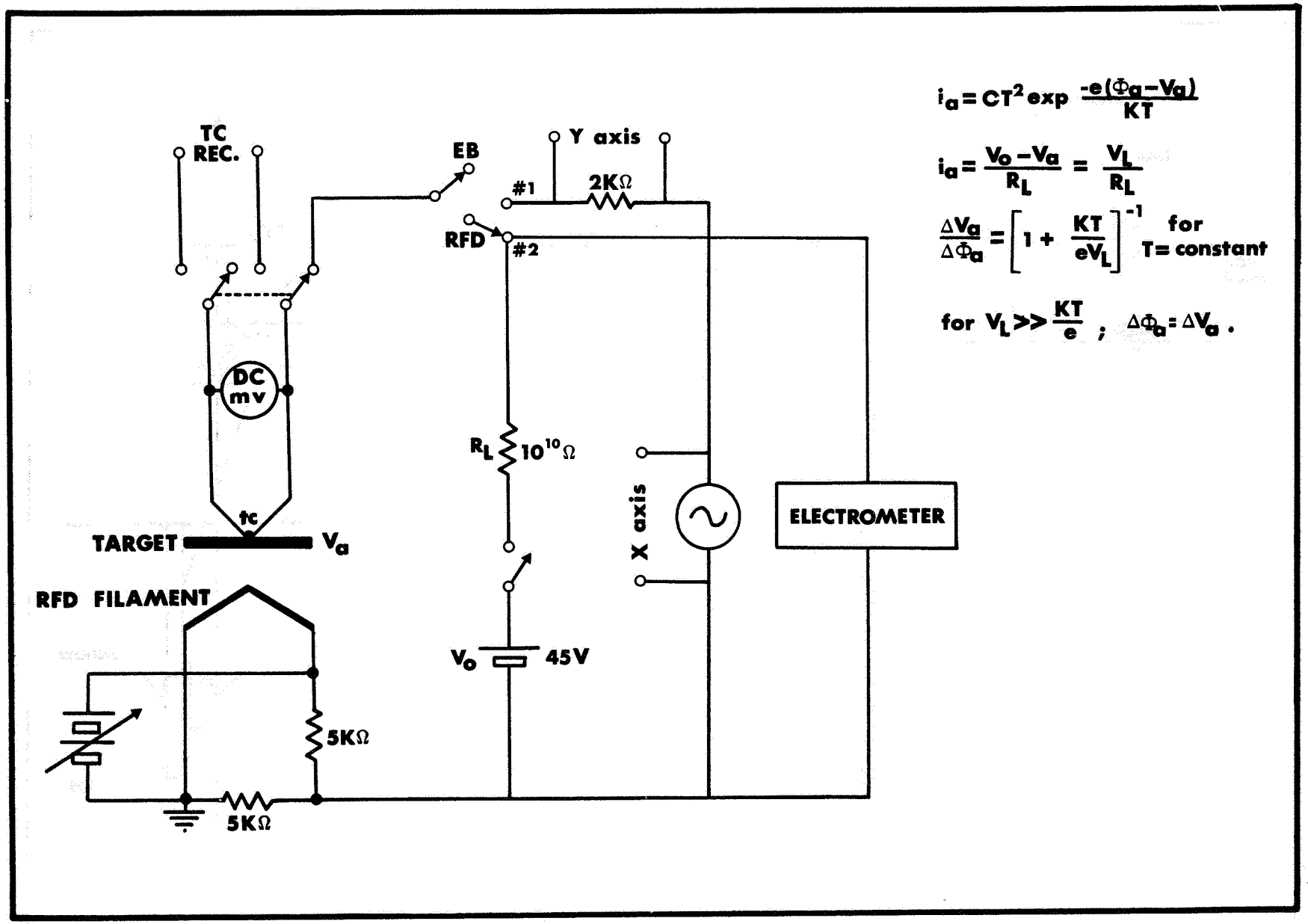

FIG. 2.5.12 CIRCUIT DIAGRAM OF RETARDING FIELD DIODE

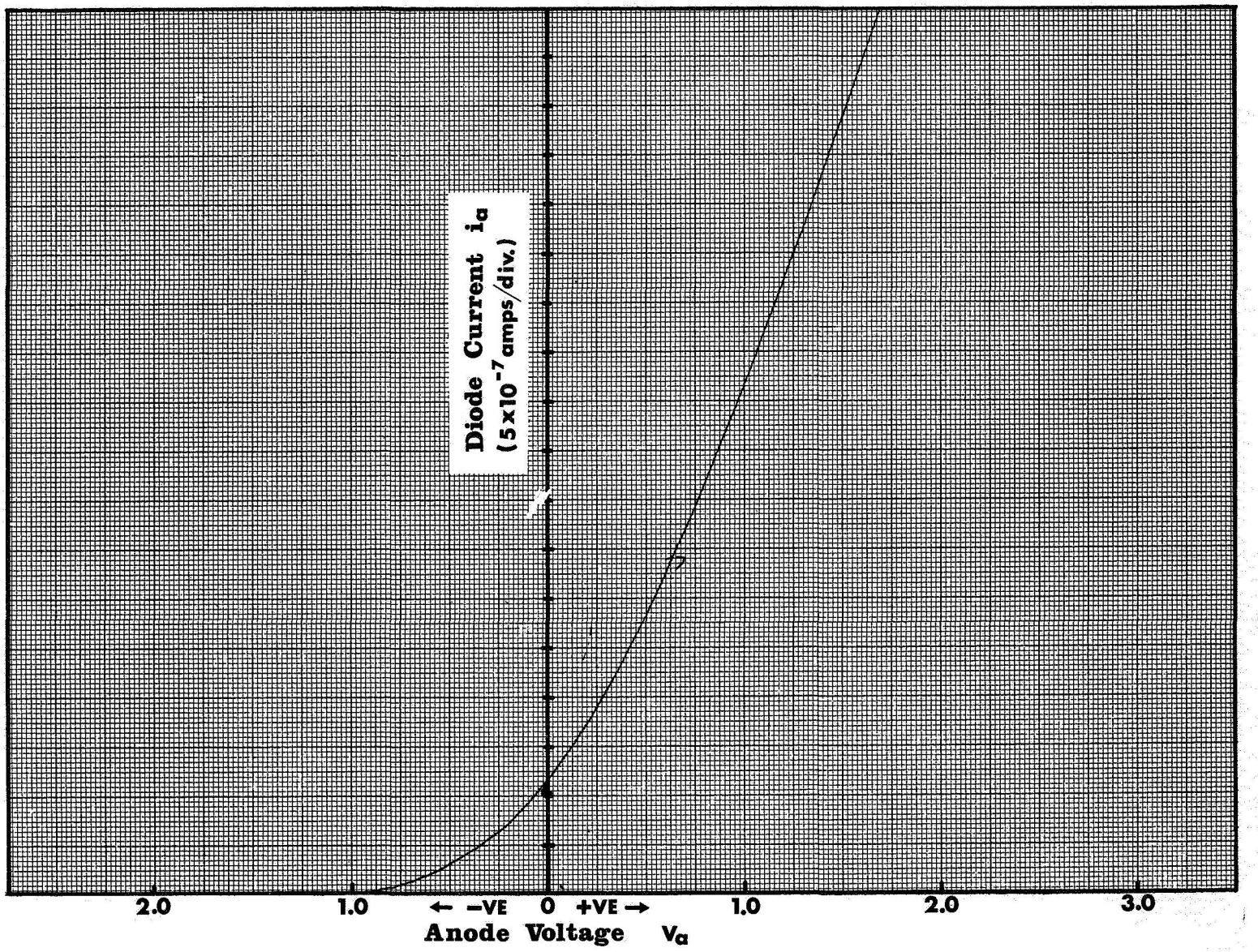

FIG. 2.5.13 RETARDING FIELD DIODE CURRENT-VOLTAGE CHARACTERISTIC

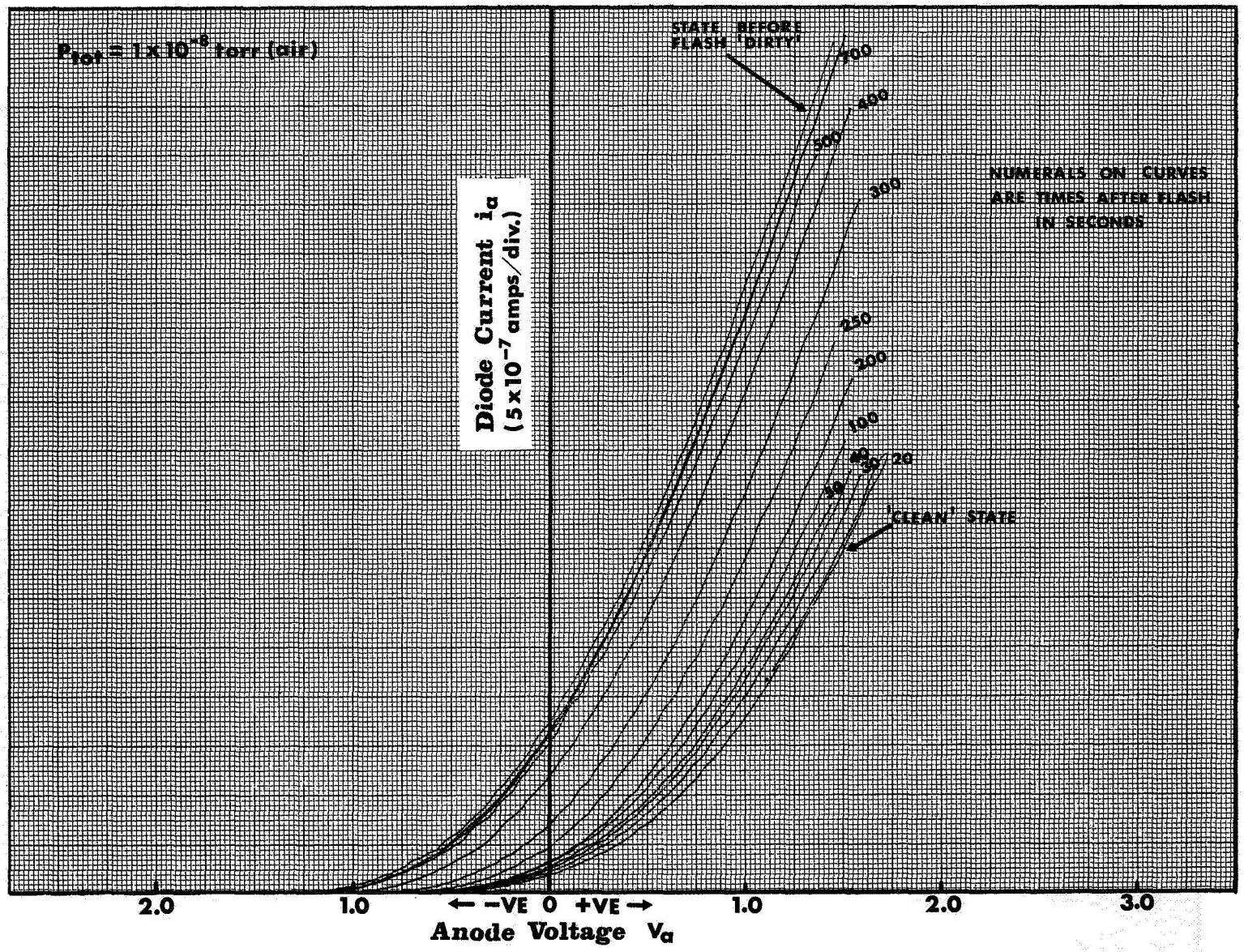

FIG. 2.5.14 SHIFT IN THE RETARDING FIELD DIODE CURRENT-VOLTAGE CHARACTERISTIC DUE TO THE ADSORPTION OF NITROGEN

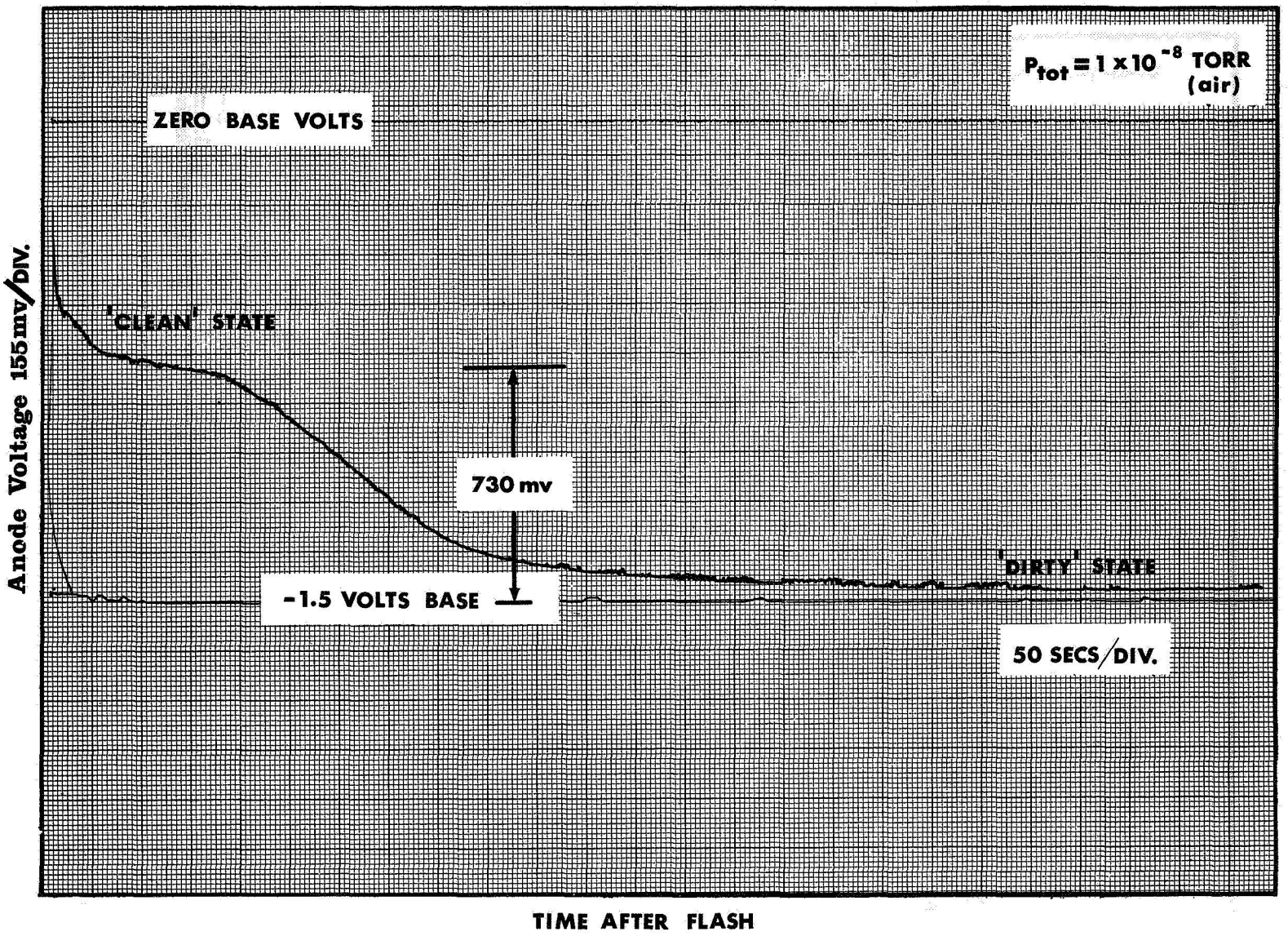

FIG. 2.5.15 VARIATION OF THE RETARDING FIELD DIODE ANODE VOLTAGE FOR THE ADSORPTION OF NITROGEN (CURRENT OF DIODE = CONSTANT)

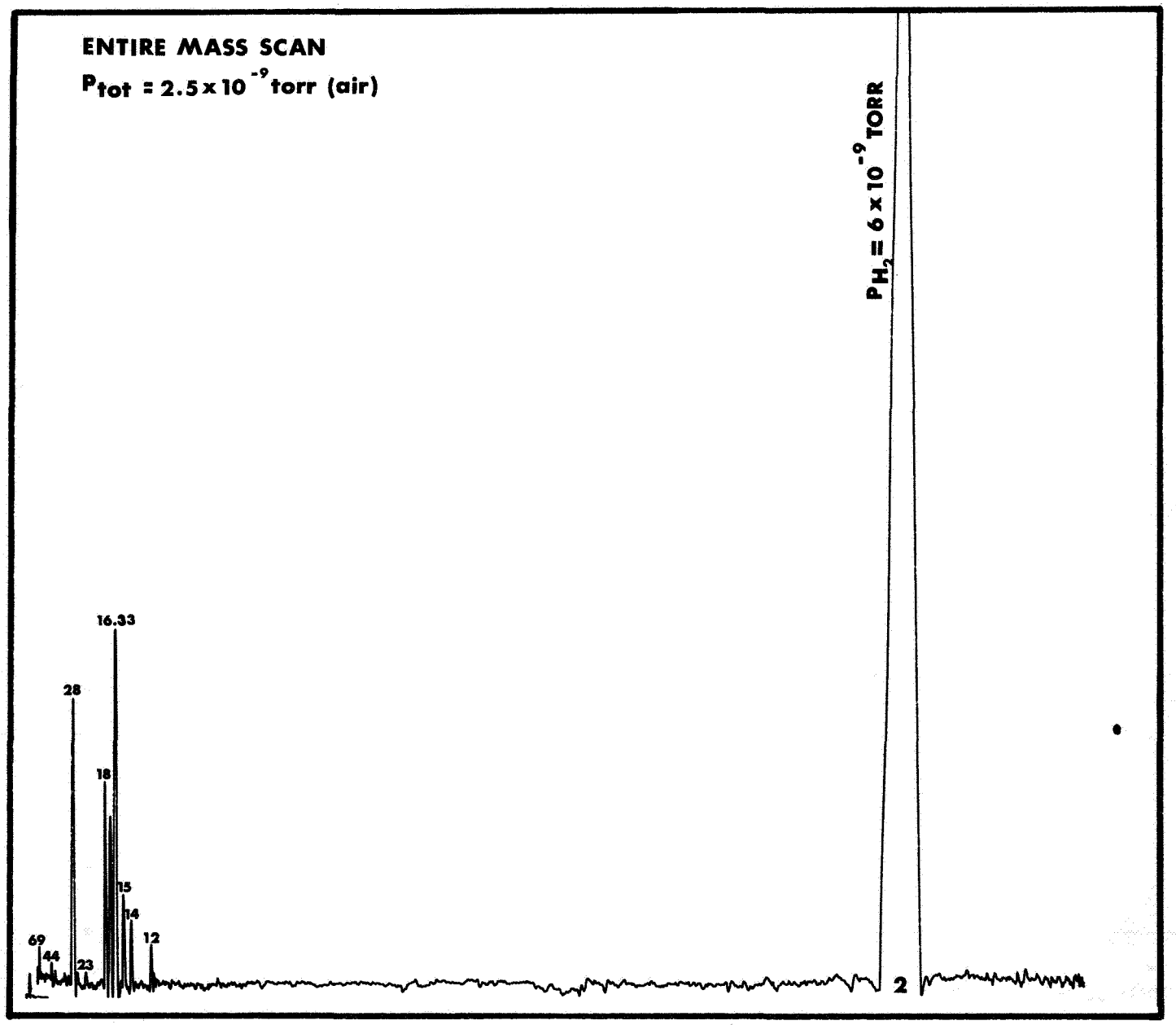

FIG. 3. 1. 1 ENTIRE MASS SCAN (2 to 70 amu)

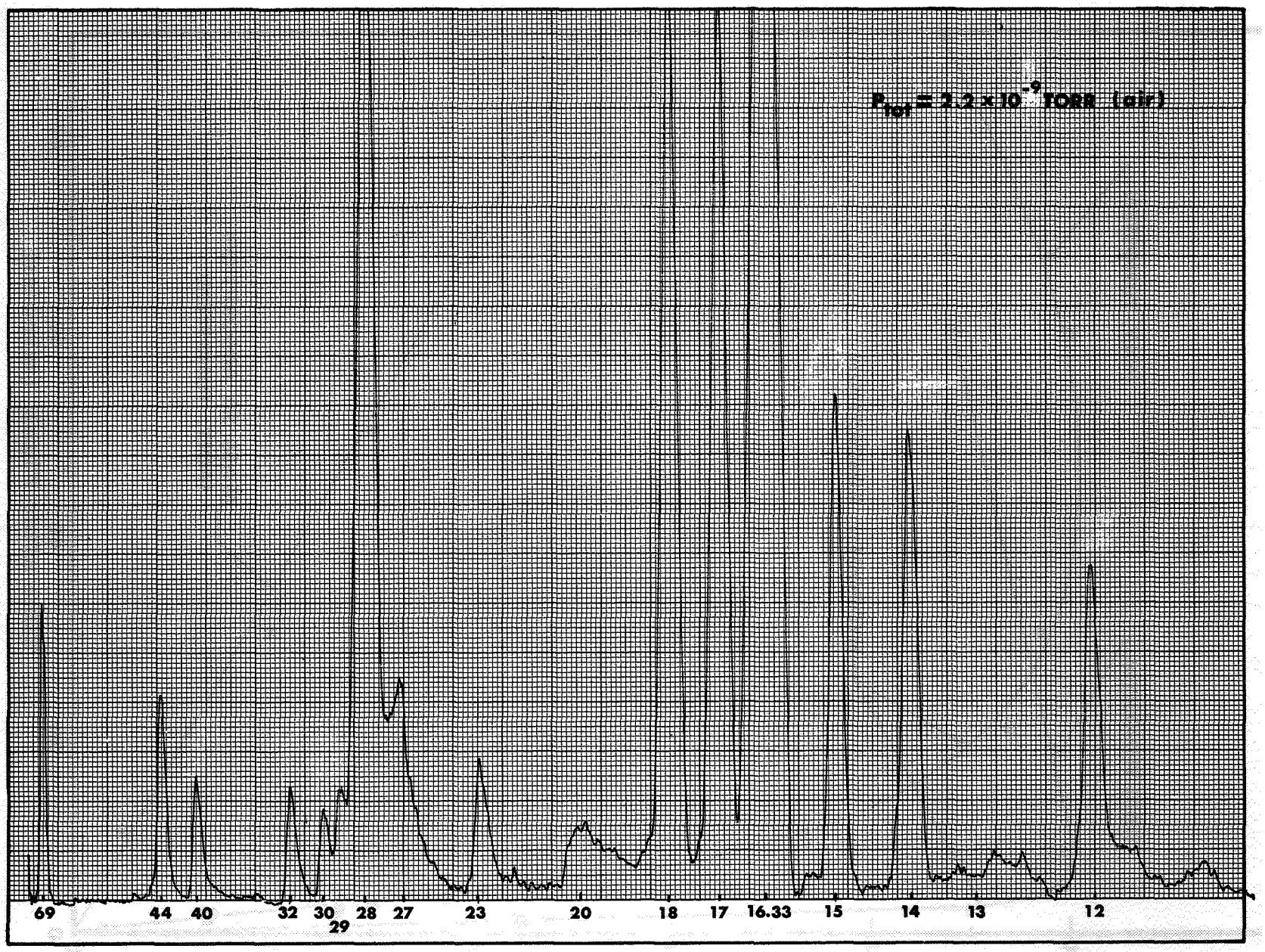

FIG. 3.1.2 PARTIAL MASS SCAN (12 to 70 amu)

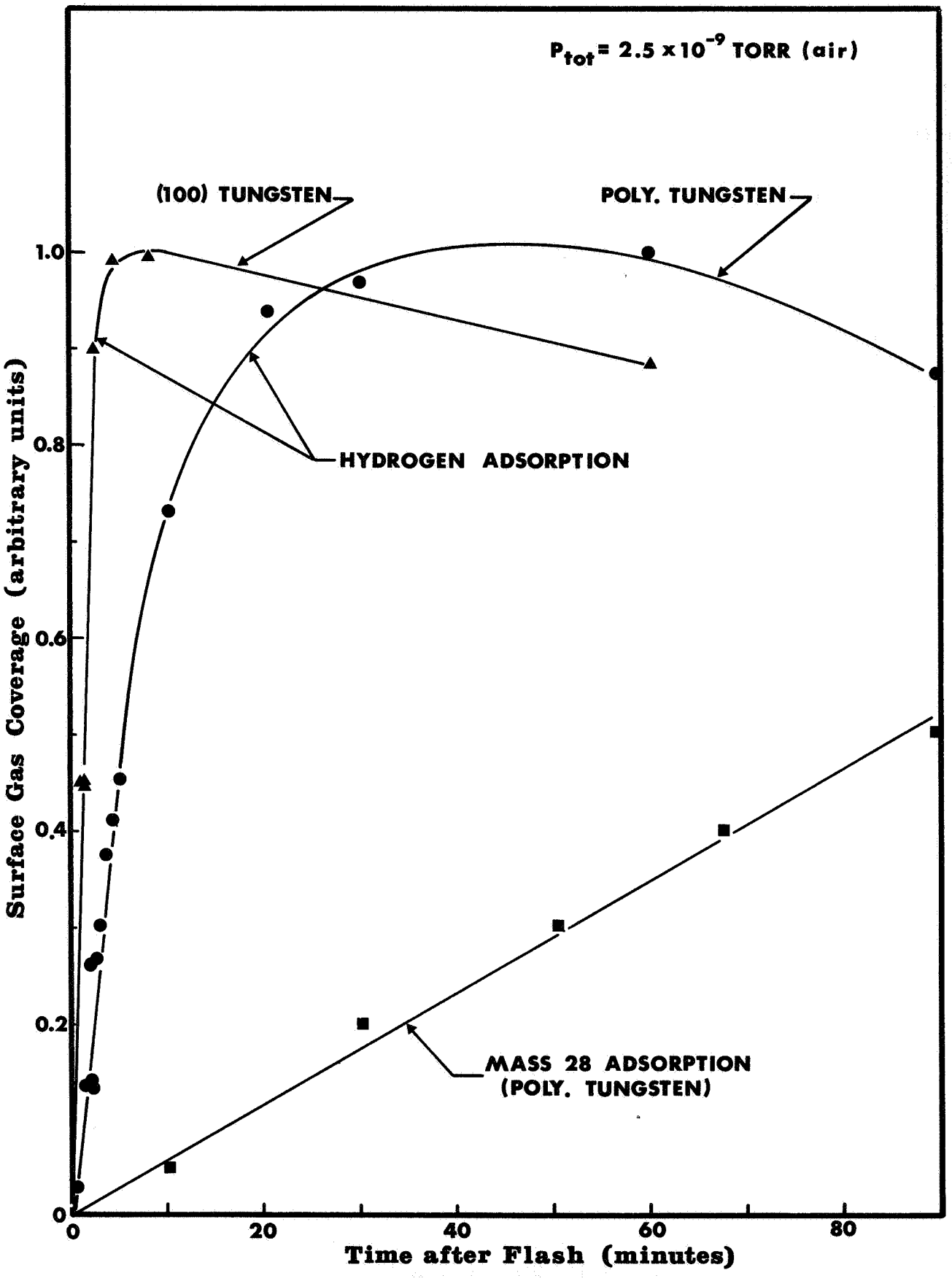

FIG. 3. 1. 3 SURFACE GAS COVERAGE DUE TO BACKGROUND GAS VS ADSORPTION TIME

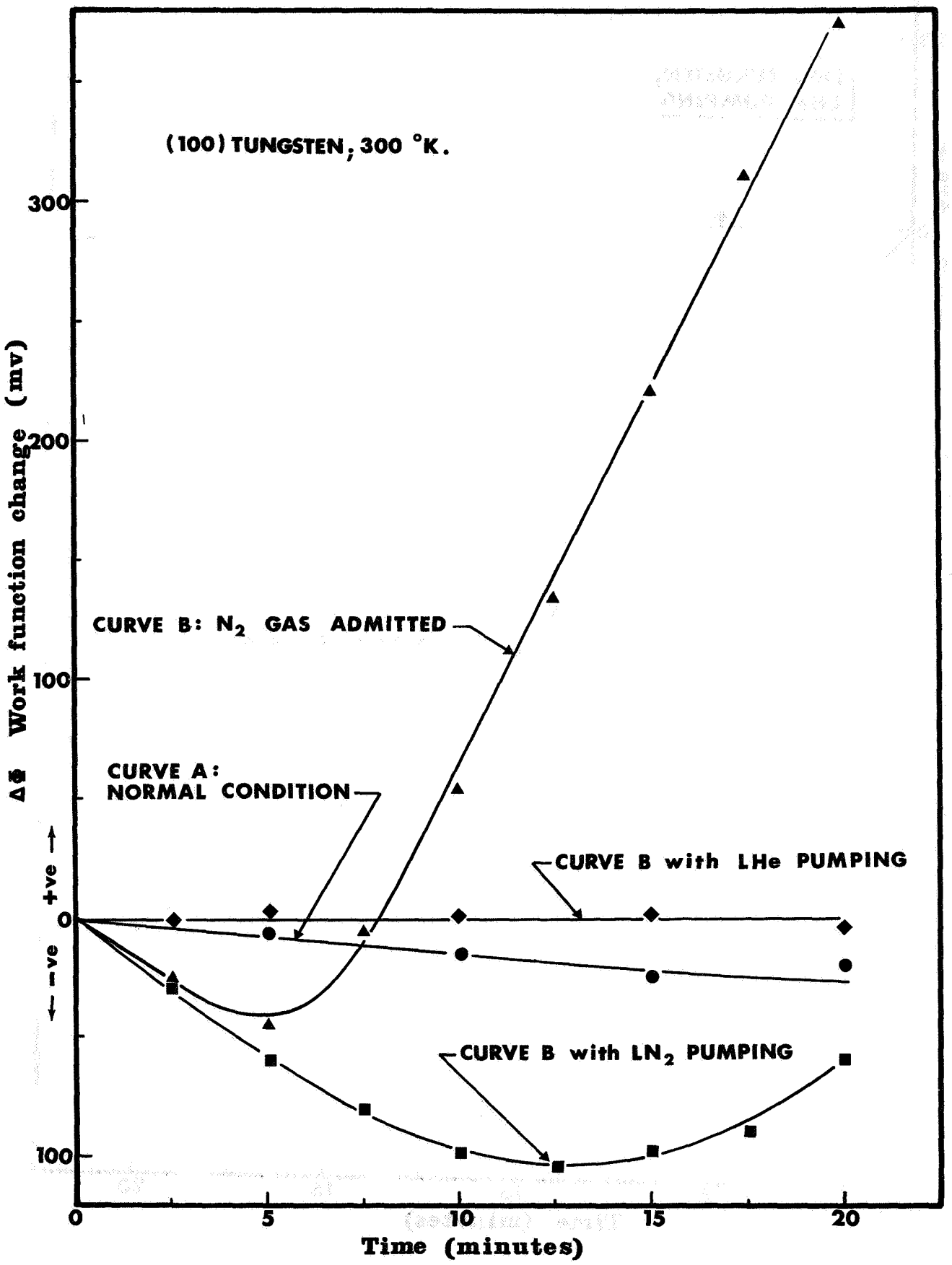

FIG. 3.1.4 WORK FUNCTION CHANGE DUE TO ADSORPTION OF BACKGROUND GASES ON THE SURFACE

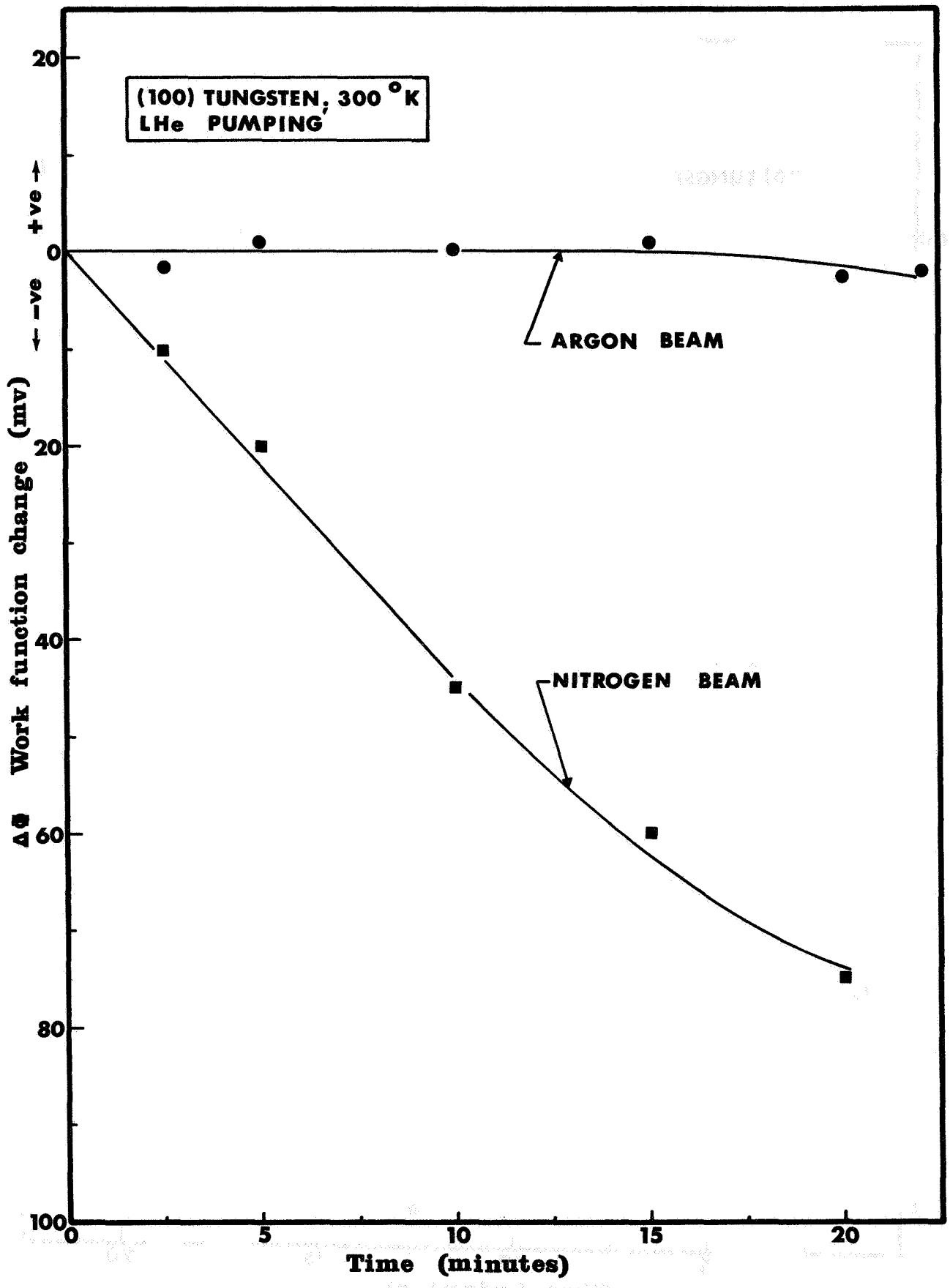

FIG. 3.1.5 WORK FUNCTION CHANGE DUE TO ADSORPTION OF BEAM ON THE SURFACE

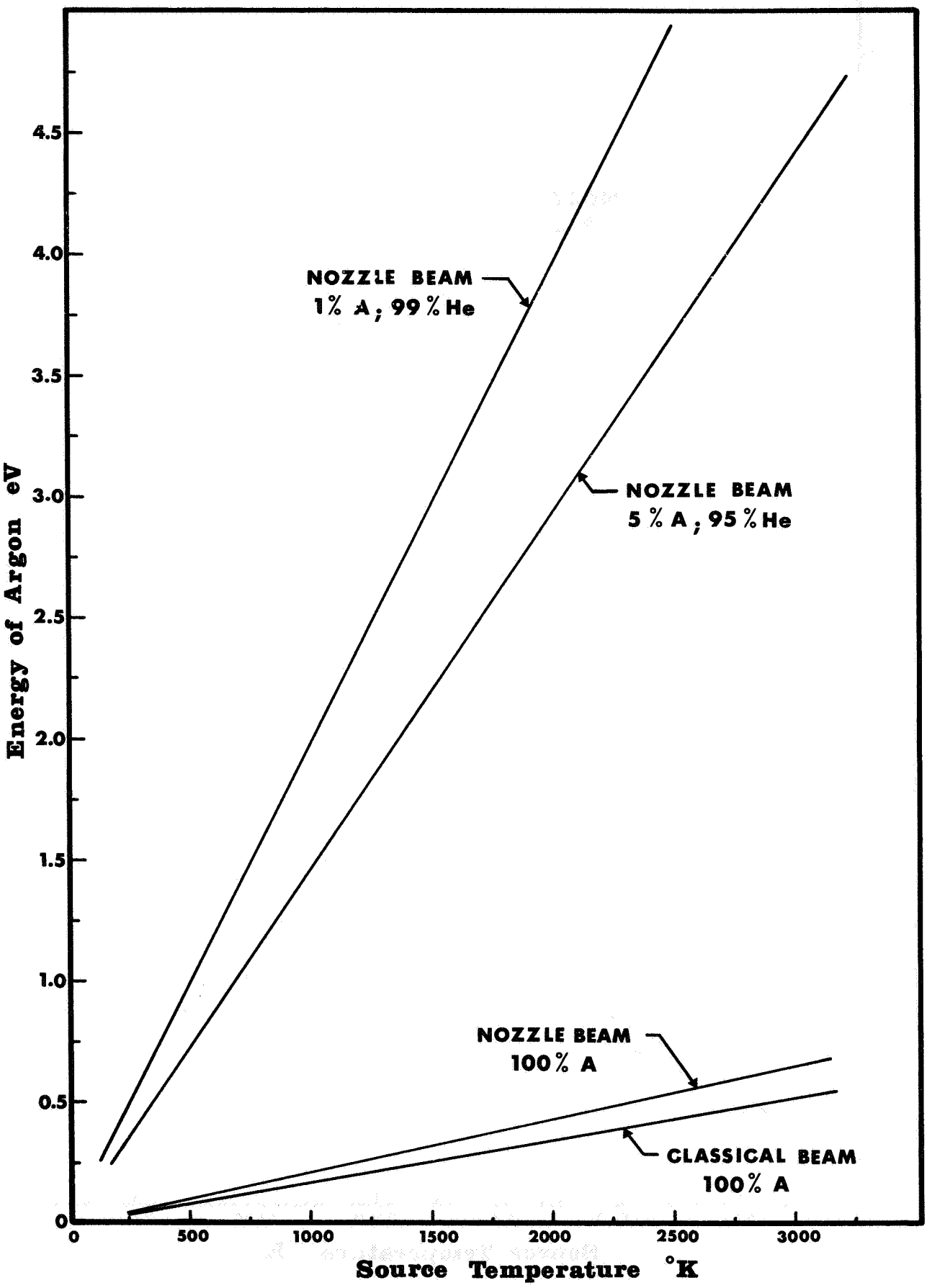

FIG. 3.2.1 ARGON BEAM ENERGY AS A FUNCTION OF SOURCE TEMPERATURE AND MIXTURE

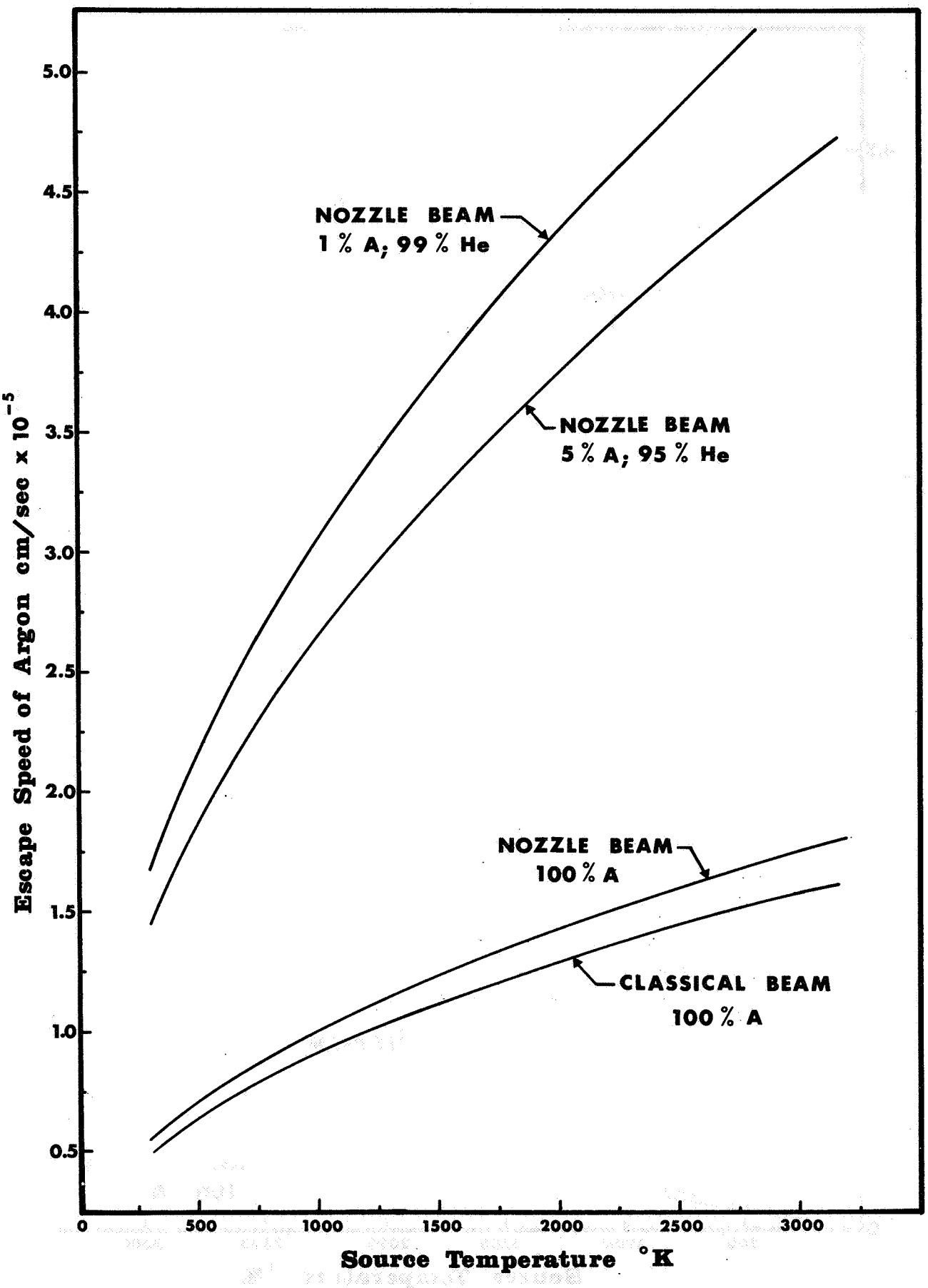

FIG. 3.2.2 ARGON BEAM VELOCITY AS A FUNCTION OF SOURCE TEMPERATURE AND MIXTURE

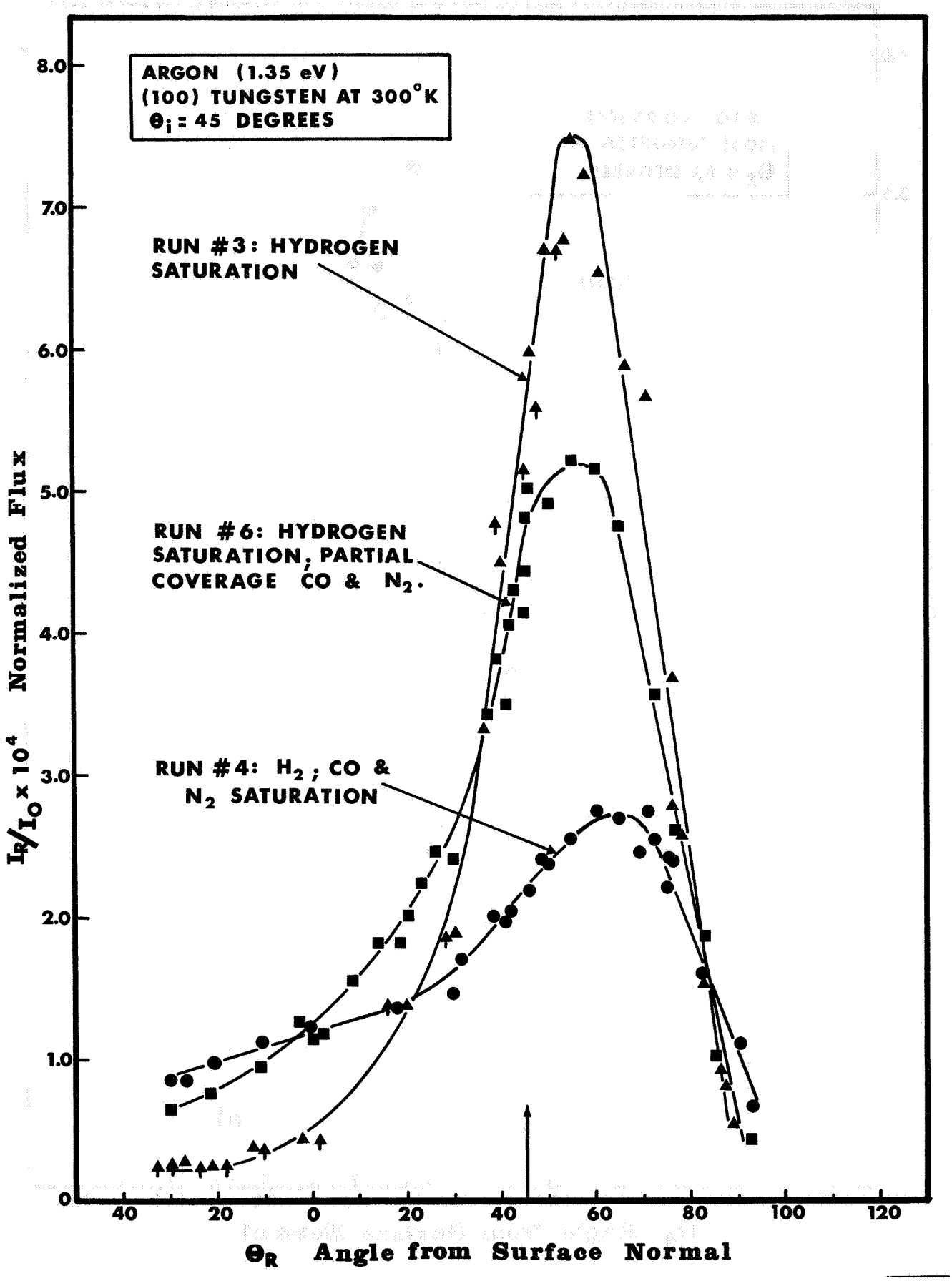

FIG. 3.2.3 THE EFFECT OF GASEOUS MONOLAYERS ON THE SCATTERED NUMBER FLUX DISTRIBUTION FOR AN INCIDENT BEAM ENERGY OF 1.35 eV. To convert to the ratio of the number of reflected particles per second per steradian (ψ) to the total number incident per second (N_o) use the expression $\psi/N_o = 2.94 \times 10^3 \, I_R/I_o$.

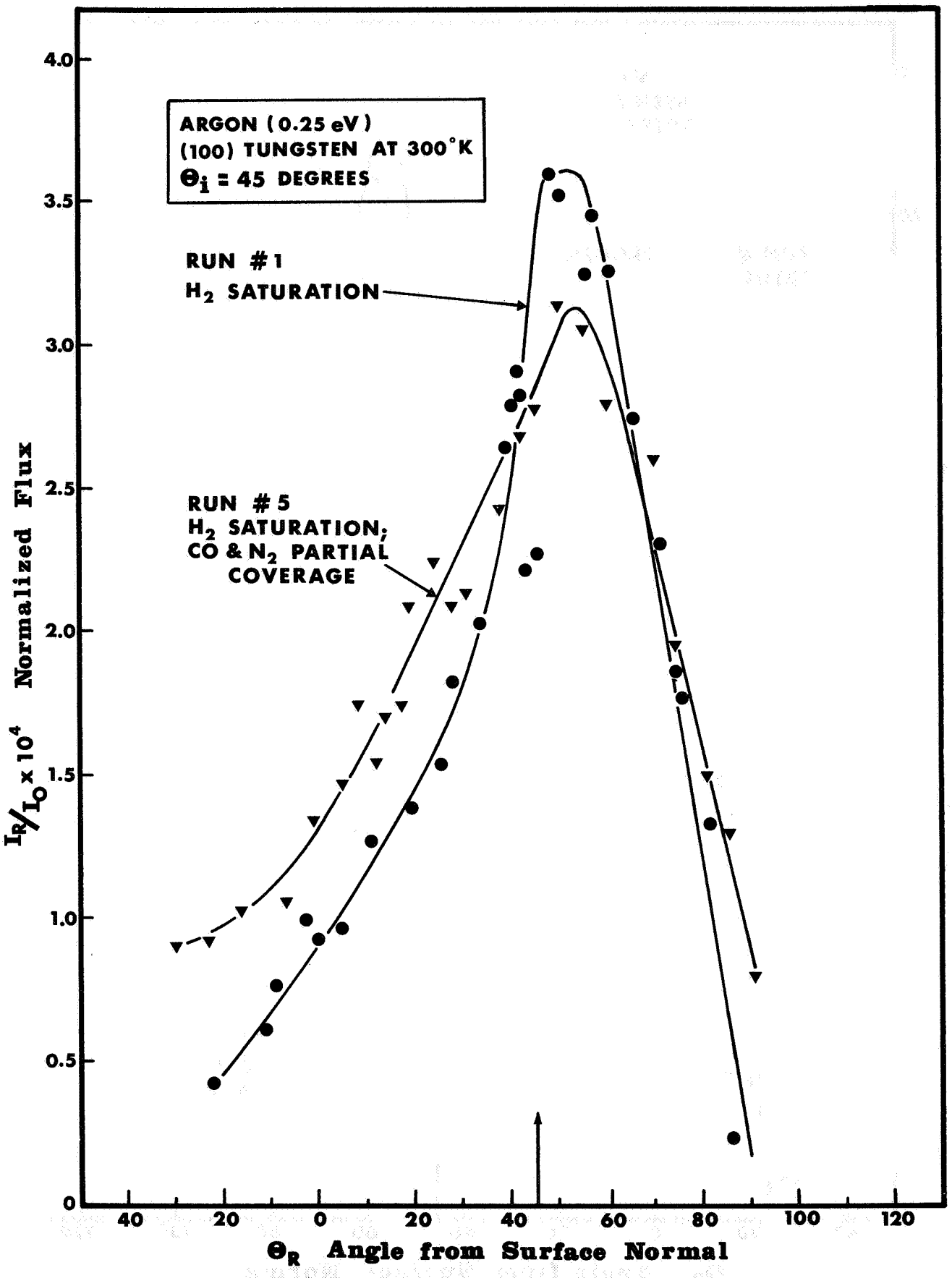

FIG. 3.2.4 THE EFFECT OF GASEOUS MONOLAYERS ON THE SCATTER. NUMBER FLUX DISTRIBUTION FOR AN INCIDENT BEAM OF 0.25 eV. To convert to the ratio of the number of reflected particles per second per steradian (ψ) to the total number incident per second (N_o) use the expression

$$\psi/N_o = 2.94 \times 10^3 \, I_R/I_o$$

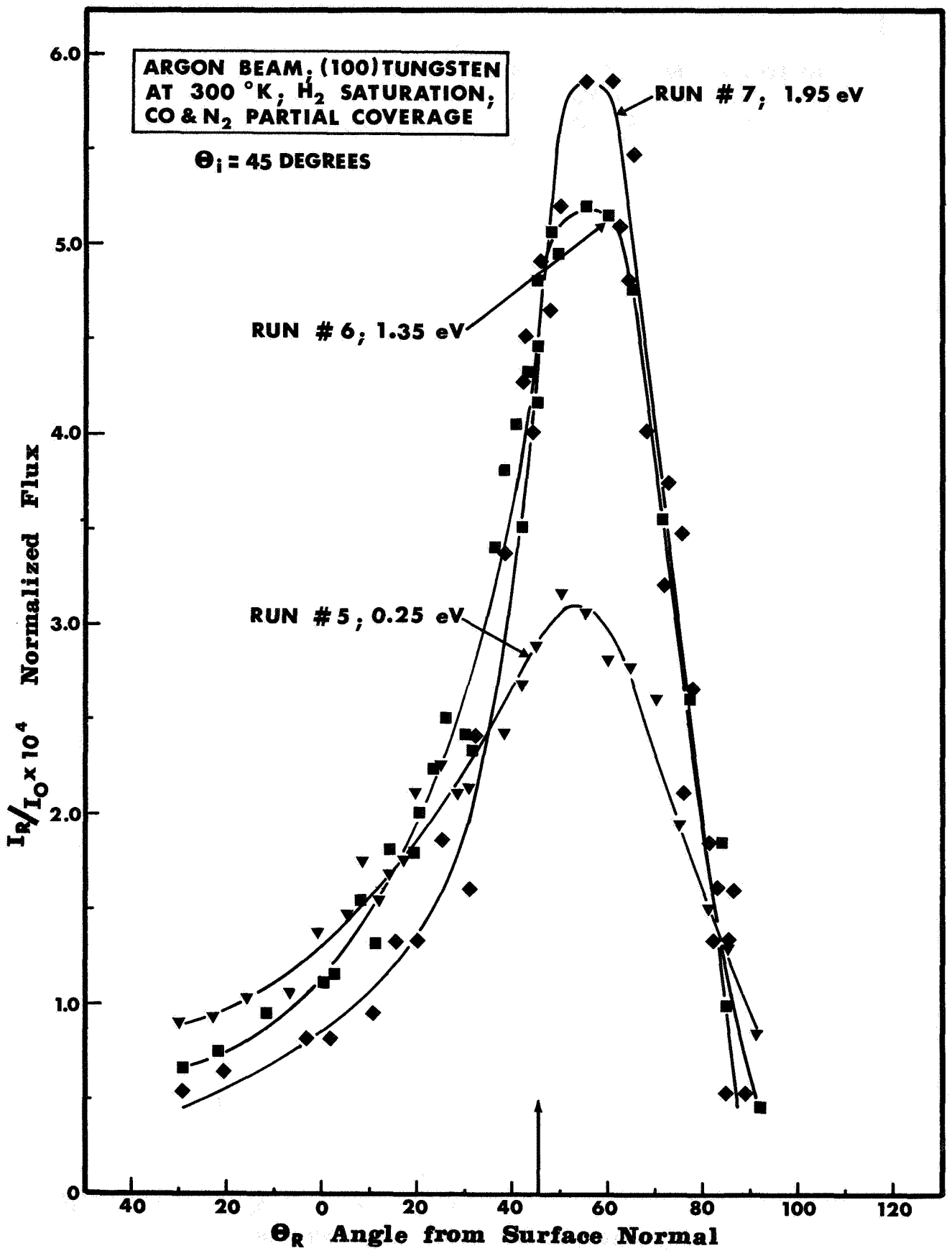

FIG. 3.2.5 THE EFFECT OF INCIDENT BEAM ENERGY ON THE SCATTERED NUMBER FLUX DISTRIBUTION (H_2 SATURATION, PARTIAL COVERAGE OF CO AND N_2). To convert to the ratio of the number of reflected particles per second per steradian (ψ) to the total number incident per second (N_o) use the expression $\psi/N_o = 2.94 \times 10^{-3} I_R/I_o$

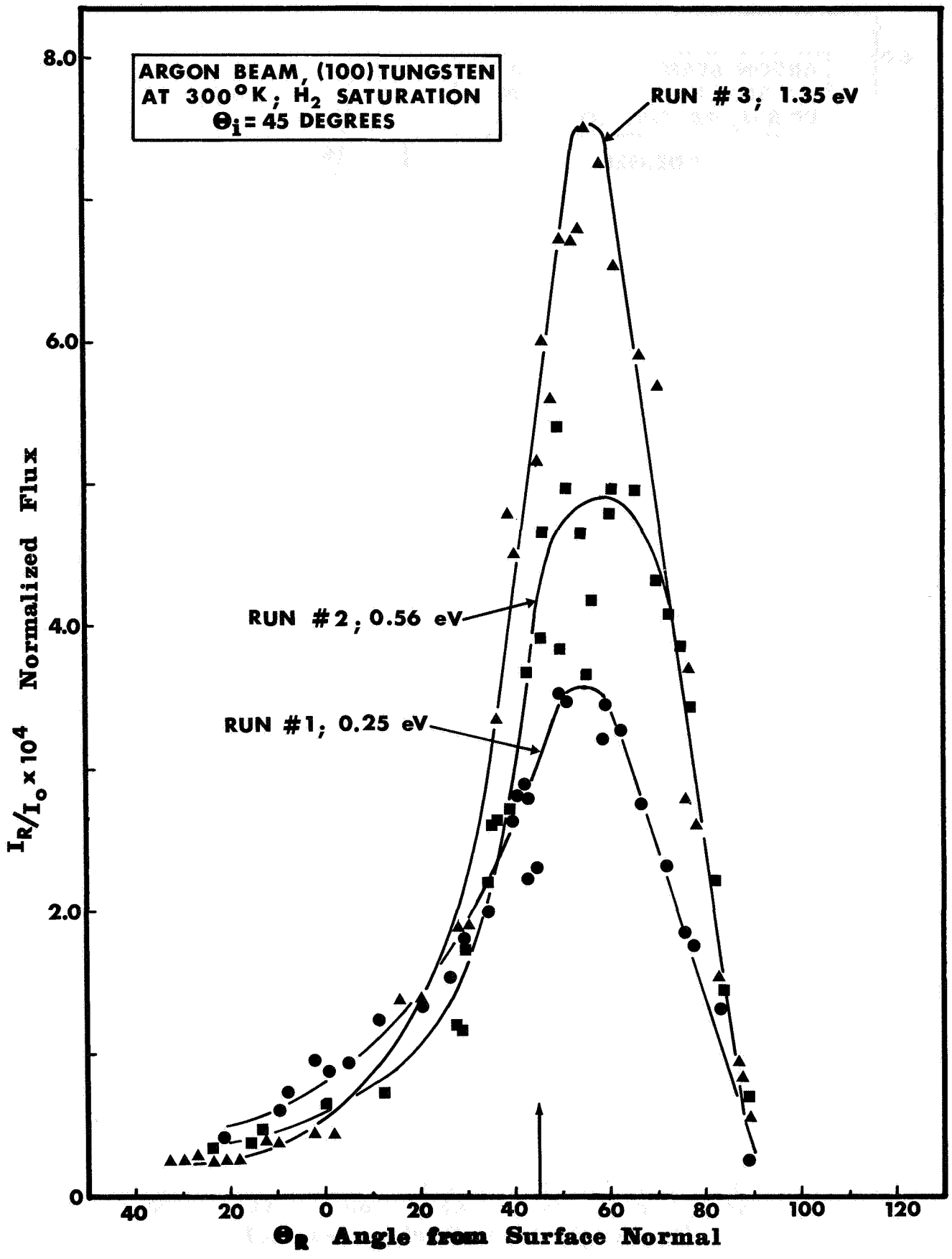

FIG. 3.2.6 THE EFFECT OF INCIDENT BEAM ENERGY ON THE SCATTERED NUMBER FLUX DISTRIBUTION (H_2 SATURATION) To convert to the ratio of the number of reflected particles per second per steradian (ψ) to the total number incident per second (N_o) use the expression $\psi/N_o = 2.94 \times 10^3 \, I_R/I_o$

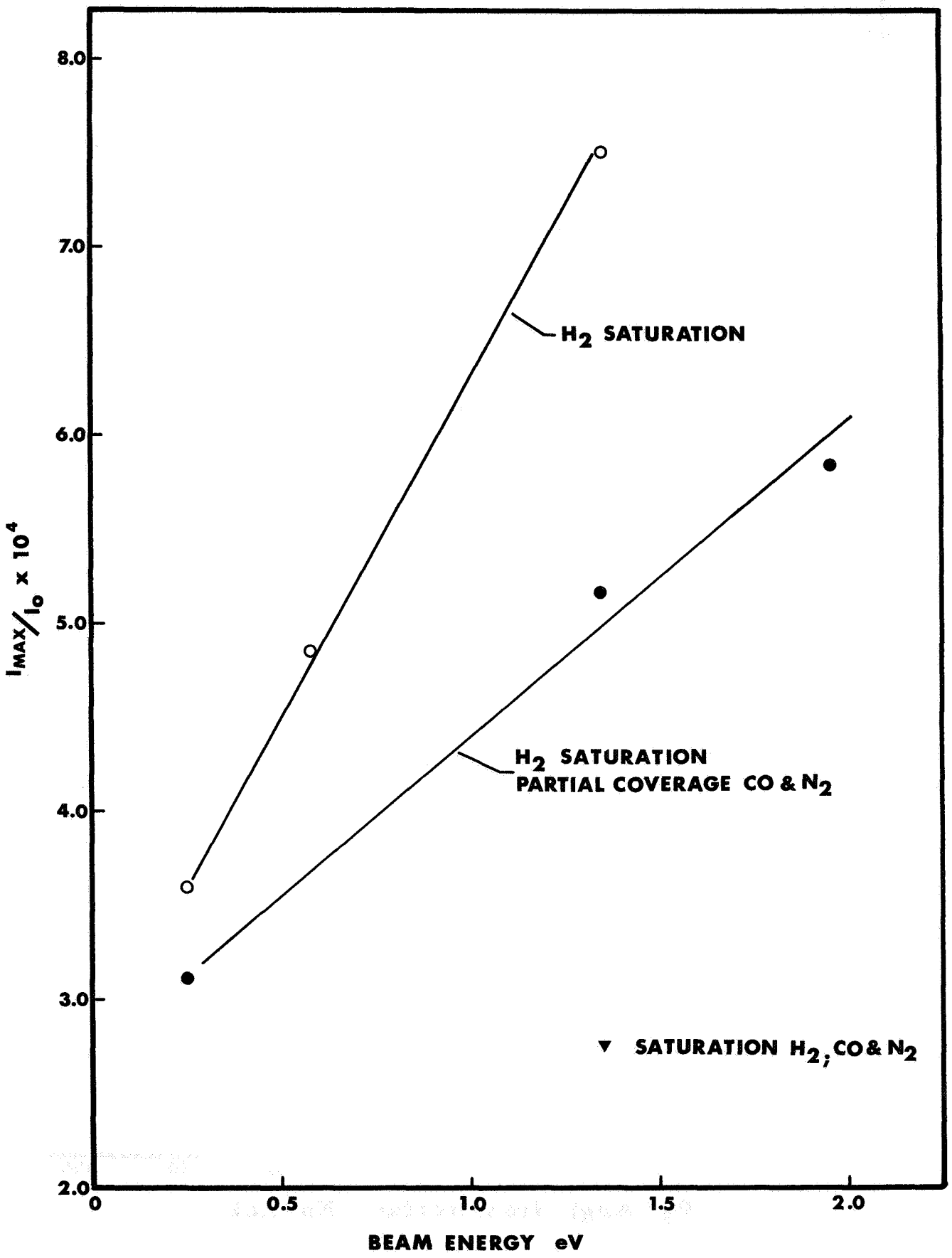

FIG. 3.2.7 VARIATION OF THE SIGNAL LEVEL AT THE POSITION OF THE MAXIMUM OF THE REFLECTED FLUX WITH INCIDENT BEAM ENERGY

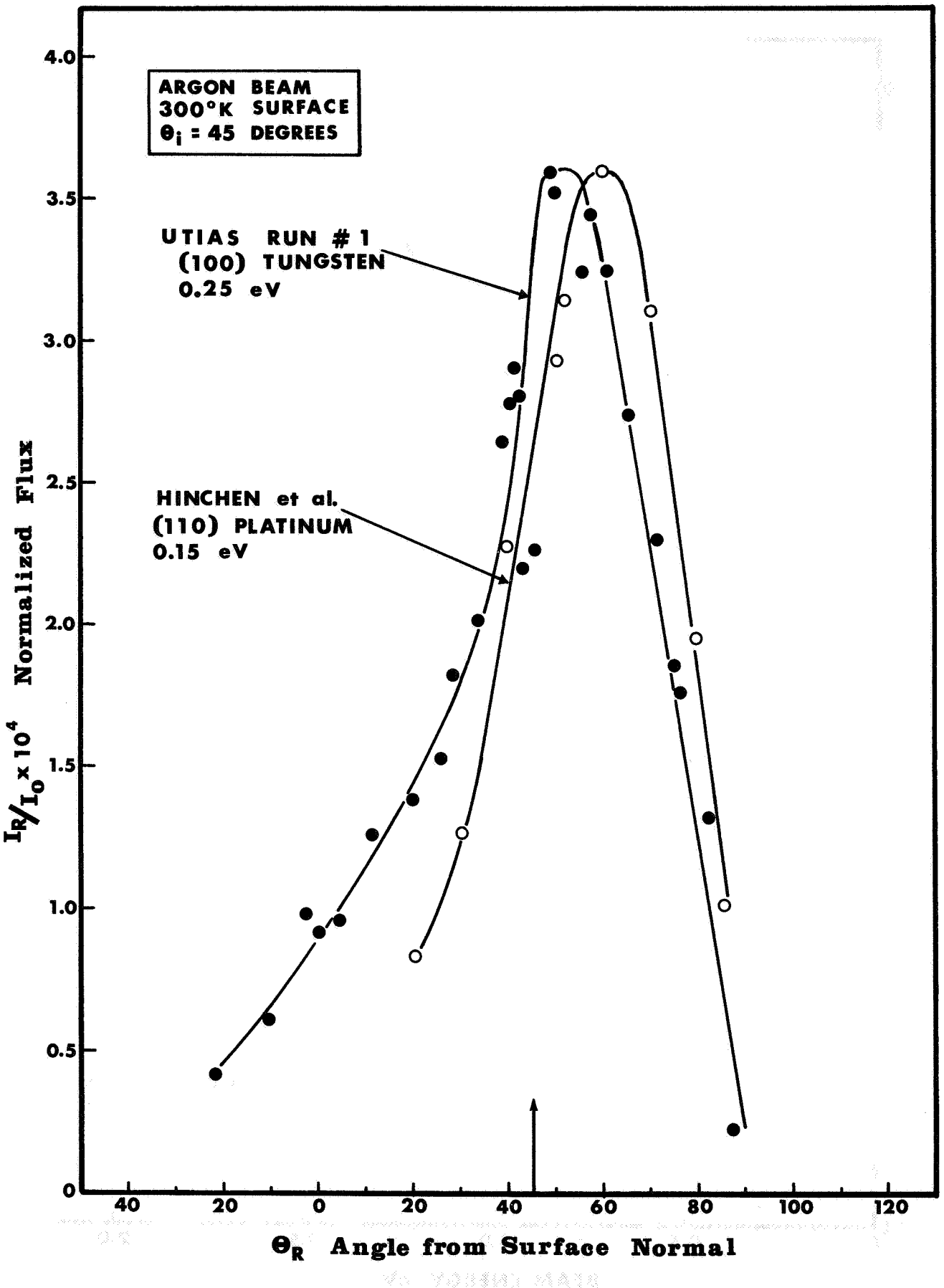

FIG. 3.2.8 COMPARISON OF PRESENT DISTRIBUTION (0.25 eV on 100 W) WITH THAT OF HINCHEN ET AL (0.15 eV on 110 Pt)

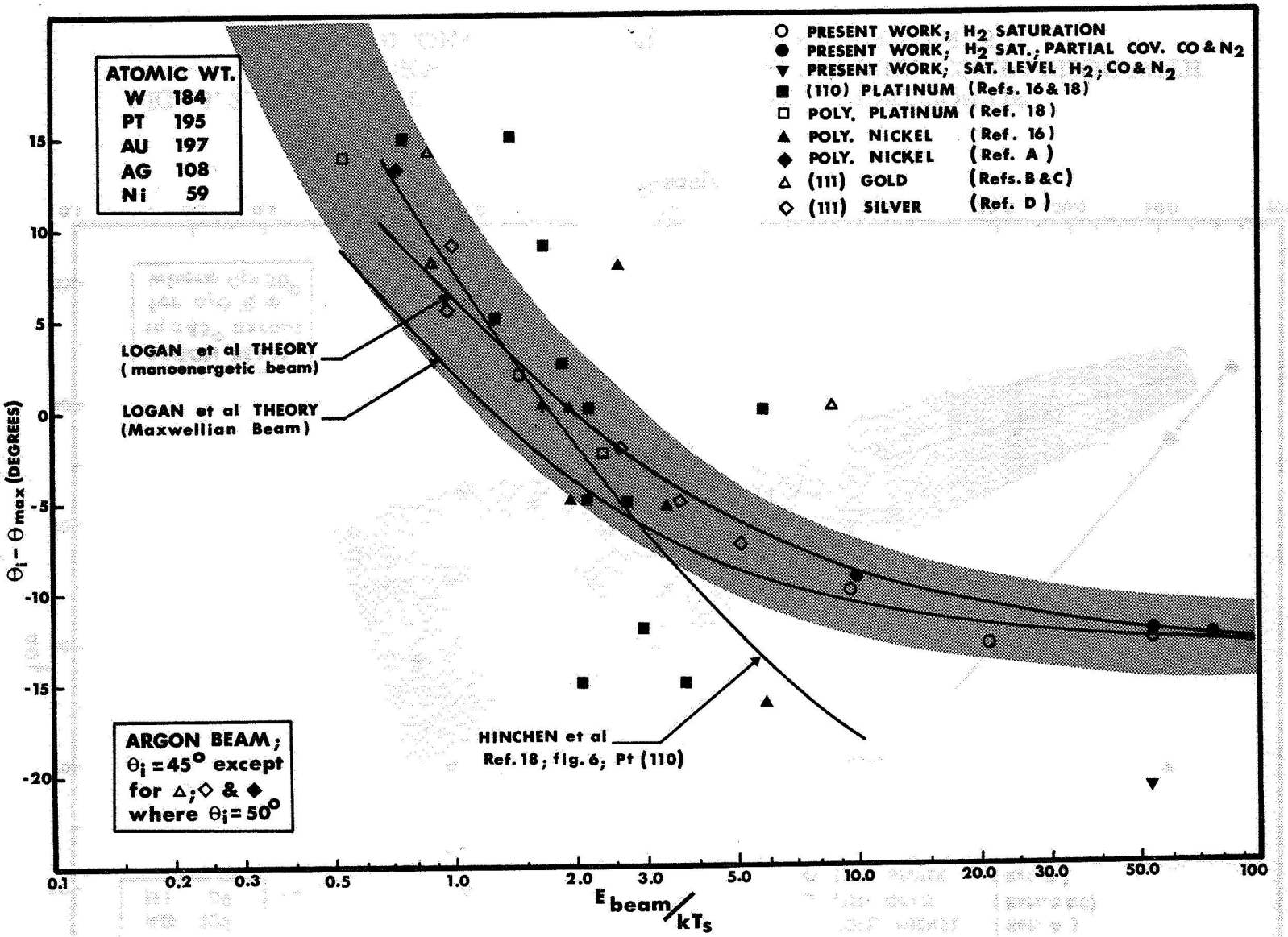

FIG. 3.2.9 ANGULAR DEVIATION OF THE DISTRIBUTION MAXIMUM FROM THE SPECULAR POSITION AS A FUNCTION OF NORMALIZED INCIDENT BEAM ENERGY. COMPARISON WITH THEORY AND LOWER ENERGY EXPERIMENTS.

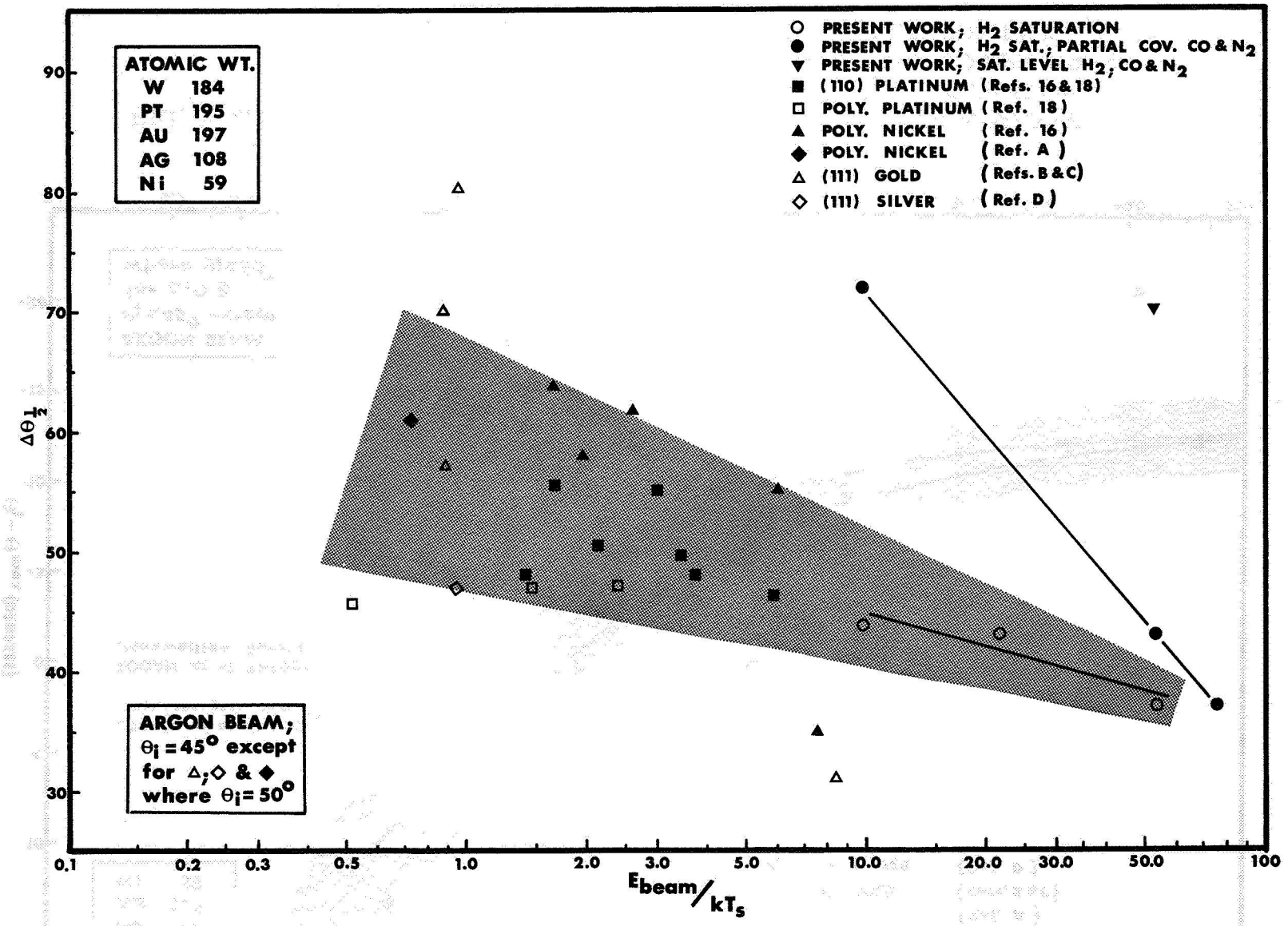

FIG. 3.2.10 DISTRIBUTION HALF-WIDTH AS A FUNCTION OF NORMALIZED INCIDENT BEAM ENERGY. COMPARISON WITH THEORY AND LOWER ENERGY EXPERIMENTS.

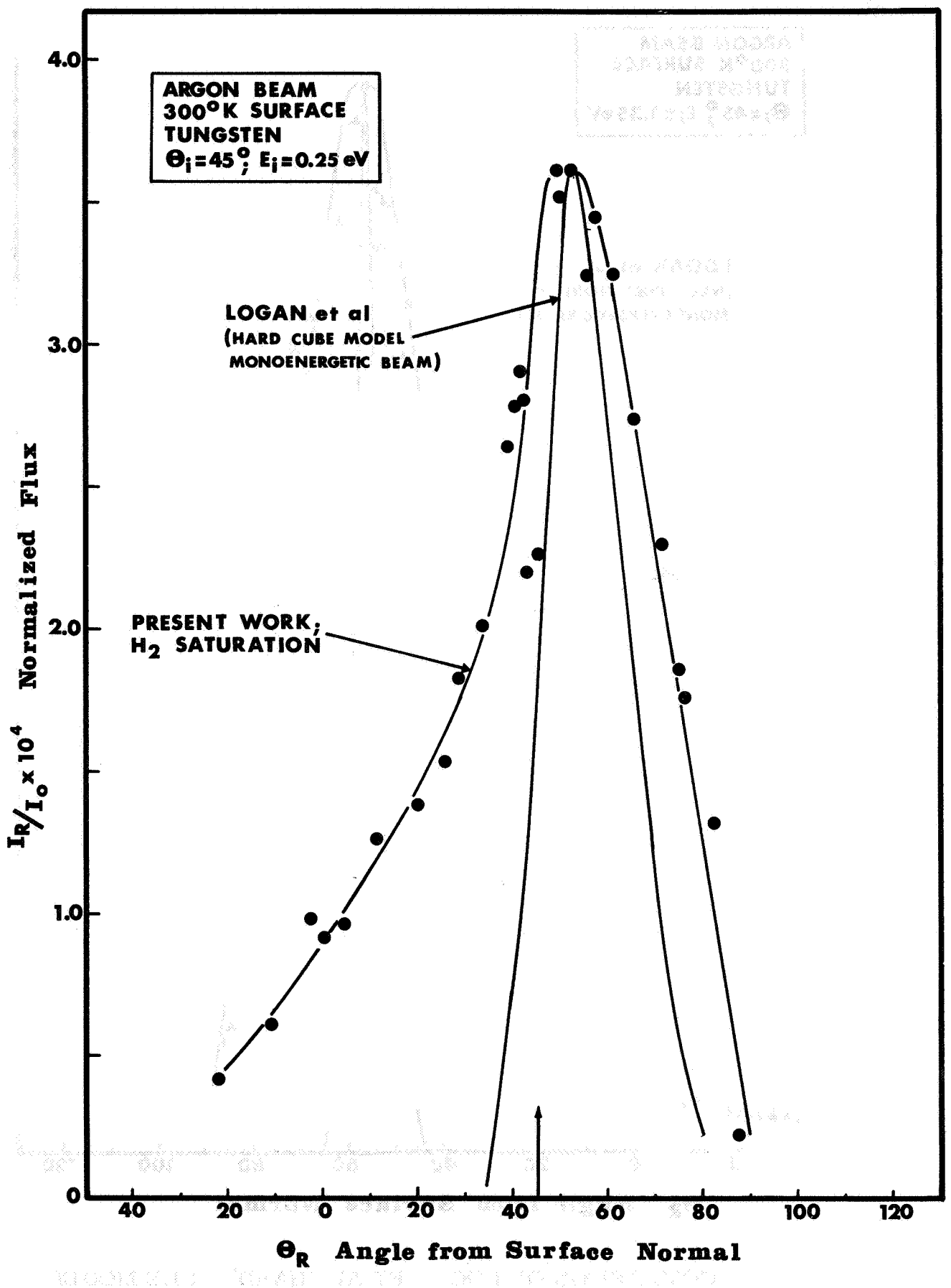

FIG. 3.2.11 COMPARISON OF LOGAN ET AL "HARD" CUBE MODEL AT 0.25 eV INCIDENT BEAM ENERGY

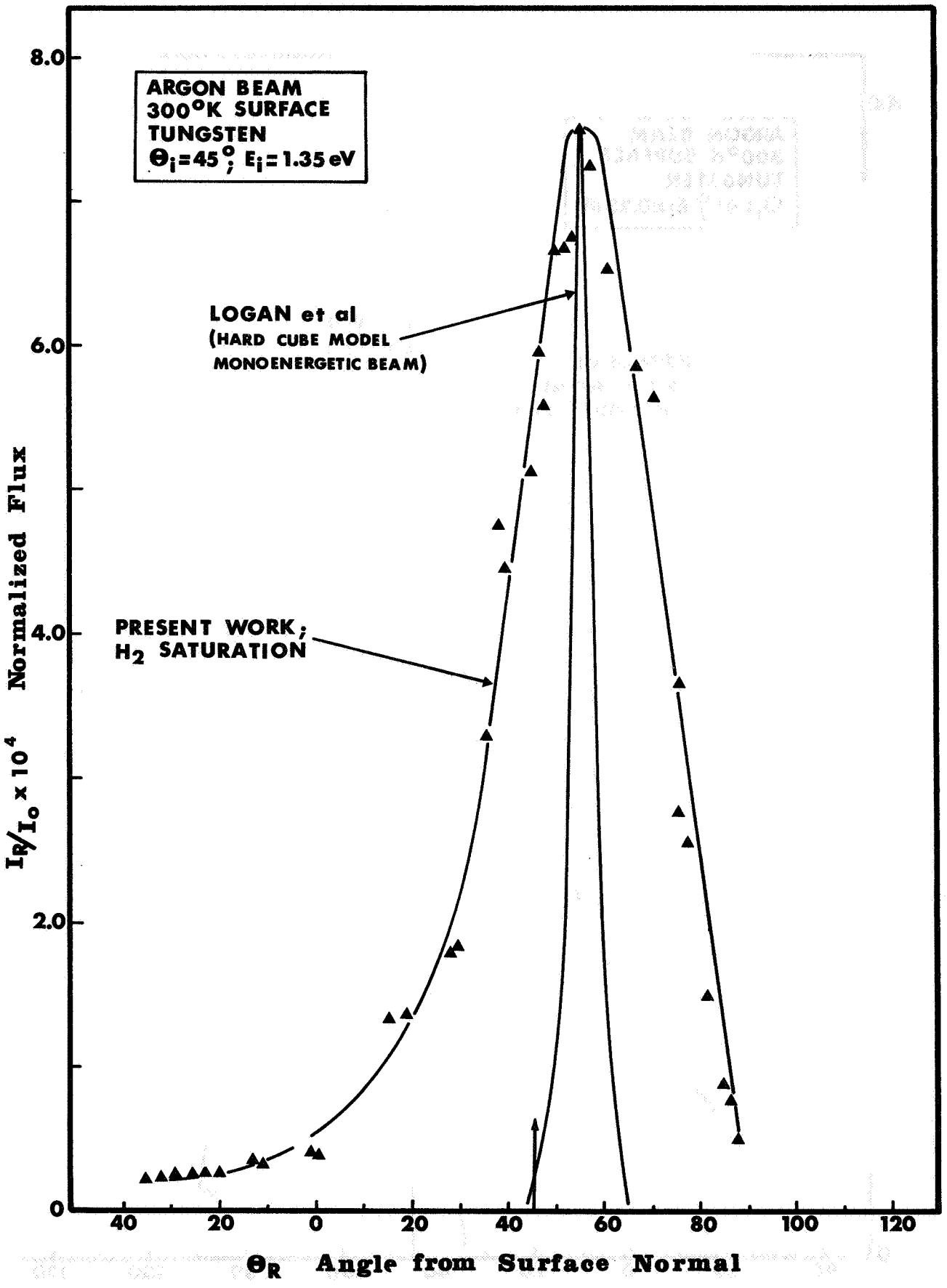

FIG. 3.2.12 COMPARISON OF LOGAN ET AL "HARD" CUBE MODEL AT 1.35 eV INCIDENT BEAM ENERGY